

The Smallest Shape Spaces. III.

Triangles in 2- and 3- d

Edward Anderson*

Abstract

This is an innovative treatise on triangles, resting upon 1) 3-body problem techniques including mass-weighted relative Jacobi coordinates. 2) Part I's detailed layer-by-layer topological and geometrical study of Kendall-type shape spaces – configuration spaces of all possible shapes – which, for triangles, are (pieces of) spheres. 3) Hopf mathematics. Triangles are moreover prototypical through being the smallest models which carry relative-angle as well as length-ratio information. Both 1) and 3) produce insightful new versions of Heron's formula, 3)'s moreover simultaneously providing new foundations for 2). Medians, and regular triangles bounding between tall and flat triangles, also play prominent roles. Right triangles form three kissing cap-circles on the shape sphere, from which a shape-theoretic answer to the well-known conundrum of what is the probability that a triangle is obtuse very readily follows: $3/4$. The differential-geometric aspects of this answer moreover generalize to numerous variant problems: conditioning on tallness and/or isoscelesness, generalizing from right angles to arbitrary maximal angles via the maximal angle flow on the shape sphere...

Hopf mathematics moreover gives a general bundle section interpretation to Kendall's iconic spherical blackboard of vertex-unlabelled mirror-image-identified triangles, and of its two variants where one of these two conditions are dropped. We attribute a monopole to each of these spaces and to the full shape sphere, one due to Dirac, one to Iwai and the other two are new to this paper. We finally make insightful comparison of triangles in 2- d with a) Part II's 4 points on the line. b) Triangles in 3- d , which are particularly significant as the smallest model exhibiting stratification. Stratified manifold–sheaf pairs [66, 84] – sheaves [42, 58] adding useful local and global structure to general bundles – lie at the heart of Shape Theory's future development.

PACS: 04.20.Cv, Physics keywords: background independence, inhomogeneity, configuration space, Killing vectors, monopoles, 3-body problem.

Mathematics keywords: triangles, spaces of triangles, Shape Geometry, Shape Statistics, Applied Topology, Applied Geometry, applications of fibre and general bundles, Hopf map, simple but new applications of Graph Theory to Shape Theory, simple examples of stratified manifolds.

* Dr.E.Anderson.Maths.Physics@protonmail.com

1 Introduction

We continue this treatise on the smallest shape spaces by considering the triangle shapes made by 3 points in 2- and 3- d . Some of the ways in which these are critical models are through providing the smallest models exhibiting the following features.

- 1) They contain relative angle information (whereas Parts I and II's shapes consisted solely of side-ratio information).
- 2) They manifest nontrivial Configurational Relationalism (a concept outlined in Part I; see [98, 108] for more details).
- 3) They exhibit nontrivial bundle mathematics [52].
- 4) The 3- d version moreover exhibits nontrivial stratification [10, 15, 22, 30] of configuration space.
- 5) Thereby, the 3- d version furthermore requires a general bundle [52] or sheaf [42, 58] treatment, given that fibre bundles do not suffice to study stratified manifolds. In fact, as the current paper first reveals, the 2- d version also requires this as regards quotienting out mirror image identification and point-or-particle distinguishability.
- 6) The 3-body problem is much more typical of N -body problems [45, 55] than the 2-body problem is.
- 7) Triangular shapes are also the smallest model which makes contact with widely studied flat geometry problems [6, 31, 50, 49, 65, 87]. For instance, Shape Theory provides new versions of Heron's formula [113], and a nice way of addressing Lewis Carroll's pillow problem [5] of what is the probability that a triangle is obtuse, $\text{Prob}(\text{Obtuse})$ [54, 100, 112, 115].

In the above ways, for instance, (3, 2) and (3, 3) models already support a complex theory of Background Independence [21, 23, 37, 48, 73, 75, 91, 98, 97, 95, 104, 102, 101, 105, 108, 122, 123, 117, 126] and thus, as argued in Part I and [91, 94, 98, 108], an in many ways nontrivial realization of the Problem of Time [26, 27, 36, 46, 47, 48, 61, 70, 71, 83, 91, 98, 108]. These are foundational topics in General Relativistic and Quantum Gravitational Physics, for which the current treatise' detailed mastery of configuration space topology and geometry is a crucial and substantial first step. (3, 2) and (3, 3) moreover have distinct elements of the eventual (N, d) theory of inhomogeneities from those in Part II. In the case of (3, 2)'s features, these and (4, 1) features are first combined in Paper IV's treatment of (4, 2).

For 3 points in 2- d , the shape space is a 2-sphere S^2 [62] or some quotient thereof. In particular, this is the hemisphere \mathbb{RP}^2 [62] for the mirror image identified shapes, a lune covering 1/3 of the sphere for the indistinguishable shapes [78, 89], or an isosceles spherical triangle covering 1/6 of the shape sphere the mirror image identified *and* indistinguishable particle case [78, 89]. This last space is the *Leibniz space* [109] for 3 points in 2- d , $\mathfrak{Leib}_{\mathfrak{g}}(3, 2)$, alias Kendall's spherical blackboard [38, 43, 54, 62] from Shape Statistics (see additionally [92, 106]). The shape sphere for 3 points in 2- d is tessellated by each of the aforementioned isosceles and scalene spherical triangles [78]; these are two of the simpler tessellations of the sphere [34].

In the current treatise, we move from outlay of techniques and (3, 1) example in Part I to (3, 2) example. This is in many ways an alternative to Part II's increased complexity in going from (3, 1) to (4, 1) models. Triangles [28, 65, 44], the space of triangles [43, 54, 62, 72, 67, 69, 79, 89, 100, 108] and corresponding constellational viewpoints: the 3-body problem [9, 24, 41, 55, 59, 67, 69, 45, 74, 76, 77, 79, 89] in $d \geq 2$ are comparatively often studied relative to 4 points-or-particles on a line [78, 82, 89, 110].

We first consider topological shapes and topological graph shape spaces in Sec 2. These are simpler than for (4, 1) models.

We next give a Lagrangian-level metric treatment of triangular shapes and shape spaces in Secs 3, 5 and 4 respectively, and extend these to the Jacobian level in Secs 10 and 13.

Our Lagrangian-level treatment includes where collinearity, isoscelesness and equilaterality are located in the shape spaces. Medians, associated radii, and area and perimeter variables are also considered. We give furthermore a simple differential-geometric characterization of rightness on the shape sphere. These turn out to trace three cap-circles kissing each other in pairs, the cap interiors of which are the obtuse triangles. This is an example of the shapes-in-space to shape space correspondence tackling shapes-in-space flat geometry problems by mapping them to Differential Geometry problems in shape space. This far more general and widely applicable scheme is

moreover rendered particularly simple in the current case by both spheres and their caps having particularly simple Differential Geometry that is widely studied years before some people progress to study Differential Geometry. A more complicated example we consider is the maximal angle flow over the shape sphere [115].

The Jacobian-level treatment (Secs 13-14), on the other hand, introduces the concepts of tall and flat triangles, as separated by regular triangles: those whose base-side and median partial moments of inertia coincide. We also show here that regularity affords further characterization of equilateral triangles. We additionally give the Jacobian versions of congruence and similarity conditions, now involving a side and its median (or the ratio thereof, respectively) along with the ‘Swiss-army-knife’ angle between these. We furthermore solve for the triangle’s other sides and angles there-between in terms of such ‘Jacobi data’. We consider the forms taken by mergers and Jacobi-uniformity for triangles, locate these notions in each type of shape space, and finally count out the number of qualitatively distinct types of triangle afforded by inclusion of these Jacobi notions (and significant subsets). Secs 3 to 7’s levels of structure on shape space are furthermore supported by summary and inter-relation webs in Appendix B. Finding the cap-circles of rightness gives access to a very simple solution to Prob(Obtuse); tche value Shape Theory allots to this is moreover well-known from a priori distinct methods: $3/4$. Numerous variants of this problem are also formulated and solved: obtuse given isosceles, obtuse or acute conditioned on (or vice versa) the triangle being tall or flat, use of other critical angles in place of rightness, such as $2\pi/3$, below which triangles have a nontrivially-located Fermat point.

We also take advantage (Sec 15) of some ‘Hopf’ structures and techniques well-known in Dynamics and Theoretical Physics which however has largely yet to enter the Shape Statistics literature. From this point of view, the Jacobian notion of regularity is placed on the same footing as the Lagrangian and directly geometrical notions of collinearity and isoscelesness. All are mutually perpendicular planes, whose perpendiculars form an axis system in the halfway shape, equilateral shape and B directions. Hopf structures being bundle-theoretic gives a deep differential-geometric underpinning to considering the notions in each of these triples of notions as coprimary. In this way, Shape Theory provides a unified model of both geometrical and dynamical triangles. This provides differential-geometrical means by which a shape-theoretic unified study goes further than studies rooted on just one of traditional geometrical practise or 3-body problem considerations. There is moreover an analogous ‘generalized Hopf structure’ for arbitrary N -a-gons (Part IV), by which this unified approach has many fertile extensions (it also persists under at least some further choices of \mathfrak{g} [123]). Its partly involving Jacobian structure further motivates the current treatise’ inclusion of Jacobian considerations from the geometrical point of view as well as from the N -body problem point of view in which these were a priori considered to be more primary.

Sec 15 moreover provides novel interpretation of the Hopf quantities as ellipticity, anisoscelesness and area, showing what functions of the triangle’s sides and angles these correspond to. Furthermore, Hopf congruence and similarity conditions are now given, and the triangle’s sides and angles there-between are solved for in terms of ‘Hopf data’.

We next consider (Sec 16) Killing vectors for each $(3, 2)$ triangle space in Sec 16, including similarity Killing vectors for the scaled version. The axes produced by the Hopf map are useful in phrasing and interpreting this. Subsequently, in Sec 17, we interpret the space of spaces of representatives over the full \mathfrak{S} [79, 89], mirror-image-identified \mathfrak{S} [79, 89], indistinguishable \mathfrak{IS} , and Leibniz $\mathfrak{Leib}_{\mathfrak{S}}$ [38, 43] shape spaces. For the shape sphere $\mathfrak{S}(3, 2)$ this is the section of a principal fibre bundle – the Hopf fibre bundle – but in the other cases a general bundle is needed to define a section. This is because quotienting out by S_3 and/or \mathbb{Z}_2 creates a discrete version of the stratification effect, turning everywhere-equivalent fibres into in places inequivalent classes of bundle objects. We then identify Kendall’s spherical blackboard picture locating triangles on $\mathfrak{Leib}_{\mathfrak{S}}$ as a *section construct* which is a fortiori not at the level of fibre bundles but at the more broader level of general bundles or (with more tools available) of Sheaf Theory. We provide various sections which are globally valid over $\mathfrak{Leib}_{\mathfrak{S}}$ and others of interest which are however singular on one corner. On the other hand, fibre bundle sections will do for the $\mathfrak{S}(3, 2)$ sphere, though of course this problem admits no global section. In this case, we provide a section which only goes bad at the equilateral triangle poles. So there is a trade-off: $\mathfrak{Leib}_{\mathfrak{S}}(3, 2)$ is simpler in admitting a global section, but is less simple in that it is a general bundle rather than a fibre bundle. In Sec 18, we add – to the Dirac monopole’s realization in the \mathbb{R}^3 relational space, and Iwai’s monopole in the corresponding half-space – two new monopoles corresponding to \mathfrak{IS} , and $\mathfrak{Leib}_{\mathfrak{S}}$. See the Conclusion and [116] for yet further monopoles realized by further models of triangleand.

In the Conclusion (Sec 19), after summarizing Part III’s results, we end with firstly a $(3, 2)$ versus $(4, 1)$ comparison, i.e. Part III versus Part II. This reveals that complex features of $(4, 1)$ and $(3, 2)$ are largely distinct; Part IV’s $(4, 2)$ then combines these to create considerable further complexity than either (Paper IV). Secondly, we compare $(3, 2)$ and $(3, 3)$, noting that in particular, stratification plays a substantial further role for $(3, 3)$. In each case in which stratification appears in Part III, general bundles are required, and it looks to be further useful and powerful to model this with sheaf mathematics. In this way, $(3, 2)$ and especially $(3, 3)$ make for a useful testing ground for GR’s Background Independence, especially at the global level [108, 126, 128].

2 Topological level of structure

2.1 Topological shapes

Proposition 1 There are three topological types of 3-point configuration: Fig 1. These coincide with the 1- d case's 3 topological classes, albeit with the G class now more broadly interpreted.

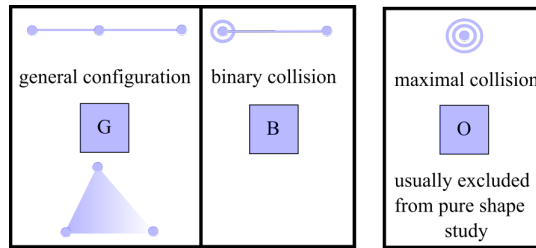


Figure 1: Topological classes of configurations for 3 particles in 1- d . Namely, the coincidence-or-collision-less generic configuration G, now covering both triangular and collinear metrically distinguished subcases, the binary coincidence-or-collisions B, and the maximal coincidence-or-collision O usually excluded from pure shape study.

Remark 1 As for $(3, 1)$, these are all partitions, unless labels or mirror image distinctions further discern between types of B.

Remark 2 Regardless of whether the points-or-particles are labelled or mirror image configurations are held to be distinct,

$$\#(G) = 1 \quad (1)$$

the generic rubber triangle (including collinear cases but excluding binary or maximal collisions) can be deformed from any labelling to any other. Thus topologically there is only one face or 2-cell. For a labelled triangle, regardless of whether mirror images are identified,

$$\#(B) = (\text{ways of leaving one particle out}) = 3 \quad (2)$$

The above represent two salient differences with the 1- d case.

2.2 Topological shape spaces

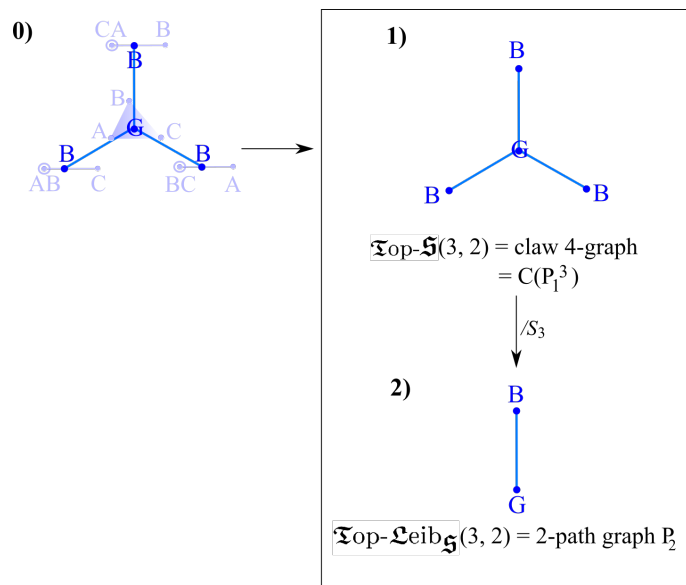


Figure 2: 0) Continuity method for determining the topology of $\mathfrak{Top}\text{-}\mathfrak{S}(3, 2)$ to be the claw graph alias 3-star (Appendix I.A); the 3 'talons' are labelled equally with B's (up to cluster labelling choice). 2- d gives no choice of regarding mirror images to be distinct at the topological level: the 'left' and 'right' topological shapes can be deformed into each other. Thus $\mathfrak{Top}\text{-}\mathfrak{S}(3, 2)$ is the same; $\mathfrak{Top}\text{-}\mathfrak{S}(3, 2)$ likewise coincide and are the 2-path graph depicted.

Proposition 1 For distinguishably labelled points-or-particles, the topological shape space is

$$\mathfrak{Top}\tilde{\mathfrak{S}}(3, 2) = \text{claw} = \mathfrak{Top}\mathfrak{S}(3, 2) : \quad (3)$$

the 4-vertex *claw graph* with equally labelled ‘talons’ as per Fig 2.1).

Proof Continuity considerations show that these shapes fit together in the manner of Fig 2.0), which closes up to form Fig 2.1). \square

Proposition 2 For indistinguishable points-or-particles,

$$\mathfrak{Top}\mathfrak{IS}(3, 2) = \frac{\mathfrak{Top}\mathfrak{S}(3, 2)}{S_3} = P_2 = \mathfrak{Top}\mathfrak{Leib}_{\mathfrak{S}}(3, 2) : \quad (4)$$

the 2-vertex path graph with distinct end-point labels as per Fig 2.2).

Remark 1 Acting on the topological shape space claw graph, identifying mirror images has no separate effect. Thus

$$S_3 \times \mathbb{Z}_2 \text{ acts as } D_3 \text{ (dihedral group of order 6) ,} \quad (5)$$

permitting us to rewrite the labelling and mirror image based definition (4) of the topological configuration in space as

$$\mathfrak{Top}\mathfrak{Leib}_{\mathfrak{S}}(3, 2) = \frac{\mathfrak{Top}\mathfrak{S}(3, 2)}{D_3} . \quad (6)$$

This is very natural in configuration space since the unlabelled claw graph has automorphism group D_3 .

2.3 The topological coincidence-or-collision structure

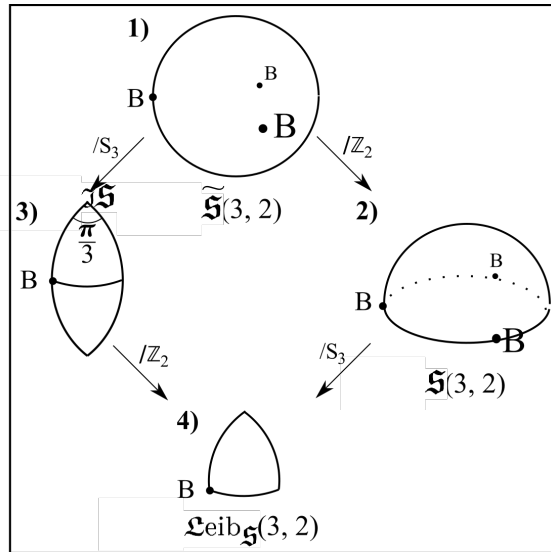


Figure 3: Topological-level configurations and configuration spaces for 3 particles in 2-d.

We include 5) and 6) for comparison and clarification, since these have on occasion been discussed as well. Since these correspond to a type of partial distinguishability [116], they do not feature further in the current treatise. While 6) and 3) both cover $1/6$ of the shape sphere, it suffices to observe that 6) involves 2 labellings of the equilateral triangle whereas 3) involves just one to establish that these are not equivalent. If the B’s in 1) are excised, one obtains the quite well-known ‘pair of pants’ [67, 69]. See [116] for a wider variety of modelling situations’ configuration spaces.

Among the normalizable shapes, this is just 3 points, corresponding to the 3 different labellings of the binary coincidence-or-collision, or just one point in the case in which these labellings are indistinguishable (Fig 3).

3 Triangular shapes at the Lagrangian metric level.

3.1 Metric shapes of triangle that are characterized by symmetries in space

At this point, much material familiar from elementary Flat Geometry is encountered. This is since triangles have been much more studied than 3 or 4 points on a line. Benefits from reconcile this material with how we have been developing Shape Theory so far are considerable and mutual as regards a number of further insights, variables and techniques.

Let us first recollect which variety of notions of triangles can be envisaged in terms of symmetries in space

Qualitative type 1) The *equilateral triangle* E is the most symmetric triangle in space; it possesses a D_3 symmetry (order 6).

Qualitative type 2) *Isosceles triangles* I are the next most symmetric in space, possessing \mathbb{Z}_2 reflection symmetry (order 2); note that this characterization of isosceles includes B.

Qualitative type 3) *Scalene triangles* S have no element of symmetry in space at all.

3.2 Metric shapes of triangle that are characterized by relative separations

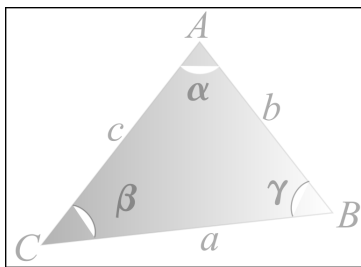


Figure 4: Cyclic notation for a triangle's vertices, sides and angles. It is also useful for us to denote a, b, c by $s_i, i = 1$ to 3.

Qualitative type 0) A zero edge, $a = 0$ say (see Fig 4 for the triangle notation in use) returns the binary coincidence-or-collision shape B which already had topological-level meaning.

At the metric level this is moreover now accompanied by basic and familiar and intuitive notions of non-coincident vertex triangles, 1) to 3) below, of which admit a relative-separation characterization. For triangles, relative separations reduce entirely to edges rather than diagonals. All in all, we consider here the notion of edge-uniformity.

Qualitative type 1) Maximal edge uniformity consists of all three edges being equal in length, $a = b = c$, giving the equilateral triangle E.

Qualitative type 2) The minimal element of edge uniformity is for two edges to be equal in length, $a \neq b = c$ say, giving the isosceles triangles, I.

Qualitative type 3) Finally, if no element of edge uniformity is present, $a \neq b \neq c$, one has a scalene triangle, S.

Remark 2 Uniformity is nontrivially realized by E. Note that one has no notion of linearly-ordered separations in non-degenerately $2-d$ configurations. However for $N = 3$, there is still a notion of adjacent separations: all separations are adjacent and without having to specify any ordering. We can thus use separations to qualify maximum uniformity.

Remark 3 We can view E's features as arising from two clusters being isosceles (this implies that the third is as well).

$$E = I \cap I = I \cap I \cap I . \tag{7}$$

Remark 4 E also plays the role of most uniform state $U(3, 2)$ for triangleand:

$$U(3, 2) = E . \tag{8}$$

Remark 5 These shapes have, respectively, the symmetry groups S_2 and S_3 acting upon

$$(\text{separation space}) = (\text{side space}) . \tag{9}$$

Qualitative type 4) The relative separation characterization of collinearity is that one separation is the sum of the other two, say

$$a = b + c . \tag{10}$$

Remark 6 For all (3, 2) shapes, moreover,

$$a \leq b + c \text{ and cycles : the } \textit{triangle inequality} . \tag{11}$$

Collinear shapes C are then the only shapes that saturate this, returning (10). The normalized such both have the same amount of diversity as the mirror image identified (3, 1) shapes of Part I. Thus these include B and U(3, 1).

Remark 7 This U(3, 1) moreover possesses an element of relative separation uniformity, by which it is a subcase of isoscelesness I according to the current section's criterion. B can moreover also be viewed as another limiting case of I; see Sec 3.6 for further comments. Overall,

$$I \cap C = \{B, U(3, 1)\} . \tag{12}$$

Definition 1 The *perimeter* of a triangle is

$$S := a + b + c ; \tag{13}$$

the *semi-perimeter* is then

$$s := \frac{S}{2} . \tag{14}$$

3.3 Metric shapes of triangle that are characterized by relative angles

Qualitative types 1) to 3) admit yet another standard characterization in terms of uniformity of relative angles (which, for triangles, are between edges).

Qualitative type 1) The equilateral triangle E has maximal angle uniformity: all three angles are equal (*equiangularity* condition):

$$\alpha = \beta = \gamma = \frac{\pi}{3} . \tag{15}$$

Qualitative type 2) The isosceles triangles I have the minimal angle uniformity: two angles equal (let us refer to this as 'isoangularity'): $\alpha \neq \beta = \gamma$, say.

Qualitative type 3) Scalene triangles S have no element of angle uniformity: $\alpha \neq \beta \neq \gamma$.

Remark 1 Isoscelesness \Leftrightarrow 'isoangularity' and equilaterality \Leftrightarrow equiangularity, by which each of these notions can be thought of either in pure-ratio terms or in pure-angle terms.

Qualitative type 4) The relative angle manifestation of collinearity¹ is that one of the relative angles is 0 and another is π . This includes U(3, 1) but now not B, since no relative angles are defined within B, so one is now really characterizing C¹ rather than C.

Remark 2 Secs 3.1-3's criteria only agree if degenerate triangles – C including B and U(3, 1) – are excluded.

3.4 Summary figure so far

See Fig 5.

3.5 A first few standard congruence and similarity conditions for triangles

For later comparison and use in proofs, we remind the reader of the usual congruence and similarity conditions for triangles.

Congruence condition 1) s-s-s: each of a pair of triangles shares the same three side lengths.

Congruence condition 2) s- α -s: each of a pair of triangles shares 2 side lengths and angle included between these.

¹ $N = 3$ supports only the overlapping index case of Remark 7 of Sec I.6.3, so the entirety of its parallelism equations are in this case collinearity equations. It takes Part IV's consideration of quadrilaterals to realize parallel but not collinear configurations: trapeziums and parallelograms. The corresponding ϵ -tolerant collinearity inequalities have been considered by Kendall [62].

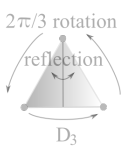
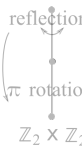
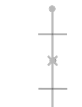
	E	I	S	U(3,1)	B	C ²
Symmetry in space						
Separation uniformity structure			—		—	—
Angular uniformity structure			—	—	—	—

Figure 5: Lagrangian properties of equilateral E, isosceles I, and scalene S triangles, alongside binary coincidence-or-collision B, collinear-uniform U(3, 1), and other collinear C² shapes.

Congruence condition 3) α -s- α : each of a pair of triangles shares two angles and the side included between these.

Congruence condition 4) α - α -s: each of a pair of triangles shares two angles and a non-included side.

Similarity condition 1) r-r: each of a pair of triangles shares two side-ratios.

Similarity conditions 2) and 3) r- α : each of a pair of triangles shares a side ratio and angle, whether included or not.

Similarity condition 4) α - α each of a pair of triangles shares two angles (and thus all three, by angles in a triangle adding up to π).

Remark 1 Congruence conditions are Euclidean-relational, whereas similarity conditions are similarity-relational. The above and subsequent enumeration of congruence and similarity conditions match upon quotienting scale out of the former. Moreover, all of the above conditions are Lagrangian, whereas the current Part III shall furthermore point to further shape-theoretically useful *Jacobian* characterizations of congruence and similarity.

Remark 2 In the current treatise's context, we view the above conditions as *well-posed data sets*, from which the entirety of the features of a given geometrical conception of a triangle can be determined. In particular, congruency conditions are data to fully solve a Euclidean triangle, whereas similarity conditions are data to fully solve a triangle in the sense of similarity geometry.² These equations for which these are data sets are moreover algebraic, so well-posedness reduces to well-determinedness. This has a counting element to it: 3 parts to a congruency condition versus 2 to a similarity condition; this counting corresponds to the dimension of the corresponding configuration space: $\dim(\mathcal{R}(3,2)) = 3$ and $\dim(\mathfrak{S}(3,2)) = 2$. Such counting need not however suffice to tie down existence or uniqueness. For instance, not all triples of lengths constitute s-s-s data since some violate the triangle inequality. Also, not all triples of angles correspond to a Euclidean triangle; they must sum to π in order to do so. This then gives a dependency equation by which α - α - α reduces to α - α , which cannot uniquely specify Euclidean triangles out of not restricting size. To relate to general relativist and physicist readers' experiences, well-posedness for triangles is indeed analogous to well-posedness for physical laws, though, these in general being modelled by PDEs, there are further PDE-specific aspects to well-posedness there. More specifically well-posedness for instantaneous laws such as Gauss' Law of electrostatics or the GR initial-value problem is furtherly analogous: configurational problems, for which far from all functions solve these problems due to their constraints.³

²[123] extends this to equiareal and affine notions of triangle.

³Conversely, for readers whose background is geometry, topology, shape theory, or its applications, Gauss's law is here cast in a gauge in which it is a constraint, whereas data for the GR initial-value problem need satisfy the Hamiltonian and momentum constraints: the time-time and time-space components of the Einstein field equations. 'Constraint' is here characterized as an equation which is less than the habitual second-order in its time derivatives.

Remark 3 The motivation for the current section is then clear: we will be providing *relationally adapted* well-determined data for similarity shape and Euclidean shape-and-scale triangles, and this will be in the form of new congruence and similarity conditions. (Their novelty is rather probably at the level of these being *motivated* as the primary congruence and similarity conditions from the Jacobi 3-body, Hopf bundle and Kendall Shape Theory points of view.) Secs 5.1, 5.3, 10.3 and 15.10 continue this discussion after more structure has been laid out.

3.6 Labelling and mirror image distinctions

Remark 1 scalene, isosceles and equilateral triangles admit 6, 3 and 1 labellings respectively.

Remark 2 Non-collinear triangles admit 2 choices of orientation (*clockwise* and *anticlockwise*), whereas collinear ones admit just a single undifferentiated orientation. For instance, one can distinguish between 2 choices of orientation for the equilateral triangle (denoted by E and \bar{E} in Paper III).

Remark 3 The effect of labelling on collinear shapes C is as per Part I. All C shapes are immune to the clockwise-anticlockwise distinction which doubles the number of all non-degenerate (non-collinear) triangles.

Remark 4 Isosceles triangles' label choice can be thought of as picking a base pair of vertices.

Remark 5 Triangles with mirror image distinction support a meaningful difference between *left-leaning* and *right-leaning* triangles, with isosceles triangles separating these (Fig 6.1).

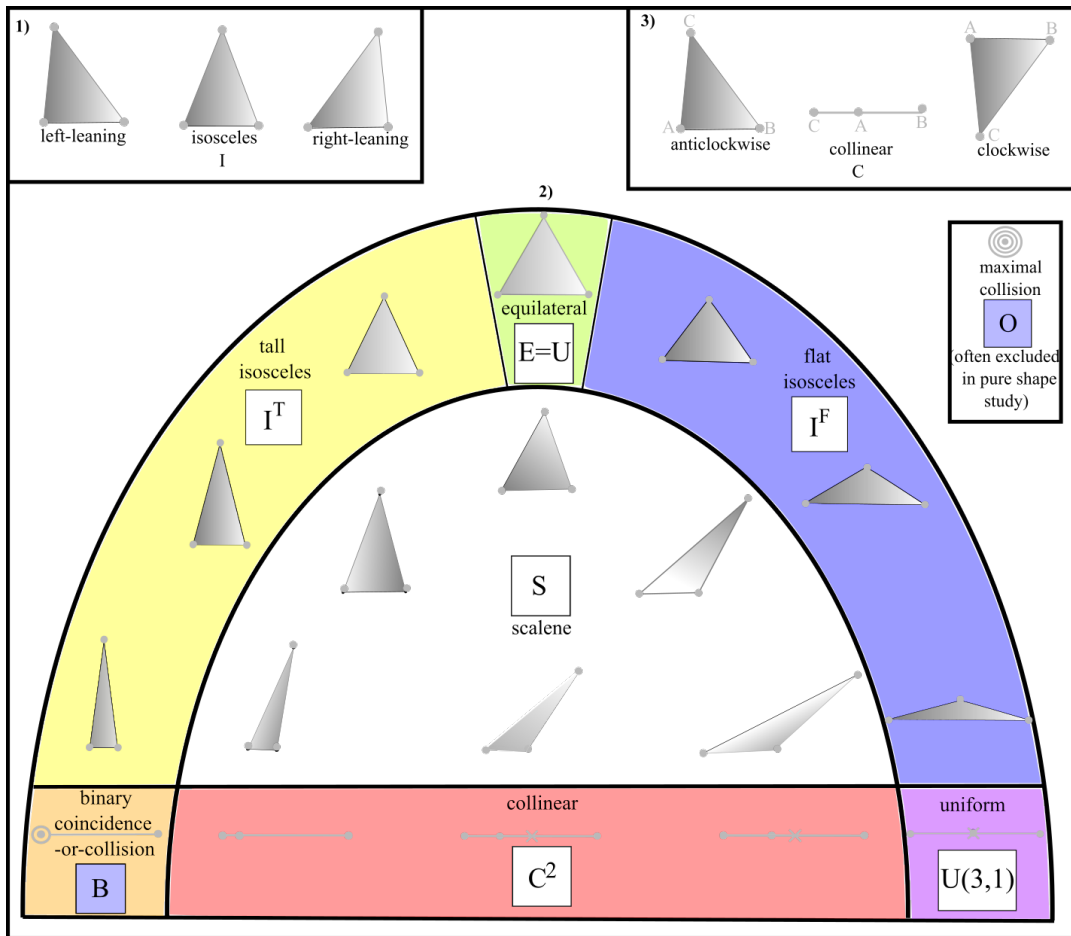


Figure 6: 1) Isosceles triangles separate left-leaning and right-leaning triangles.

2) As Sec 4 will characterize further, isoscelesness is split by the equilateral triangle. The lower corners where isoscelesness I meets collinearity C are the B and U(3, 1) shapes. The interior of this so-far heuristic wedge of notions of triangles is itself made up of the generic scalene triangles. For now, this is a shape-space-topological-manifold-level diagram of the metric types of shape; an accurate metric counterpart of it is set up in the next Section.

3) Furthermore, for labelled triangles, collinear configurations separate clockwise and anticlockwise labelled triangles.

3.7 Splits so far of G, C and I notions of shape

In support of Fig 6.3, firstly the collinear configurations have been split to the exclusion of the topologically distinct binary coincidence-or-collision B:

$$C = C^1 \amalg B, \quad (16)$$

followed by the further split

$$C^1 = C^2 \amalg U(3, 1). \quad (17)$$

Also, the topological-level generic configuration G has been decomposed according to

$$G = I \amalg S \amalg C^1, \quad (18)$$

for I isosceles and S scalene. Finally I has been furthermore decomposed into

$$I = I^T \amalg E \amalg I^F. \quad (19)$$

The T and F superscripts here refer to tall and flat triangles, a notion we further detail in Sec 10. For now, we note that for isosceles triangles, tallness and flatness are relative to the equilateral shape, which splits the isosceles part of $\mathfrak{L}eib_{\mathfrak{G}}(3, 2)$'s perimeter into its I^T and I^F parts.

3.8 Lagrangian angle uniformity

Remark 1 For triangleland, the element of angle-uniformity is the same as the element of separation-uniformity, i.e. isoangularity – two angles equal – is equivalent to isoscelesness: two sides equal.

Remark 2 Moreover the presence of two elements of angle uniformity imposes a third: the equiangularity characterization of equilaterality.

Remark 3 Isoangularity and equiangularity involve, respectively, the groups S_2 and S_3 acting on angle space.

Remark 4 For triangles, the groups acting on space, relative separations and relative angles are moreover isomorphic in each case.

4 Shape spaces of triangles at the Lagrangian metric level

The previous section's metric-level observations are accounted for by the following topological shape space structure.

Proposition 1 The shape space topology topological features are as per Fig 3 and these and the Lagrangian-level metric features obtained by the continuity method, as per Fig 7.

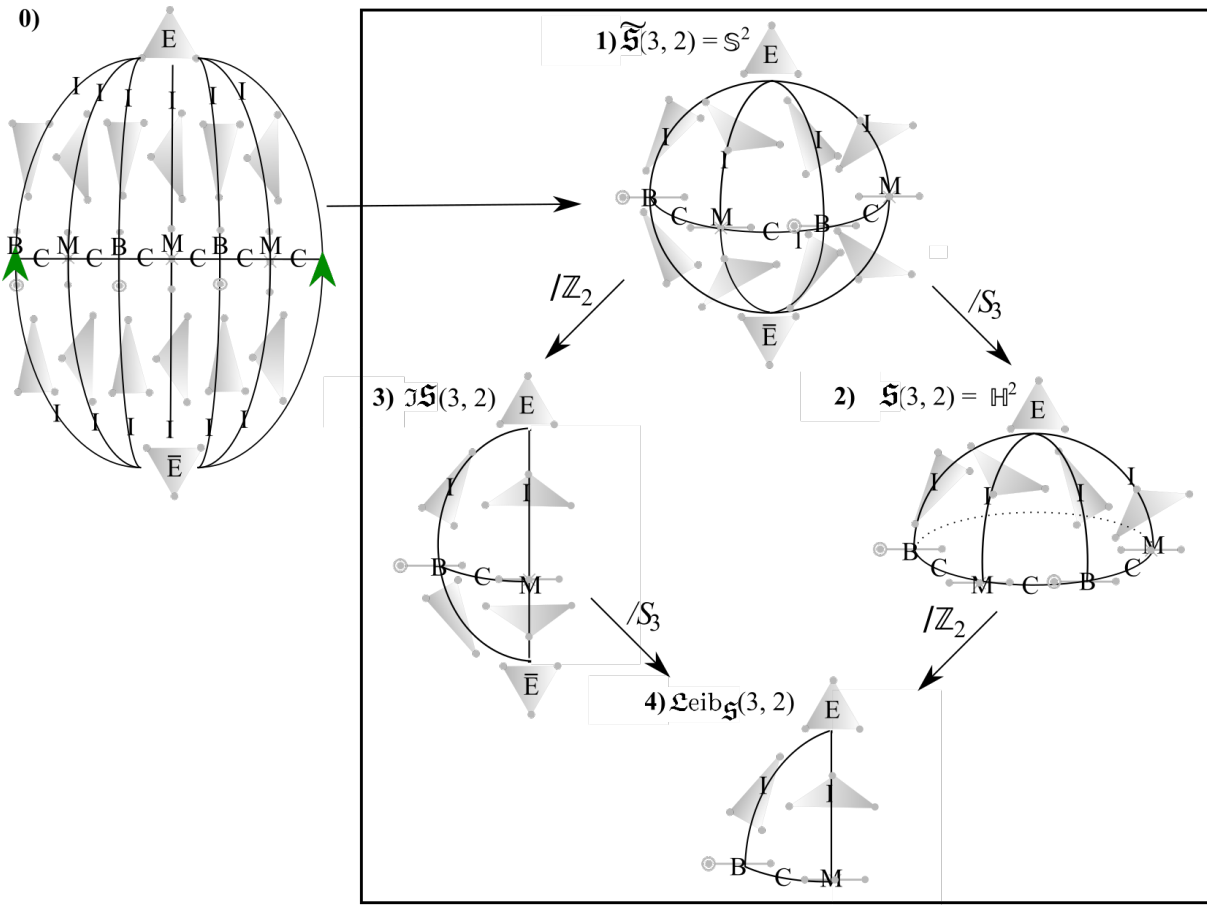


Figure 7: 0) The continuity method gives the shape sphere 1). This Figure is moreover drawn to be metrically correct with respect to the naturally induced spherical metric, with azimuthal and polar angles as given by eqs (I.171-172) and Fig I.18.a). Isoscelesness and collinearity decorate this as a 6-segmented orange cut in half perpendicular to its segments.

2) Applying mirror image identification kills off one hemisphere while preserving the equator, thus giving a hemisphere with edge. [This is often misinterpreted as $\mathbb{R}P^2$ in the literature, out of not detailedly investigating the shapes in question and which action in configuration space the mirror image \mathbb{Z}_2 symmetry in space corresponds to.]

3) Applying label indistinguishability instead leaves one with a lune of width $\frac{\pi}{3}$.

4) Applying both at once leaves one with a the Leibniz space demilune of width $\frac{\pi}{3}$: *Kendall's spherical blackboard* [43].

4.1 Axis systems

We point to the following two axis systems, for now postponing naming the third mutually perpendicular axis until Sec 6.1.

Axis System 1) BE: with B as principal axis and E as secondary axis. As we shall see in Sec 6, this is natural in Jacobi coordinates and thus commonly arises as an adapted coordinate system in 3-body problems. The simplest spherical angle interpretations are for the corresponding angles, denoted by Θ, Φ

Axis System 2) EB: with E as principal axis and B as secondary axis. This is more geometrically natural and also accords axis principality to the democratic concept. The price to pay is that its spherical angles, denoted $\tilde{\Theta}, \tilde{\Phi}$, has a more complicated in interpretation in spatial (formulae in terms of \underline{q}^I). These are of course however related to Θ and Φ by basic spherical trigonometry formulae [89].

Remark 1 It turns out to often be useful to check whether one has remembered to pass from tilded to untilded variables. Failure to emphasize this point can cause arguments to sound wrong. This is an important point to make in an introductory account, as it avoids much confusion including obscuring what would otherwise be encouraging intuitions. This lacuna is moreover compounded by an axis switch usually being irrelevant in geometrical problems, but none the less making a huge interpretational difference in passing between shape space and shapes-realized-in-physical-space, since the axes now mean very different things: a binary collision to an equilateral triangle. For axis

switches usually being irrelevant in practise means that one may not spot that an undeclared axis switch is why one's interpretation of a presentation's words do not match one's intuitions using what *one thinks* the paper or seminar's notation is referring to...

Example 1 For instance, the equator of collinearity C corresponds to $\Phi = 0$ or π , or, in tilded coordinates, to $\tilde{\Theta} = \pi/2$.

Remark 2 On the other hand, one of the bimeridians of isoscelesness I is at $\Phi = \frac{\pi}{2}$ or $\frac{3\pi}{2}$, or, in tilded coordinates, at $\tilde{\Phi} = 0$ or π .

Remark 3 We postpone physical interpretations of Φ , Θ to Sec 6.

4.2 Coincidence, collinearity, symmetry and uniformity structures over the shape sphere.

Proposition 1 Triangleland's *metric-level coincidence-or-collision structure* – consult Fig 56.a) – consists of 3 points at $\frac{2\pi}{3}$ to each other on the equator: the B's.

Proposition 2 Triangleland's *collinearity structure* – Fig 56.d) – is a purely metric-level concept, and consists of the equator of collinearity C.

Remark 1 This realizes $\mathfrak{S}(3, 1)$, as another example of the Shape-Theoretic Aufbau Principle. The current model's second spatial dimension automatically identifies mirror image collinear configurations, explaining this realization (rather than that of $\mathfrak{S}(3, 1)$). This contains a total of six alternating equally spaced out B and M configurations.

Remark 2 C separates northern and southern hemispheres of clockwise and anticlockwise triangles.

Proposition 3 The (Lagrangian) symmetric configurations are distributed as follows.

The isosceles configurations I form bimeridian great circles at $\frac{\pi}{3}$ to each other. Each clustering choice of I separates the triangleland sphere into hemispheres of corresponding right-leaning and left-leaning triangles with respect to the same clustering choice.

These intersect at the poles (in the new coordinates) which are the equilateral triangle shapes E.

This observation, and computation of Part II's symmetry element counting function over the shape sphere, establishes the following.

Proposition 4 E (and \bar{E} when distinct) maximizes

- i) symmetry in space.
- ii) separation uniformity.
- iii) angle uniformity.

Remark 3 ii) and iii) make use of Part II's separation and angle-uniformity counting functions respectively.

Remark 4 See Figures 58 and 59 for each level of structure's full topological and metric structure over shape space respectively. These are arrived at by solving the coincidence equations, collinearity equations redux of the parallelism equations, symmetry in space equations, separation uniformity equations, and angle uniformity equations respectively. In particular,

i) the symmetry structure is topologically the disc with five punctures and metrically the edges of the 'orange of 3 segments' tessellation.

ii) The Lagrangian separation uniformity structure is topologically and metrically the symmetry structure with the collision structure removed. This is because isosceles triangles have two sides of the same length – an element of uniformity – excepting the coincidence-or-collision points in shape spaces, since we defined uniformity to not include features already implied by coincidences-or-collisions.

iii) The Lagrangian angle uniformity structure coincides with ii). This is by Remark 1 of Sec 3.3's basic observation that isoscelesness and equilaterality can be reformulated as 'isoangularity' and equiangularity respectively.

Remark 5 For triangleland, the pure-ratio structure coincides with the uniformity structure: Fig 56.c).

Remark 6 The pure-angle collinearity–perpendicularity structure is the 3 circles linking at the B's cut in half (Fig 56.d); the M are not distinguished points here.

Remark 7 The full pure-angle structure is the 3 circles linking at the B's cut in half and the I meridians (Fig 56.j), since I is an angular as well as side-ratio concept.

4.3 Mirror image identified counterpart

The figure looks the same from the bird's eye view but lower hemisphere part is of course now missing. This leads to the topological differences of row 2 of Fig 58 relative to row 1 (see Appendix A for how this computes out).

4.4 Indistinguishable shape space and Leibniz space counterparts

Indistinguishable shape space is a $\frac{\pi}{3}$ lune with corners E and \bar{E} and edges I^T and I^F .

Proposition 1 The coincidence-or-collision, collinearity, symmetry and uniformity structures at the level of indistinguishable space are as per Fig 55. Topologically, these are as per row 3 of Fig 58.

Leibniz space is an isosceles spherical triangle with corners E, B, M and edges I^T , I^F and C.

Proposition 2 The collision, collinearity, symmetry and uniformity structures at the level of Leibniz space are as per Fig 54. Topologically, these are as per row 4 of Fig 58.

Remark 1 As regards levels of structure on $\mathfrak{L}eib_5(3, 2)$ and $\mathfrak{J}5(3, 2)$, see now Fig 54 and 55 in place of Fig 56.

4.5 Count of qualitative types so far

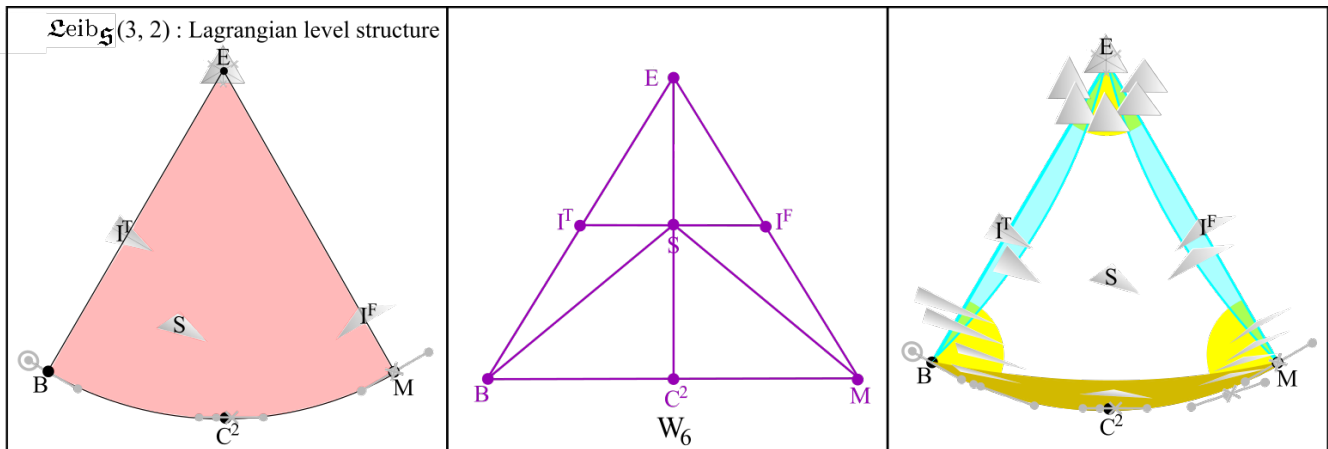


Figure 8: Shape-space-metric-level detail of $\mathfrak{L}eib_5(3, 2)$ for shapes-in-space at the metric Lagrangian separation level.

Remark 1 At the level of Lagrangian separations, there are $V = 3$ types of special points: E, B and $U(3, 1)$.

Remark 2 These are also $E = 3$ types of edges C^2 , I^T and I^F .

Remark 3 There is just the one type of face ($F = 1$): the generic non-collinear scalene triangles, S.

Remark 4 These can be located, and counted off, as per Fig 8.a).

Remark 5 Thus the number of qualitative types in Leibniz space is

$$Q := V + E + F = 3 + 3 + 1 = 7 . \quad (20)$$

Remark 6 The adjacency graph Fig 8.b), $V(\text{Adj}) = Q = 7$ and $E(\text{Adj}) = 12$, and is moreover the 6-wheel W_6 .

Remark 7 See Figs 54–56 for an end-summary of special arcs and special points among the (3, 2) shapes. See Fig 9 for further counts of qualitative types in the four (3, 2) shape spaces, as exhibited in Fig 37 in the case of Leibniz space.

shape space	$V = G $	$E = e(G)$	F	χ	p	Q	Q_{approx}	Q_{total}	Q_{Approx}	Q_{Total}
$\mathfrak{L}eib\mathfrak{S}(4, 1)$	3	3	1	1	3	7	12	18	19	25
$\mathfrak{I}\mathfrak{S}(4, 1)$	4	5	2	1	4	11	22	34	33	45
$\mathfrak{S}(4, 1)$	7	12	6	1	6	25	60	96	85	121
$\mathfrak{S}(4, 1)$	8	18	12	2	0	38	108	180	146	218

Figure 9: Number of qualitative types with Lagrangian separation decor. Note that the first rows the current Figure and of Fig II.18 are the same due to underlying isomorphic graphs, and that the same applies again to their second rows.

5 Right, acute and obtuse triangles

5.1 Overview

Qualitative type 5) The relative angle notion of perpendicularity supports the notion of *right-angled triangles*, \perp .⁴

Qualitative type 6) Moreover, if a triangle contains an angle which is larger than the right angle, it is an *obtuse triangle*, \searrow .

Qualitative type 7) Finally if none of a triangle's angles are as large as a right angle, it is an *acute triangle*, \angle .

Remark 1 Obtuse comes in three labelling choices, but acute is a labelling-independent concept.

Remark 2 For a right-angled triangle, the side opposite the right angle, say a , is known as the *hypotenuse*, and the other two sides as the *legs*. Pythagoras' Theorem applies:

$$a^2 = b^2 + c^2 . \quad (21)$$

Given one of the non-right angles therein, say α the legs are designated *opposite* and *adjacent* relative to it (Fig 10.a). Trigonometric definitions ensue

$$\sin \alpha := \frac{\text{opposite}}{\text{hypotenuse}} , \quad \cos \alpha := \frac{\text{adjacent}}{\text{hypotenuse}} , \quad \tan \alpha := \frac{\text{opposite}}{\text{adjacent}} ; \quad (22)$$

by Pythagoras,

$$\sin^2 \alpha + \cos^2 \alpha = 1 . \quad (23)$$

Remark 2 For the general triangle, Pythagoras generalizes to the *cosine rule*

$$a^2 = b^2 + c^2 - 2bc \cos \alpha ; \quad (24)$$

One also has the *sine rule*

$$\frac{a}{\sin \alpha} = \frac{b}{\sin \beta} = \frac{c}{\sin \gamma} . \quad (25)$$

Remark 3 Given s-s-s, the perimeter S follows immediately. Given s- α -s, the cosine rule supplies the final side, thus giving another formula for S .

Remark 4 Right angles involve picking a hypotenuse pair of vertices, now with mirror image distinction (except for the isosceles right triangle).

Remark 5 The right isosceles triangle, detailed in Fig 10.b), will play a significant role in this treatise.

⁴As all relative separations are edges for triangles, these right angles are between edges. On the other hand, Part IV's quadrilaterals will also have to contend with edge-diagonal and diagonal-diagonal perpendicularities.

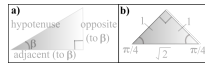


Figure 10: a) Notation for right-angled triangles. b) The right isosceles triangle I^\perp . Its symmetry, separation uniformity and angular uniformity are as for any other isosceles triangle.

5.2 Right angled triangle specific congruence and similarity conditions

Congruence condition 5) \perp -h-s: two right angled triangles with shared-length hypotenuses and another pair of equal side-lengths.

Similarity condition 5) \perp -r: two right angled triangles with a shared hypotenuse-to-side ratio.

Remark 2 Qualitative types 5) to 7) give splits for, firstly, the scalene triangles (see also Fig 11),

$$S = \angle \coprod \perp \coprod \setminus , \quad (26)$$

and, secondly, for the isosceles triangles,

$$I = I^\angle \coprod I^\perp \coprod I^\setminus . \quad (27)$$

(see Fig 10 for I^\perp). This split moreover affects exclusively the flat isosceles triangles –

$$I^F = I^{F\angle} \coprod I^\perp \coprod I^\setminus \quad (28)$$

– since the equilateral triangle and all the tall isosceles triangles are acute.

Remark 3 \perp itself is further split into

$$\perp = \perp^1 \coprod I^\perp . \quad (29)$$

The furthermore degenerate case B is arbitrarily close to all of obtuse, right and acute triangles, though there is a sense in which is the 2-right-angle limit of the arbitrarily tall isosceles triangle, by which it belongs to the right and isosceles arcs.

Remark 4 The degenerate shapes C^1 can moreover be adjoined to the obtuse triangles to make a slightly more general notion of obtuse.

Remark 5 Let us also comment on \perp -h-s and \perp -r only applying to some triangles: right-angled ones, which are moreover not generic. This is of limited value when the aim is to treat the entirety of the triangles on a common footing, as is the case in Shape Theory through setting up the (scale-and-)shape space.

5.3 On which congruence and similarity conditions are complete as regards degenerate configurations

Remark 1 This is a good point at which to assess which of the remaining, generically applicable standard congruence and similarity conditions extend well-determinedly to include the non-generic degenerate cases. Namely, the collinear C and binary coincidence-or-collision B normalizable shapes, and, in the Euclidean case, the maximal collision O as well. This is motivated by most pure-shape considerations including the former, and most shape-and-scale considerations additionally including the latter.

Remark 2 Let us start by considering C.

Congruence condition 1) s-s-s's triangle inequality is now saturated, so s-s data is fully determining.

Congruence condition 2) s- α -s data functions as usual, for a taking a collinear value (i.e. 0 or π).

Congruence conditions 3) and 4) α -s- α and α - α -s data have both their a's take collinear values, but their remaining s information does not suffice to uniquely determine the shape-and-scale.

Similarity condition 1) r-r inherits a dependency from the saturated triangle inequality, so r data is fully determining.

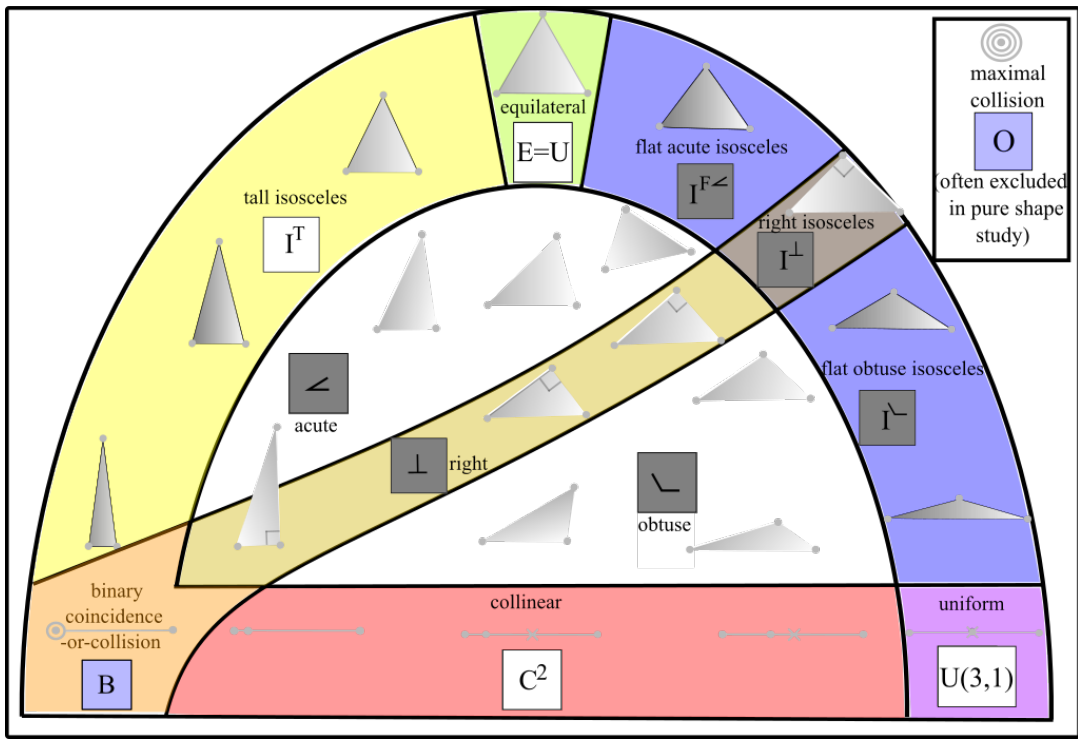


Figure 11: Shape-space-topological-manifold-level diagram of the shapes-in-space metric Lagrangian level decor, now updated to include rightness and the ensuing acute-to-obtuse distinction.

Similarity conditions 2) and 3) r - α functions as usual, for a taking a collinear value.

Similarity condition 4) α - α takes collinear values but, being bereft of length ratio information, does not uniquely determine the configuration.

So s - s - s remains operational subject to an interpretational caveat, whereas s - α - s carries over *without comment*. r - r and r - α then follow suit.

Remark 3 We next comment on B.

Congruence condition 1) s - s - s here reduces to s - s -0 which is determined by a single s datum.

Congruence condition 2) s - α - s reduces to α 's collinear value and 1 nonzero side datum (the nonzero s 's are equal).

Congruence conditions 3) and 4) α - s - α and α - α - s break down as only 1 relative angle is defined.

Similarity condition 1) r - r reduces here to a single finite nonzero ratio $r = 1$.

Similarity condition 2) r - α included reduces to $r = 1$ and $\alpha = 0$.

Similarity condition 3) r - α not included reduces to $r = 0$ or ∞ and $\alpha = 0$.

Similarity condition 4) α - α breaks down as only 1 relative angle is defined.

Thus, by somewhat different arguments, s - α - s and r - α (now specifically included) are the most desirable for the extension, whereas s - s - s and r - r also pass muster with interpretational caveats. This suffices to crown s - α - s as the conventional congruence condition that is most suitable to the entirety of the shape space of triangles.

Remark 4 For the shape-and-scale case, we also need consider the maximal coincidence-or-collision O.

Congruence condition 1) s - s - s here reduces to 0-0-0.

Congruence conditions 2) to 4) all break down since now no relative angles are defined.

Thus for Shape-and-Scale Theory, it is s-s-s which extends to the final point. One interpretation of this is to make do with s-s-s for all shapes; another is to view s-s-s as a valid shape-and-scale space coordinate chart to approach O, whereas s- α -s could be in use everywhere else.

6 Medians and further Cevian structure

Definition 1 The *medians* of a triangle are as per 12.a)-b). It will also be useful for us to use m_i , $i = 1$ to 3 to denote m_a, m_b, m_c .

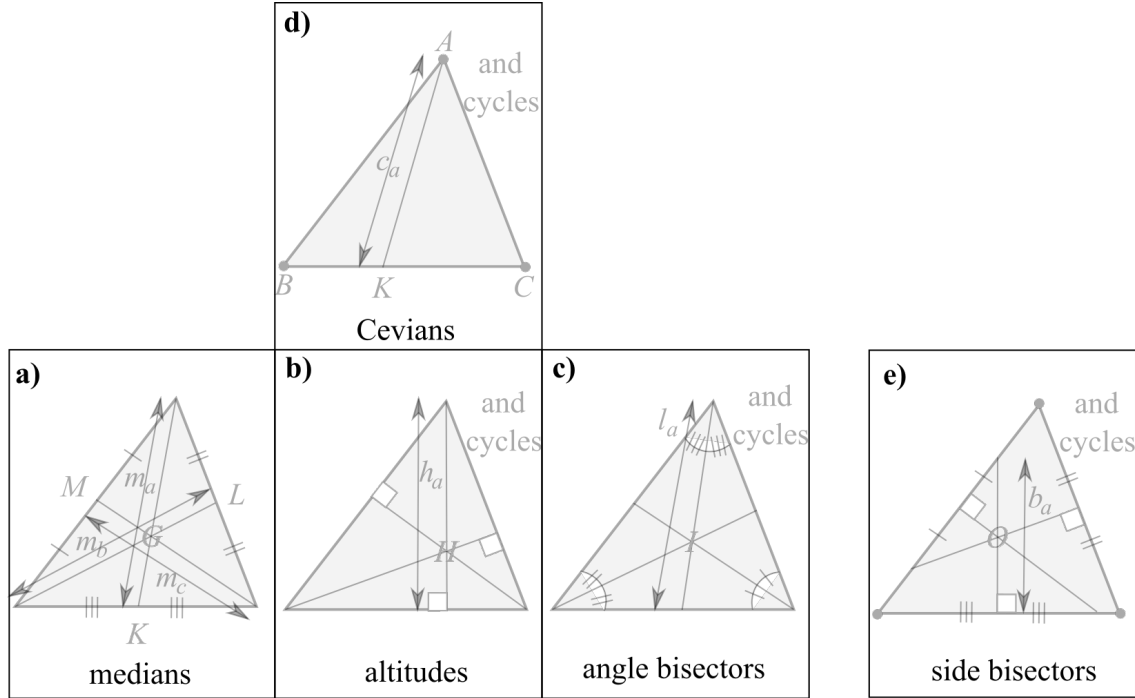


Figure 12: a) Definition of the medians; these concur at the *centroid*, alias *centre of mass*, G . b) Definition of the altitudes, which intersect at the *orthocentre* H . c) The internal angle bisectors h_a from each vertex to its opposite side; these intersect at the *incentre* I . d) General Cevian set-up, of which medians and internal angle bisectors are a particular subcase. e) The sides' perpendicular bisectors; note that these are not in general Cevians, via their not going through the vertex opposite the side; these moreover intersect at the *circumcentre* O .

Remark 1 By treating the sides and the medians on an equal footing – which we motivate in Secs (11.3) and (10.2) – we have more definitions (or at least accordances of equal significance) than in hitherto standard treatments of triangles, starting with the following.

Definition 2 The *medimeter* M is

$$M := m_a + m_b + m_c = \sum_i m_i, \quad (30)$$

whereas the *semi-medimeter* is

$$s = \frac{M}{2}. \quad (31)$$

Remark 2 The perimeter and medimeter can furthermore be viewed as first moments of sides and medians respectively. The second moments counterparts of each of these also enter the current treatise, as follows.

Definition 4 The segment

$$c_a := AK \quad (32)$$

from a triangle's vertex A to a point K on the opposite side BC is known as a *Cevian* (pronounced 'Chevian', and depicted in Fig 12.d). We also denote c_a, c_b and c_c collectively by c_i .

Remark 3 This is a more general concept than a median; further examples of Cevian are Fig 12.b)'s *altitudes* h_i and Fig 12.c)'s *internal angle bisectors* l_i .

<i>first moment of sides</i> alias <i>perimeter</i> , <i>semi-perimeter</i> <i>arithmetic mean of sides</i>	$S := \sum_i s_i$ P $s := \frac{S}{2} = \frac{1}{2} \sum_i s_i$ $S_A := \frac{S}{3} = \frac{1}{3} \sum_i s_i$	<i>first moment of medians</i> alias <i>medimeter</i> <i>semi-medimeter</i> <i>arithmetic mean of medians</i>	$M := \sum_i m_i$ $m := \frac{M}{2} = \frac{1}{2} \sum_i m_i$ $M_A := \frac{M}{3} = \frac{1}{3} \sum_i m_i$
<i>root sum of squares of sides</i> <i>quadratic mean of sides</i>	$S_{RSS} := \sqrt{\sum_i s_i^2}$ $S_Q := \frac{S_{RMS}}{\sqrt{3}} = \sqrt{\frac{\sum_i s_i^2}{3}}$	<i>root sum of squares of medians</i> <i>root mean square average of medians</i>	$M_{RSS} := \sqrt{\sum_i m_i^2}$ $M_Q := \frac{M_{RMS}}{\sqrt{3}} = \sqrt{\frac{\sum_i m_i^2}{3}}$
<i>geometric mean of sides</i>	$S_G := \left(\prod_{i=1} s_i \right)^{1/3}$	<i>geometric mean of medians</i>	$M_G := \left(\prod_{i=1} m_i \right)^{1/3}$

Figure 13: Three pairs of variables, with one inter-relation and various useful and conceptually meaningful rescalings. Note that we are using the letters 'M' and 'S' to denote quantities which are dimensionally lengths, while also keeping track of which are side-based and which are median-based.

Remark 4 The *Cevian-based ratios*

$$\frac{KC}{BC} \text{ and } \frac{BK}{BC} \quad (33)$$

moreover have affine significance, entering the following Theorem by Ceva himself.

Theorem 1 (Ceva's Concurrence Theorem) AK , BL and CM are collinear iff

$$\frac{BK}{KC} \cdot \frac{CL}{LA} \cdot \frac{AM}{MB} = -1. \quad (34)$$

(See e.g. [31, 65] for proofs.)

Exercise 1 Use Ceva's Concurrence Theorem to show that each of medians, altitudes, and internal angle bisectors are concurrent. Also give a simpler physical argument for median concurrence.

Remark 5 In Euclidean geometry, moreover, Cevians have lengths as well as affine properties, and it is in fact the following 'Cevian length theorem' that we make use of.

Theorem 2 (Stewart's Cevian-length Theorem) Let $\triangle ABC$ be a triangle with K an arbitrary point on side BC . Then

$$AK^2 = \frac{KC}{BC} AB^2 + \frac{BK}{BC} AC^2 - BK KC. \quad (35)$$

(See e.g. [31] for a proof.)

Corollary 1 i) The squares of the medians' lengths are given by

$$m_a^2 = \frac{2b^2 + 2c^2 - a^2}{4} \text{ and cycles.} \quad (36)$$

ii) The quadratic means of sides and of medians are related by

$$S_Q = \frac{2}{\sqrt{3}} M_Q = \kappa M_Q, \quad (37)$$

for

$$\kappa := \frac{2}{\sqrt{3}}. \quad (38)$$

Proof i) This readily follows from Stewart's Theorem, as per Problem 1 of [87].

ii) then follows immediately from summing i) over all cycles, and square-rooting. \square

Remark 6 Thus the middle pair of quantities defined in Fig 13 are in fact not independent from each other, leaving us with five independent quantities.

Remark 7 κ is for now to be treated as a number, powers of which are recurrent in the geometrical theory of the triangle. A conceptual and physical meaning for κ will moreover be elucidated in Sec 10.2.

Corollary 2 i) An incipient Linear Algebra form for this is [113]

$$m_i^2 = \frac{1}{4} B_{ij} s_j^2, \quad (39)$$

for

$$\underline{\underline{B}} := \begin{pmatrix} -1 & 2 & 2 \\ \frac{2}{2} & -1 & \frac{2}{2} \\ 2 & 2 & -1 \end{pmatrix} \quad (40)$$

a symmetric matrix

$$\underline{\underline{B}} = \underline{\underline{B}}^T, \quad \text{i.e. in components } B_{ij} = B_{ji}. \quad (41)$$

ii) Inverting,

$$s_i^2 = \frac{4}{9} B_{ij} m_j^2. \quad (42)$$

Remark 8 That the same B_{ij} appears in the inverted expression indicates that B_{ij} is proportional to an *involution* J_{ij} , i.e. it is a matrix such that

$$\underline{\underline{J}}^2 = \underline{\underline{1}}: \text{ the identity matrix.} \quad (43)$$

We can thereby further tidy up [113] Corollary 2 Linear Algebra formulation by identifying and using $\underline{\underline{J}}$, as follows.

Corollary 3 (Sides–Medians involution) [113] i)

$$m_i^2 = \kappa^{-2} J_{ij} s_j^2, \quad (44)$$

where

$$\underline{\underline{J}} := \frac{1}{3} \begin{pmatrix} -1 & 2 & 2 \\ \frac{2}{2} & -1 & \frac{2}{2} \\ 2 & 2 & -1 \end{pmatrix} \quad (45)$$

is the *sides-medians involution*. This of course remains symmetric,

$$\underline{\underline{J}} = \underline{\underline{J}}^T, \quad \text{i.e. in components } J_{ij} = J_{ji}. \quad (46)$$

ii) Inverting,

$$s_i^2 = \kappa^2 J_{ij} m_j^2. \quad (47)$$

(See [114] for a proof.)

Lemma 1 (Perimeter bounds on the sum of the medians M)

$$\kappa^{-2} S \leq M \leq S. \quad (48)$$

(See [6] for a proof.)

Remark 6 Including degenerate triangles – as is required in Shape Theory – means that indeed the saturated version of these inequalities is required. The value 1 occurs at the binary coincidence-or-collision B, and κ^{-2} at the uniform collinear configuration U(3, 1).

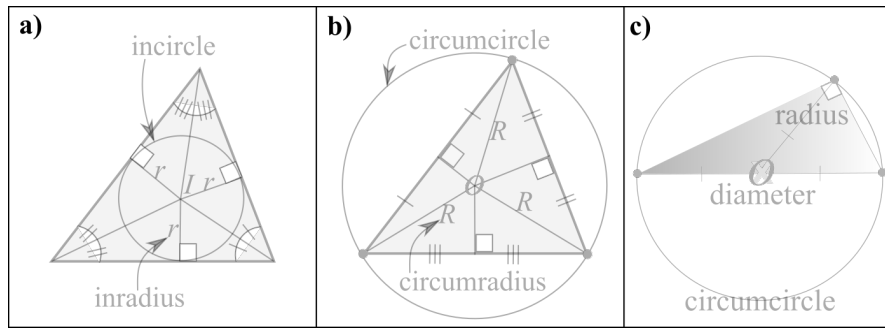


Figure 14: a) The angle bisectors define the incircle as indicated, with incentre I and inradius r .

b) The perpendicular bisectors of the sides define the circumcircle as indicated, with circumcentre O and circumradius R .

c) Diameter subtends a right angle, which can be reinterpreted as the circumcircle of a right-angled triangle, for which the hypotenuse is a diameter, $2R$. The corresponding median is, moreover, the corresponding radius R , and thus is in 1: 2 proportion with the hypotenuse.

7 Associated circles

Definition 1 The *inradius* r is defined as per Fig 14.a), and the *circumradius* R as per Fig 14.b).

Remark 1 At least prima facie, these are secondary features extrinsic to the triangle itself.

Remark 2 Right-angled triangles' circumcircles play a subsequent role in the current Part as per Fig 14.c).

Remark 3 Inradius and circumradius moreover provide bounding inequalities on sums of (squares of) sides or medians; these are either very simple or quite well-known.

Lemma 1 (Preliminary crude joint bounds on sides and medians)

$$2r < s_i, \quad m_i \leq 2R, \quad (49)$$

$$6r < S, \quad M \leq 6R, \quad \text{and} \quad (50)$$

$$12r^2 \leq S_{\text{RSS}}^2, \quad M_{\text{RSS}}^2 \leq 12R. \quad (51)$$

(See [114] for a proof.)

Remark 4 (50) and (51) are mostly provided for comparison with subsequent sharper inequalities, which do discern between sides and medians.

Lemma 2 The root sum of squares is bounded by the square of the semi-perimeter length, s , according to

$$s^2 \leq \kappa^{-2} S_{\text{RMS}}^2 = M_{\text{RMS}}^2. \quad (52)$$

(See [114] for a proof.)

8 The (tetra-)area variable

Definition 1 We use $\text{Area}(ABC)$, or Area for short when unambiguous, to denote the area of $\triangle ABC$.

Lemma 1 Area is given by, in terms of s - α - s data,

$$\text{Area} = \frac{1}{2} ab \sin \gamma \quad \text{or cycles} . \quad (53)$$

Theorem 1 (Heron's formula) Area is given by, in terms of 3-sides data

$$\text{Area} = \sqrt{s(s-a)(s-b)(s-c)}. \quad (54)$$

This is a classical result, known since the first century A.D. [2]; see e.g. [44] for a modern-era proof.

Corollary 1 (Expanded Heron’s formula) The square of the *tetra-area* T is given by

$$T^2 := \{4 \times Area\}^2 = (2a^2b^2 - c^4) + \text{cycles} . \quad (55)$$

Corollary 2 The expanded form (55) of Heron’s formula (54) can be recast in Linear Algebra terms as the quadratic form – in squares a_i^2 , so it is quartic in the a_i themselves –

$$T^2 = H_{ij} s_i^2 s_j^2 \quad (56)$$

for ‘*Heron matrix*’

$$\underline{\underline{H}} := \frac{1}{3} \begin{pmatrix} -1 & 1 & 1 \\ 1 & -1 & 1 \\ 1 & 1 & -1 \end{pmatrix} . \quad (57)$$

Theorem 2 (Medians’ Heron formula) [51], alias ‘area from median data’ formula.

$$Area = \kappa^2 \sqrt{s(s - m_a)(s - m_b)(s - m_c)} . \quad (58)$$

(See [113] for a proof.)

Remark 2 While traditional geometric proofs of this are not uncommon [68], my Linear Algebra proof above contains an insight that these miss. Namely, that the side–median involution matrix $\underline{\underline{J}}$ and the ‘Heron matrix’ $\underline{\underline{H}}$ commute,

$$[\underline{\underline{J}}, \underline{\underline{H}}] = 0 , \quad \text{i.e. } \underline{\underline{J}}\underline{\underline{H}} = \underline{\underline{H}}\underline{\underline{J}} . \quad (59)$$

Remark 3 It is because of this that the ‘median-Heron’ matrix $\underline{\underline{M}}$ in the a priori conceptual form of the medians-data Heron’s formula,

$$Area^2 = M_{ij} m_i^2 m_j^2 , \quad (60)$$

is just proportional to the ‘Heron matrix’ itself,

$$\underline{\underline{M}} = \frac{1}{9} \underline{\underline{H}} . \quad (61)$$

Remark 4 In summary, the sides-Heron and medians-Heron formulae are

$$\sqrt{s(s - a)(s - b)(s - c)} = Area = \kappa^2 \sqrt{s(s - m_a)(s - m_b)(s - m_c)} . \quad (62)$$

Lemma 2 (r and R recast in terms of intrinsic variables) i)

$$Area = r s . \quad (63)$$

ii)

$$Area = r_a(s - a) \quad \text{and cycles} . \quad (64)$$

iii)

$$S_G^3 = a b c = 4 s r R = 4 Area R = R T . \quad (65)$$

Proof These are all standard; see e.g. [44] for i), ii), as well as for a neat way of obtaining Heron’s formula (54) from ii). The first equality of iii) is Fig 13.e)’s definition, the third follows from the extended sine rule and formula (53) for the area, the second then follows from i). The new fourth equality then just follows from the third by the definition of tetra-area, T . \square

8.1 Inequalities reformulated intrinsically

Lemma 1 (Inradius–circumradius bounds) i) The medimeter is bounded according to

$$r \leq \frac{M}{9} \leq \frac{R}{2} . \quad (66)$$

ii) The sum squared of medians is bounded according to

$$r^2 \leq \frac{M_{\text{RMS}}^2}{27} \leq \frac{R^2}{4} . \quad (67)$$

Proof This is a subset of worked Problems 1 and 2 of [88]. \square

Remark 1 On the one hand, i) tightens Lemma 2.ii) from $6r$ to $9r$ – a factor of $3/2$ – and from $6R$ to $9R/2$: a factor of $4/3$.

On the other hand, ii) tightens Lemma 2.iii) from $12r$ to $27r$ – a factor of $9/4 = (3/2)^2$ – and from $12R^2$ to $27R^2/4$: a factor of $16/9 = (4/3)^2$.

Remark 2 Inradius r and circumradius R are moreover not natural or primary constructs from a shape-theoretic point of view, being ‘extrinsic’ features of triangles. We can instead reformulate these quantities as per Lemma 1.i) and iii), giving the following further form for the inequalities.

Corollary 1

$$\frac{T}{S} < s_i, m_i, S_A, M_A \leq 2 \frac{S_G^3}{T}, \text{ and} \quad (68)$$

$$\left(\frac{T}{S}\right)^2 < S_Q^2, M_Q^2 \leq 4 \left(\frac{S_G^3}{T}\right)^2. \quad (69)$$

Corollary 2

$$\sqrt{3} \frac{T}{S} \leq \kappa M_A \leq \sqrt{3} \frac{S_G^3}{T}, \text{ and} \quad (70)$$

$$3 \left(\frac{T}{S}\right)^2 \leq S_Q^2 = \kappa^2 M_Q^2 \leq 3 \left(\frac{S_G^3}{T}\right)^2. \quad (71)$$

Theorem 1 These two inequalities furthermore admit a joint repackaging, as

$$\sqrt{3} \frac{T}{S} \leq \kappa M_A \leq \kappa M_Q = S_Q \leq \sqrt{3} \frac{S_G^3}{T}. \quad (72)$$

(See [114] for a proof.)

8.2 Ratio quantities

Structure 1 We started with seven quantities, but showed two to be equal up to proportion. Thus five independent ratios are supported. For reasons which later become clear, we pick two side-quantity ratios, two median-quantity ratios and the isoperimetric ratio for this purpose, as follows.

<i>arithmetic to quadratic mean ratio of sides</i>	$\mathcal{S} := \frac{S_A}{S_Q}$	<i>arithmetic to geometric mean ratio of sides</i>	$\mathcal{G} := \frac{S_A}{S_G}$
<i>arithmetic to quadratic mean ratio of medians</i>	$\mathcal{M} := \frac{M_A}{M_Q}$	<i>arithmetic to geometric mean ratio of medians</i>	$\mathcal{H} := \frac{M_A}{M_G}$
<i>isoperimetric ratio</i>		$\mathcal{I} := \frac{T}{\sqrt{3} S_A^2}$	

Figure 15: A choice of five independent ratios, as supported by *Area* and Figure 13 and five other independent quantities.

Definition 1 The five independent ratios the current treatise conceives in terms of are given in Fig 15.

Remark 1 These are all scaled to have range 0 to 1. Setting this up requires finding and evaluating their maxima (see [125] for this and further extremization calculations).

Remark 2 To carry over to Shape Theory, we first recast all the inequalities in Sec 2 in terms of ratios. We first define the quantities to appear in these ratios, which are composites of some of the above five ‘most natural’ ratios.

Definition 2

$$\mathcal{F} := \frac{M}{S} = \frac{M_A}{S_A} \quad (73)$$

is the *medimeter to perimeter ratio*.

Remark 3

$$\frac{M_Q}{S_Q} \tag{74}$$

is sterile by the constancy implied by (98). The following alternative quantity, however, does have nontrivial shape-theoretic content (and is what occurs in the below inequalities).

Definition 3 The second ratio featuring in our inequalities is the *quadratic-to-arithmetic mean ratio of medians*,

$$\mathcal{L} := \frac{M_Q}{S_A}. \tag{75}$$

Definition 4 and Proposition 1 The third and fourth ratios featuring in the ratio version of the traditional form of the inequalities are the *inradius per unit perimeter*

$$\mathcal{N} := \frac{r}{S} = \frac{T}{2S^2} = \frac{\mathcal{I}}{6\sqrt{3}}, \tag{76}$$

and the *circumradius per unit perimeter*.

$$\mathcal{N} := \frac{R}{S} = \frac{S_G^3}{TS} = \frac{1}{3\sqrt{3}\mathcal{I}\mathcal{G}^3}. \tag{77}$$

8.3 Rational form of inequalities

Lemma 1)

$$\kappa^{-2} \leq \mathcal{F} \leq 1. \tag{78}$$

Remark 1 The maximum of \mathcal{F} is thus also 1 in accord with our standardization convention, but its range is $[\frac{3}{4}, 1]$ rather than $[0, 1]$. As [125] shows, the range for \mathcal{L} is $[\frac{1}{2\sqrt{2}}, 1]$. \mathcal{F}_{\max} is at the binary coincidence-or-collision B, whereas \mathcal{L}_{\max} is at the equilateral triangle E. Both \mathcal{F}_{\min} and \mathcal{L}_{\min} are at the uniform collinear configuration U(3, 1).

Theorem 1

$$\mathcal{I} \leq \kappa \mathcal{F} \leq \kappa \mathcal{L} = S^{-1} \leq \mathcal{I}^{-1} \mathcal{G}^{-3}. \tag{79}$$

Remark 3 This is an intrinsic reconceptualization of in-and-circumradius bounds on median moments of Sec 8.1, to now be in terms of the isoperimetric ratio and arithmetic-to-geometric sides ratio shape quantities.

9 Lagrangian-level shape space structures including rightness

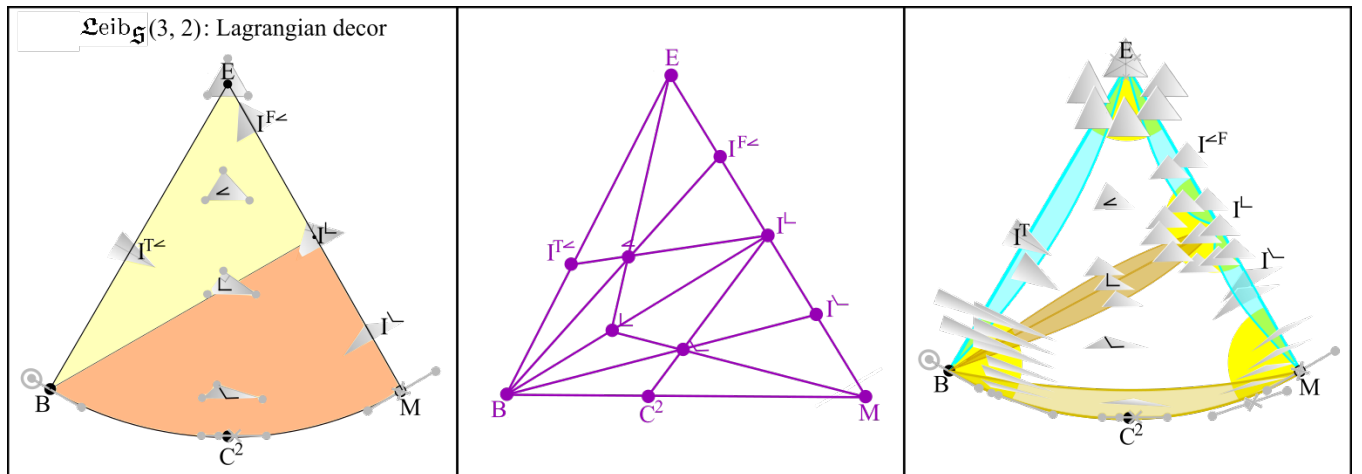


Figure 16: a) Metric-level shape space structure of $\mathfrak{L}eib_5(3, 2)$ corresponding to the full metric Lagrangian level structure of triangular shapes-in-space at the Lagrangian level.

Remark 1 Including rightness, there are now $V = 4$ types of special vertices: E, B, M, I^\perp .

Remark 2 There are also $E = 5$ edges: C , \perp , I^T , $I^{F\angle}$, and $I^{F\setminus}$ which can be denoted just I^{\setminus} .

Remark 3 Finally there are now $F = 2$ faces: obtuse and acute triangles, denoted by \setminus and \angle respectively (explaining also 2 of the previous item's suffices).

Remark 4 These vertices, edges and faces can be located, and counted off, as per Fig 16.a).

Remark 5 The number of exact qualitative types is thus

$$Q := V + E + F = 4 + 5 + 2 = 11 . \quad (80)$$

Remark 6 The adjacency graph 16.b) has $V(\text{Adj}) = Q = 11$, and is moreover $2 W_6$ wheel subgraphs with 2 common edges, so

$$E(\text{Adj}) = 12 \times 2 - 2 = 22 . \quad (81)$$

Remark 7 See Figs 54–56 for an end-summary of special arcs and special points among the $(3, 2)$ shapes. See Fig 18 for further counts of qualitative types in the four $(3, 2)$ shape spaces, as exhibited in Fig 37 in the case of Leibniz space.

	Bird's eye view	Side view perpendicular to S	Side view perpendicular to M	Side view perpendicular to B
a) Right circles alone				
b) Right circles, collinear equator and tall isosceles meridians				
c) Lagrangian structure Right circles, collinear equator and all isosceles meridians				

Figure 17: Each shape space decoration is given a bird's eye view from above the pole in the left column and an equatorial view in the right column.

- a) Cap-circles of rightness, kissing in pairs at the B points. The bird's eye view of these is the inscribed equilateral triangle.
- b) The meridians of tall isoscelessness are moreover related to this as the bird's eye view's equilateral triangle's medians; the numbers in round brackets here serve to distinguish between the various clustering choices.
- c) Considering flat isosceles triangles as well yields a 24-face pattern, the bird's eye view of which is the smaller of the current treatise's two 'kaleidoscopes'.

shape space	$V = G $	$E = e(G)$	F	χ	p	Q	Q_{approx}	Q_{total}	Q_{Approx}	Q_{Total}
$\mathfrak{L}eib_{\mathfrak{S}}(4, 1)$	4	5	2	1	4	11	22	34	33	45
$\mathfrak{I}\mathfrak{S}(4, 1)$	6	9	4	1	6	19	42	66	61	85
$\mathfrak{S}(4, 1)$	10	21	12	1	6	33	114	186	147	219
$\mathfrak{F}(4, 1)$	14	36	24	2	0	74	216	360	290	434

Figure 18: Number of qualitative types including the full Jacobian decor. Note that the first row is the same as row 2 of Fig II.18 due to underlying isomorphic graphs; the second row's graph is isomorphic to the 4-fan, F_4 .

10 Jacobi level of structure for shapes in space

10.1 Mass-unweighted version

Definition 1 For triangleland, we furthermore denote the Jacobi masses μ_1 by μ_s – *side Jacobi mass* – and μ_2 by μ_m : *median Jacobi mass*. This is *possible* since the μ_i are cluster choice independent, and *useful* by its replacing the 1 and 2 labels with more conceptually meaningful and memorable labels, s for side and m for median.

Definition 2 We follow suit by calling the triangle model's first and second relative Jacobi vectors the *side* and *median* vectors (for all that these are cluster-dependent). I.e.

$$R_1^{(a_i)} = s_i, \quad R_2^{(a_i)} = m_i. \quad (82)$$

Corollary 1

$$R_2^{(i)2} = \kappa^{-2} J_{ij} R_1^{(i)2}, \quad \text{inverting to } R_1^{(i)2} = \kappa^2 J_{ij} R_2^{(i)2}. \quad (83)$$

Proof Substitute $R_1 = a$ and $R_2 = m_a$ into the Linear Algebra form of the sides–medians relation (44). \square

10.2 Relative Jacobi separations inter-relations

We now work in terms of the mass-weighted relative Jacobi coordinates provided in eq. (I.67).

Corollary 1

$$\rho_2^{(i)2} = J_{ij} \rho_1^{(i)2}, \quad \text{inverting to } \rho_1^{(i)2} = J_{ij} \rho_2^{(i)2}. \quad (84)$$

Remark 1 Note that the mass-weighting cleans out the awkward numerical factor of $\frac{4}{3} = \kappa^2$ in eqs (83), revealing this factor to be

$$\kappa^2 = \frac{4}{3} = \frac{\mu_m}{\mu_s} = \frac{(\text{median Jacobi mass})}{(\text{side Jacobi mass})}. \quad (85)$$

Lemma 1 i) The mass-weighted version of the formula for median lengths (36) is

$$\rho_2^{(1)2} = \frac{2(\rho_1^{(2)2} + \rho_1^{(3)2}) - \rho_1^{(1)2}}{3} \quad \text{and cycles}. \quad (86)$$

Proof Apply definition (I.34) and mass weighting (I.47) to Corollary 1 of Sec 6. \square

Remark 2 In [113], we furthermore interpret this as a mass-weighted counterpart to Stewart's Theorem, in the special case in which the Cevians under consideration are medians.

Definition 1 The *first mass-weighted moment sums* are, for $a = 1, 2$,

$$F_a := \sum_i \rho_a^{(i)}. \quad (87)$$

Remark 1 The mass-weighted Jacobi separations are moreover related to the more widely used partial moments of inertia ι_a by

$$\iota_a = \rho_a^2. \quad (88)$$

In particular, with clustering labels explicit,

$$\iota_1^{(a)} = \rho_1^2 = \mu_1 R_1^2 = \frac{a^2}{2} \quad \text{and cycles}, \quad (89)$$

and

$$\iota_2^{(a)} = \rho_2^2 = \mu_2 R_2^2 = \frac{m_a^2}{2} \text{ and cycles .} \quad (90)$$

Definition 2 More familiarly, summing over disjoint partial moments rather than over clusters, the *total moment of inertia* is

$$\iota^{(a)} := \iota_1^{(a)} + \iota_2^{(a)} . \quad (91)$$

The definition here is that the total object is the sum of all disjoint partial contributions.

Lemma 2 i)

$$\iota = \rho_2^2(1 + \mathcal{R}^2) . \quad (92)$$

ii) (Democratic formula for the moment of inertia)

$$\iota = \frac{a^2 + b^2 + c^2}{3} = \langle \text{side}^2 \rangle , \quad (93)$$

where $\langle \rangle$ denotes ‘democratic average’.

(See [113] for a proof.)

Remark 3 The right hand side of the first equality being cluster-independent, we are entitled to rewrite

$$\iota := \iota_1^{(a)} + \iota_2^{(a)} \text{ or cycles .} \quad (94)$$

While trivial to prove, the Lemma’s second equality none the less has *conceptual content* as regards giving a sharp interpretation for the computational right hand side of the first equality.

Definition 3 The *second mass-weighted moment sums* are, for $a = 1, 2$,

$$Z_a := \sum_i \rho_a^{(i)2} = \sum_i \iota_a^{(i)} . \quad (95)$$

Definition 4 Let $\sigma, \mu, \sigma_{\text{RSS}}, \mu_{\text{RSS}}$ denote the mass-weighted version of the perimeter S , medimeter M , S_{RSS} and M_{RSS} respectively.

Corollary 1

$$\iota = 2\sigma_{\text{Q}}^2 = 2\mu_{\text{Q}}^2 , \text{ or, inverting ,} \quad (96)$$

$$\sigma_{\text{Q}}^2 = \mu_{\text{Q}}^2 = \frac{\iota}{2} . \quad (97)$$

Remark 4 This signifies that, in mass-weighted space, cluster summed or averaged second moments of side or of median are equivalent, and both are readily convertible to the moment of inertia up to a constant of proportionality.

Remark 5 Thus summing up over the clusterings gives

$$Z_1 := \sum_i \rho_1^{(i)2} = \sum_i \iota_1^{(i)} = \sum_i \iota_2^{(i)} = \sum_i \rho_2^{(i)2} =: Z_2 , \quad (98)$$

which is also now free of numerical factors [as compared to (52)’s factor of $\frac{3}{4} = \kappa^{-2}$]. This signifies that median partial moments of inertia contribute – over all clusterings – the *same amount* as side moments of inertia. This amounts to a statement of *Jacobi-isotropy* among the sums over all clusters of the partial moments of inertia. Furthermore, dividing both sides by 3,

$$\langle \rho_1^2 \rangle = \langle \rho_2^2 \rangle \quad (99)$$

casts this interpretation in the form of equality between (cluster-averaged median partial moment of inertia) and (cluster-averaged side partial moment of inertia).

Definition 5 The *mass-weighted inertia quadric* (I.71) is

$$\iota(\underline{\rho}_a) = \sum_a \rho_a^2 = \rho_1^2 + \rho_2^2 , \quad (100)$$

where the last equality is an $N = 3$ specialization. Computationally, this amounts to returning to the previous section’s tilded formulation. So one motivation for the mass-weighted relative Jacobi coordinates is that they are

what drops out of the Linear Algebra approach. Another follows from the matrix in the quadric being the identity, alongside the following interpretation.

Remark 7 The Cartesian equivalence in this (mass-weighted notion of) relative space of \underline{R}_1 and \underline{R}_2 moreover provides the following.

‘Jacobian’ first motivation for median coprimality. Mass-weighted medians and mass-weighted sides are on an identical geometrical footing in (mass-weighted) relative space. These are moreover what drops out of the linear algebra most directly, in obtaining Jacobi coordinates by diagonalization. Motivating relative Jacobi coordinates themselves has moreover further parts to it. For, aside from their usefulness in treating the N -body problem, they turn out to be coordinates in terms of which the shape space’s natural coordinates are simple (spherical coordinates for $N = 3$ or inhomogeneous coordinates for $N \geq 4$).

10.3 Jacobi congruence and similarity conditions

Remark 1 Mechanical naturality of medians points to various further congruence and similarity conditions.

Definition and Proposition 1 i) s-S-m – a side s , say $a = R_1$, the corresponding median m , say $m_a = R_2$, and the Swiss-army-knife angle $S = \Phi$ included between the corresponding vectors, as per Fig I.18.a) and eq (I.171) – is a further congruence condition, which we term the **Jacobi congruence condition, 6)**.

ii) R-S, for R a side-to-corresponding median ratio and $S = \Phi$ the Swiss-army-knife angle included between these is a further similarity condition, which we term the **Jacobi similarity condition, 6)**.

Let us next consider how we solve for the scaled or pure-shape triangle in question given s-m-S or R-S data respectively. If a and m_a are given, the problem turns out to be symmetric for b, c and for γ, β by which it is useful to denote these respectively by b_{\pm} and γ_{\pm}

Proposition 2 i) With reference to Fig 4, prior to mass weighting, the scaled triangle is solved in terms of the Euclidean Jacobi data: side-length R_1 , half-side length H_1 , corresponding median-length R_2 , and Swiss-army-knife angle Φ ,

$$a = R_1, \quad b_{\pm} = \sqrt{R_2^2 \pm R_1 R_2 \cos \Phi + R_1^2/4} = \|\underline{H}_1 \pm \underline{R}_2\|, \quad (101)$$

$$\cos \gamma_{\pm} = \frac{R_1 \pm 2 R_2 \cos \Phi}{\sqrt{4 R_2^2 \pm 4 R_1 \cos \Phi + R_1^2}} = \frac{H_1 \pm R_2 \cos \Phi}{\|\underline{H}_1 \pm \underline{R}_2\|}, \quad (102)$$

$$\cos \alpha = \frac{4 R_2^2 - R_1^2}{\sqrt{8 R_2^2 [2 R_2^2 + R_1^2 (1 - 2 \cos^2 \Phi)] + R_1^4}} = \frac{R_2^2 - H_1^2}{\sqrt{(R_2^2 + H_2^2)^2 - 2 (\underline{H}_1 \cdot \underline{R}_2)^2}}. \quad (103)$$

ii) The mass-weighted versions of this solution is

$$a = \sqrt{2} \rho_1, \quad b_{\pm} = \|\underline{\rho}_1 \pm \sqrt{3} \underline{\rho}_2\| / \sqrt{2}, \quad (104)$$

$$\cos \gamma_{\pm} = \frac{\rho_1 \pm \sqrt{3} \rho_2 \cos \Phi}{\sqrt{\rho_2 (3 \rho_2 \pm 2 \sqrt{3} \rho_1 \cos \Phi) + \rho_1^2}} = \frac{\rho_1 \pm \sqrt{3} \rho_2 \cos \Phi}{\|\underline{\rho}_1 \pm \sqrt{3} \underline{\rho}_2\|}, \quad (105)$$

$$\cos \alpha = \frac{3 \rho_2^2 - \rho_1^2}{\sqrt{(3 \rho_2^2 + \rho_1^2)^2 - 4 \sqrt{3} (\underline{\rho}_1 \cdot \underline{\rho}_2)^2}}. \quad (106)$$

iii) The pure-shape triangle is solved in terms of the similarity Jacobi data: median-to-base ratio \mathcal{R} and Swiss-army-knife angle Φ ,

$$\frac{b_{\pm}}{a} = \frac{1}{2} \sqrt{3 \mathcal{R}^2 \pm 2 \sqrt{3} \mathcal{R} \cos \Phi + 1} = \frac{1}{2} \sqrt{\mathcal{V}^2 \pm 2 \mathcal{V} \cos \Phi + 1}, \quad (107)$$

$$\cos \gamma_{\pm} = \frac{1 \pm \sqrt{3} \mathcal{R} \cos \Phi}{\sqrt{3 \mathcal{R}^2 \pm 2 \sqrt{3} \mathcal{R} \cos \Phi + 1}} = \frac{1 \pm \mathcal{V} \cos \Phi}{\sqrt{\mathcal{V}^2 \pm 2 \mathcal{V} \cos \Phi + 1}}, \quad (108)$$

$$\cos \alpha = \frac{3 \mathcal{R}^2 - 1}{\sqrt{(3 \mathcal{R}^2 + 1)^2 - 12 \mathcal{R}^2 \cos^2 \Phi}} + 1 = \frac{\mathcal{V}^2 - 1}{\sqrt{(\mathcal{V}^2 + 1)^2 - 4 \mathcal{V}^2 \cos^2 \Phi}}, \quad (109)$$

where we have tidied up by introducing the transformation

$$\mathcal{V} := \sqrt{3} \mathcal{R}. \quad (110)$$

Proof Five sequential uses of the cosine rule give i). Then mass-weight as per (I.34) to obtain ii). Finally form length ratios and divide tops and bottoms of right-hand-side expressions by suitable powers of ρ_i to recast them in terms of the ratio \mathcal{R} . \square

Remark 2 The transformation (110) is moreover revealed in Sec 13.7 to have further shape space significance.

Remark 3 The Jacobi conditions s-S-m and R-S moreover closely emulate the s- α -s and r- α (included) conditions argued for in Sec 5.3. Indeed, the arguments by which the latter extend to C (including B) largely carry over; the Swiss-army-knife angle now takes a collinear value 0 or π [One now has to exclude U(3, 1) since the Swiss-army-knife angle is not defined there; one can probe near there using s-s-s or r-r, by which the use of a s-s-s patch to deal with O covers this moderate inconvenience with U(3, 1) as well.]

Remark 4 Having obtained the above angle formulae, (23) and cycles give that

$$\sin \gamma_{\pm} = \frac{\mathcal{V} \sin \Phi}{\sqrt{\mathcal{V}^2 \pm 2\mathcal{V} \cos \Phi + 1}} \quad \text{and} \quad \sin \alpha = \frac{2\mathcal{V} \sin \Phi}{\sqrt{\mathcal{V}^4 + 2\mathcal{V}^2(1 - \cos 2\Phi) + 1}}. \quad (111)$$

The simplest expressions for these angles are moreover

$$\cot \gamma_{\pm} = \mathcal{V}^{-1} \operatorname{cosec} \Phi \pm \cot \Phi \quad \text{and} \quad \cot \alpha = 2^{-1} \operatorname{cosec} \Phi (\mathcal{V} - \mathcal{V}^{-1}). \quad (112)$$

11 Theory of mass-weighted area

11.1 Sides-to-medians symmetric Jacobi–Heron formula

Definition 1 The *mass-weighted area* is, in terms of relative Jacobi vectors,

$$\mathcal{A}rea := \frac{1}{2} |\rho_1 \times \rho_2|. \quad (113)$$

We also denote the *mass-weighted tetra-area* by

$$\mathcal{T} := 4 \times \mathcal{A}rea. \quad (114)$$

Definition 2 The *mass-weighted area per unit moment of inertia* is

$$area := \frac{(\text{mass-weighted area})}{(\text{moment of inertia})} = \frac{|\rho_1 \times \rho_2|}{2(\rho_1^2 + \rho_2^2)}; \quad (115)$$

We also denote the *mass-weighted tetra-area per unit moment of inertia* by

$$\tau := 4 \times area. \quad (116)$$

Remark 1 *area* and τ are shape quantities (and thus dimensionless).

Remark 2 Upon reaching preshape space, moreover, ℓ is constant, so *area* and τ continue to be proportional to the geometrical area variable.

Definition 3 Let us denote the *mass-weighted semi-perimeter* denoted by σ , and the *mass-weighted semi-median* by ς .

Remark 3 Various subsequent sections of this Part require knowing furthermore how the quantities in question scale.

Lemma 1 i) Mass-weighted semi-perimeter is a mass-weighting side-vector,⁵

$$\sigma := \sqrt{\mu_s} s = \frac{s}{\sqrt{2}}. \quad (117)$$

ii) *Mass-weighted semi-median* is a mass-weighting median-vector,

$$\varsigma := \sqrt{\mu_m} s = \sqrt{\frac{2}{3}} s. \quad (118)$$

⁵See [114] for further exposition of what ‘side-vector’, ‘median-vector’ and ‘side-median bivector’ mean.

iii) Area is a mass-weighting side–median bivector,

$$\alpha_{\text{rea}} = \sqrt{\mu_s \mu_m} \text{Area} = \frac{\text{Area}}{\sqrt{3}}. \quad (119)$$

(See [113] for a proof.)

Theorem 1 Mass-weighted area’s *Heron–Jacobi formulae* in terms of each of mass-weighted sides and mass-weighted medians is

$$\sqrt{\sigma \left(\sigma - \rho_1^{(a)} \right) \left(\sigma - \rho_1^{(b)} \right) \left(\sigma - \rho_1^{(c)} \right)} = \alpha_{\text{rea}} = \sqrt{\varsigma \left(\varsigma - \rho_2^{(a)} \right) \left(\varsigma - \rho_2^{(b)} \right) \left(\varsigma - \rho_2^{(c)} \right)}. \quad (120)$$

(See [113] for a proof.)

Remark 4 In allocating primary ratios, we already used a maximal amount of what would be mass-weighted scalars, for subsequent convenience. Thus no further mass-weighted versions of these need to be introduced at this point.

Remark 5 Note that mass-weighting places the sides and medians versions of Heron on an equal footing. I.e. without any constant prefactor difference like the κ^2 in the case of the mass-unweighted medians relative to the case of the mass-unweighted sides of (62). This amounts to explaining the κ^2 factor discrepancy between the medians’ and sides’ Heron’s formulae as resulting from formulation in terms of area rather than mass-weighted area. This is a further way in which the Jacobi formulation exhibits naturality. It is moreover a *common* explanation of the numerical factors in the sides-to-medians Heron formulae and the sides-to-medians involution, as per eq. (85).

11.2 Diagonalizing the Heron matrix gives the Hopf Map and Kendall’s Theorem

Remark 1 Furthermore, setting

$$0 = \det(\underline{H} - \lambda \underline{I}) \quad (121)$$

$\lambda = -2$ with multiplicity 2, with respective orthonormal eigenvectors

$$\frac{1}{\sqrt{3}} \begin{pmatrix} 1 \\ 1 \\ 1 \end{pmatrix}, \quad \frac{1}{\sqrt{2}} \begin{pmatrix} 1 \\ -1 \\ 0 \end{pmatrix}, \quad \frac{1}{\sqrt{6}} \begin{pmatrix} 1 \\ 1 \\ -2 \end{pmatrix}. \quad (122)$$

The diagonalizing variables are thus

$$\bar{a}^2 = \frac{a^2 + b^2 + c^2}{\sqrt{3}}, \quad \bar{b}^2 = \frac{a^2 - b^2}{\sqrt{2}}, \quad \text{and} \quad \bar{c}^2 = \frac{a^2 + b^2 - 2c^2}{\sqrt{2}}. \quad (123)$$

The Heron quadratic form (56) is thus equal to

$$\sum_i \Lambda_{ii} \bar{a}_i^2 \bar{a}_i^2 \quad (124)$$

for *diagonalized Heron matrix*

$$\Lambda_{ij} = \text{diag}(1, -2, -2). \quad (125)$$

This is related to the original Heron matrix H_{ij} by conjugation with the P_{ij} formed by using (122)’s orthonormal eigenvectors as columns. Thus we have derived that Heron’s formula also takes the following form.

Theorem 1 (Diagonal Heron formula)

$$T = \sqrt{\bar{a}^4 - 2(\bar{b}^2 + \bar{c}^2)}. \quad (126)$$

Corollary 1 (Ratio form of Diagonal Heron formula)

$$\frac{T}{\bar{a}^2} = \sqrt{1 - \left[\sqrt{2} \left(\frac{\bar{b}}{\bar{a}} \right)^2 \right]^2 - \left[\sqrt{2} \left(\frac{\bar{c}}{\bar{a}} \right)^2 \right]^2}. \quad (127)$$

Definition 1 The rescaled *ratio variables*

$$z := \sqrt{2} \left(\frac{\bar{c}}{\bar{a}} \right)^2 = \frac{a^2 + b^2 - 2c^2}{a^2 + b^2 + c^2}. \quad (128)$$

$$x := \sqrt{2} \left(\frac{\bar{b}}{\bar{a}} \right)^2 = \frac{\sqrt{3}(a^2 - b^2)}{a^2 + b^2 + c^2} \quad \text{and} \quad (129)$$

$$y := \frac{\sqrt{3}T}{a^2 + b^2 + c^2} \quad (130)$$

are then natural.

Remark 2 The denominator of the ratio is proportional to ι by Lemma 2.ii) of Sec 10.2. y is moreover to be interpreted precisely as *mass-weighted tetra-area per unit moment of inertia*, τ

Corollary 1 In terms of the rescaled ratio variables, the diagonal Heron formula has been reduced to

$$x^2 + y^2 + z^2 = 1 . \quad (131)$$

This is mathematically just the on-2-sphere condition. This moreover constitutes a derivation of the Kendall shape sphere from new first principles.

Remark 3 With the following extra computation, this also amounts to a derivation of the Hopf map \mathcal{H}_C following on from (I.180). This work amounts to identifying x, y, z in terms of the four $\underline{\rho}_i$. Firstly, it is straightforward from (130) and Lemma 2.ii) that

$$y = 2(\underline{\nu}_1 \times \underline{\nu}_2)_3 . \quad (132)$$

Secondly, using the first form of (107) and (I.174) in (129-128)

$$x = 2\underline{\nu}_1 \cdot \underline{\nu}_2 , \quad (133)$$

$$z = \nu_1^2 - \nu_2^2 . \quad (134)$$

Remark 4 x and z are to be interpreted as Heron map eigenvectors. x is furthermore to be interpreted as anisocscelness, *aniso*: departure from isoscelesness.

$$\textit{aniso} = \frac{\sqrt{3}(a^2 - b^2)}{a^2 + b^2 + c^2} , \quad (135)$$

and z as ellipticity, *ellip*: departure from regularity.

$$\textit{ellip} = \frac{a^2 + b^2 - 2c^2}{a^2 + b^2 + c^2} . \quad (136)$$

We will have more to say about these quantifiers in Sec 15.

Remark 5 See [62, 75, 89] for further derivations of the shape sphere: geometry and associated mechanical action reduction.

11.3 Median–sides interchange form invariance of diagonal Heron–Hopf formula

Corollary 1 In terms of the medians, i)

$$\textit{ellip} = - \frac{m_a^2 + m_b^2 - 2m_c^2}{m_a^2 + m_b^2 + m_c^2} , \quad (137)$$

$$\textit{aniso} = - \frac{m_a^2 - m_b^2}{\sqrt{3}\{m_a^2 + m_b^2 + m_c^2\}} , \quad \text{check downstairsness of this 3} \quad (138)$$

i.e. equality of form up to sign choice (which is an allowed ambiguity in setting up Cartesian axis systems).

Proof Use the below Lemma and the sides–medians involution. \square

Lemma 1 (Democratic medians form of total moment of inertia)

$$\iota = \kappa^2 \langle m_i^2 \rangle = \kappa^2 M_Q^2 . \quad (139)$$

(See [114] for a proof.)

Remark 1 The above Corollary can be interpreted as follows. Expressing *ellip* and *aniso* in terms of medians instead does not moreover affect the diagonality. The Heron–Hopf formula is thus independent of whether one is conceiving in terms of sides or of medians; the Hopf quantities offer a third point of view that is side–median symmetric. Thus we have arrived at the

‘Hopfian’ second motivation for median coprmality.

11.4 Heron–Hopf–Kendall, Heron–Hopf and two concomitant formulae

We conclude the previous three sections as follows. Sec 11.2’s workings readily imply the following Theorems.

Theorem 1 The diagonalized form of the mass-weighted Heron formula is

$$\tau = \sqrt{1 - \alpha niso^2 - ellip^2} . \quad (140)$$

This ‘*Heron–Hopf*’ formula is moreover sides–to–medians symmetric.

Theorem 2 The most symmetrical presentation of the diagonalized mass-weighted Heron formula is, from 131,

$$\tau^2 + \alpha niso^2 + ellip^2 = 1 . \quad (141)$$

This ‘*Heron–Hopf–Kendall*’ formula is mathematically just the on-sphere condition; moreover observing this amounts to a *recovery of Kendall’s Theorem* that the shape space of all triangles in $2-d$ is a sphere.

Remark 1 As considered in current treatise, Kendall’s Theorem is in the context of distinctly labelled point-or-particle vertices without mirror image identification. A conceptual name for this theorem is ‘*triangleland sphere theorem*’, whereas one for the more general Kendall theorem is ‘*N-a-gonland complex projective space theorem*’.

Remark 2 The Heron–Hopf formula, as the area-subject Hopf formula in terms of ellipticity and anisoscelesness data, now has two concomitant formulae in many senses. These are, firstly, the ellipticity-subject Hopf formula in terms of anisoscelesness and area data,

$$ellip = \sqrt{1 - \alpha niso^2 - \tau^2} . \quad (142)$$

Secondly, the anisoscelesness-subject Hopf formula in terms of elliptiity and area data,

$$\alpha niso = \sqrt{1 - ellip^2 - \tau^2} . \quad (143)$$

The sense in which Heron–Hopf has a further quality than these two other formulae is that it is the only one among these which has a democratic subject (in the clustering alias Jacobi sense).

11.5 Maximum and minimum *area*

Remark 1 *area* is a natural $2-d$ analogue of $(N, 1)$ ’s *diam* of eq. (I.260).

Remark 2 On the one hand, for mirror image identified versions,

$$area_{\max} \text{ is at the equilateral triangle } E \quad (144)$$

and

$$area_{\min} \text{ is shared by all collinear configurations } C . \quad (145)$$

Remark 3 On the other hand, for the mirror image distinct versions, using the unsigned version of *area*,

$$area_{\max} \text{ is at the equilateral points } E \text{ and } \bar{E} , \quad (146)$$

and $area_{\min}$ is as above. For the signed version, however, $area_{\max}$ is at \bar{E} and $area_{\min}$ is at E .

Remark 4 Collinear configurations $area = 0$ moreover bound clockwise triangles obeying the signed-area inequality,

$$area > 0 , \quad (147)$$

from anticlockwise triangles obeying the opposite signed-area inequality,

$$area < 0 . \quad (148)$$

Remark 5

$$\mathcal{P} := \frac{\sigma}{\sqrt{l}} = \frac{\sigma}{\rho} \quad (149)$$

– *mass-weighted perimeter per square root of moment of inertia* or *per (mass-weighted) configuration space radius* – is a comparably significant quantity. This however takes more work to extremize, so we leave this task to a further paper [125].

Remark 7

$$\mathcal{J} := \frac{\text{Area}}{S^2} \quad (150)$$

is the *isoperimetric ratio* that features in the classical *isoperimetric problem*; for 3 points-or-particles, this is also maximized for the equilateral triangle (see e.g. [17] for 3 elementary proofs). Moreover, the three ratios above clearly only have two degrees of freedom between them. (There is proportionality to the mass-weighted quantity

$$\left. \frac{\tau}{\sigma^2} \right). \quad (151)$$

What has happened is that naturality of moment of inertia in Shape Theory has rendered the classical isoperimetric ratio less primary, by which it is now to be regarded as the composite ration of the previous two more shape-theoretic ratios. On these grounds, extremizing the first two of these ratios has significance as a shape-theoretic replacement of the isoperimetric problem by two more primary problems whose ratio is the insoperimetric quantity itself.

Remark 8 See [125] for further study of shape-theoretically significant ratios for triangles.

11.6 Jacobi separation inequalities

Passing to mass weighted Jacobi versions of Sec 3's inequalities requires knowing how the quantities involved scale under mass-weighting.

Lemma 1 i) In Fig 13, everything in column 1 is a side-vector and median-scalar, whereas everything in column 2 is a median-vector and side-scalar.

ii) \mathcal{S} , \mathcal{G} , \mathcal{M} and \mathcal{H} are mass-weighting scalars.

iii) \mathcal{F} , \mathcal{E} and \mathcal{I} are all median-vectors and side-covectors.

(See [114] for a proof.)

Remark 2 As set up, while working at the level of ratios, everything is a biscalar or a vector-covector, whose weight is moreover κ .

Definition 1 Denote the *mass-weighted medimeter per unit perimeter* by

$$\Psi := \kappa \mathcal{F} , \quad (152)$$

the *mass-weighted root sum of medians per unit perimeter* by

$$\Lambda := \kappa \mathcal{L} , \quad (153)$$

We do not use the *mass-weighted isoperimetric ratio*

$$\Upsilon := \kappa \mathcal{I} , \quad (154)$$

so as to maintain the $[0, 1]$ range. To be clear, in each case here, 'mass weighted' means that both the numerator and the denominator are mass-weighted.

Theorem 1

$$\kappa^{-1} \leq \Psi \leq \kappa . \quad (155)$$

Proof Mass-weight (78). \square .

Theorem 4

$$\mathcal{I} \leq \Psi \leq \Lambda = \mathcal{S}^{-1} \leq \mathcal{I}^{-1} \mathcal{G}^{-3} . \quad (156)$$

Proof Mass-weight (79). \square

Remark 4 On the one hand, Theorem 1 places shape-independent bounds on the mass-weighted medimeter-to-perimeter ratio. Mass-weighting has multiplicatively centred this inequalities' bounds, meaning that one bound is now the reciprocal of the other. On the other hand, Theorem 2 places shape-dependent bounds on this and the root

sum median to perimeter ratio, the shape dependence of which is manifested as powers of the isoperimetric ratio and arithmetic-to-geometric mean side ratio shape variables. As regards lower bounds, for

$$\mathcal{I} < \kappa^{-1}, \quad (157)$$

Theorem 2's shape-dependent one is more stringent, whereas for

$$\mathcal{I} > \kappa^{-1}, \quad (158)$$

Theorem 1's shape-independent one is. As regards upper bounds, for

$$\mathcal{I} \mathcal{G}^3 > \kappa^{-1}, \quad (159)$$

Theorem 2's shape-dependent one is more stringent, whereas for

$$\mathcal{I} \mathcal{G}^3 < \kappa^{-1}, \quad (160)$$

Theorem 1's shape-independent one is. The corresponding cross-over's critical values, and consideration of the set of shapes entailed by each case, is part of [125].

12 Jacobian recharacterization of some familiar types of triangle

12.1 Jacobi-perpendicularity recharacterization of isosceles and equilateral triangles

Remark 1 Isoscelesness can furthermore be characterized by an edge being perpendicular to its median (Ex. 3.13 of [28]). [This is by the shared side-equal side-right or r-h-s congruence \Rightarrow other sides equal \Rightarrow isosceles.] In the current treatise's relational language, this result can be rephrased as the corresponding Swiss-army-knife angle being right: a Jacobi perpendicularity criterion,

$$(\text{isosceles}) \Leftrightarrow \left(\text{at least on Swiss-army-knife angle is right} : \Phi = \frac{\pi}{2} \right). \quad (161)$$

Remark 2 The sole degree of freedom isosceles triangles are left with in this Jacobi characterization is the median-to-base ratio R .

Remark 3 At the Jacobian level of structure, equilaterality's characterization as isosceles with respect to two clustering choices (implying the third as well) translates to two (also implying the third as well) edges being perpendicular to their respective median. This converts (7) to being a Jacobi perpendicularity criterion for equilaterality.

Remark 4 Note that the above is base–median perpendicularity within a given clustering. Triangleland moreover also supports Jacobi perpendicularity between one clustering's base and another's median, and median–median mutual perpendicularity between clusters; see Fig 19 (in extension of Fig I.16).

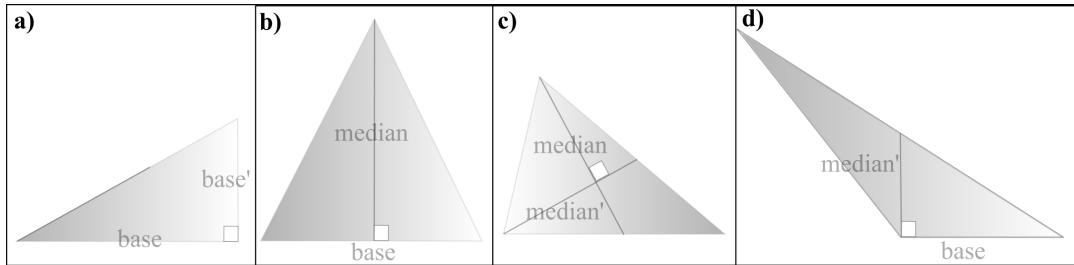


Figure 19: a) An obvious alias Lagrange right triangle.

b) Jacobi rightness is a further isoscelesness condition.

c) Median-median perpendicularity.

d) Perpendicularity between one clustering's base and another's median.

12.2 Mergers, cluster hierarchy and hierarchical coincidence structure

This is covered in Fig 20.

	E	I	S	R	B	C ^T	H	C ^F	M
Jacobi separation uniformity	 equiregular	 aregular	 aregular	 regular	 aregular	 regular	 regular	 aregular	 aregular
Jacobi angle uniformity		—	—	—	—	—	—	—	—
Hierarchical coincidence structure	—	—	—	—		—	—	—	
Hierarchical separation uniformity structure			—	—	—	—	—	—	
Hierarchical angular uniformity structure			—	—	—	—	—	—	—

Figure 20: a) Regularity, hierarchical coincidences and hierarchical uniformity for (3, 2) shapes.

12.3 Jacobi separation uniformity characterization: tall, flat and regular triangles

Remark 1 Due to its pure length-ratio content, Sec 4.5's tall-versus-flat distinction extends to scalene triangles as well. This requires bringing in the following bounding notion.

Definition 1 A triangle is *regular* if its base and median partial moments of inertia are equal:

$$l_s = l_m \Leftrightarrow \frac{\rho_1}{\rho_2} = 1. \quad (162)$$

The latter form is clearly an example of Part I's Jacobi separation uniformity criterion. Other useful descriptions or aliases for regular are *Jacobi-isotropic* – meaning side-to-median isotropy in partial moments of inertia – and *circular* (explained in Sec 15.3).

Remark 2 There are moreover 3 notions of regularity, corresponding to the 3 clustering choices,

$$l_s^{(i)} = l_m^{(i)}. \quad (163)$$

Remark 3 In space itself, due to intervention of the Jacobi masses, the regularity condition translates to

$$\frac{R_1}{R_2} = \kappa, \quad (164)$$

which is immediately recognizable as the equilateral triangle's base-to-height ratio. This gives the following further Jacobi-separation-uniformity characterization.

Proposition 1 A triangle is equilateral iff base–median equality holds in two of its Jacobi clusterings.

Remark 4 E clearly has base–median condition hold in *all three* of its clusterings, but by the Proposition, this holding in two *implies* it holds in the third as well.

Remark 5 Regularity can thus be reformulated in entirely flat space geometrical terms – without any reference to mass weighting or moments of inertia – as ‘the base and median are in the proportion found in the equilateral triangle’.

Corollary 1 The equilateral triangle E is not only twofold \Rightarrow threefold isosceles I , but also twofold \Rightarrow threefold regular R ,

$$E = R \cap R = R \cap R \cap R . \quad (165)$$

Definition 2 Let us term this twofold \Rightarrow threefold regularity *equiregularity*.

Remark 6 This is clearly a pure-ratio characterization of equilaterality E ; it involves multiple clusterings.

Remark 7 Moreover,

$$E = I \cap I \cap I \cap R \cap R \cap R , \quad (166)$$

which is a full characterization that is unique on the shape hemisphere and gives a pair of antipodal conjugate points E and \bar{E} on the shape sphere.

Remark 8 On the other hand, the following is the unique Leibniz space level characterization of equilaterality, E , as a mixed length-ratio and relative-angle concept within a single cluster.

Proposition 2 (angle-ratio symmetric, alias Jacobi–Leibniz, criterion for equilaterality) Just being one I and one R implies being E :

$$E = I \cap R : (\text{equilateral}) = (\text{isosceles}) \cap (\text{regular}) . \quad (167)$$

Proof Case 1) The median involved in the regularity condition is not relative to either of the ab initio equal sides (Fig 21.a). Here, isoscelesness forces this median to be perpendicular to its base. Also regularity fixes the height in space of the isosceles triangle to be κ^{-1} times the base. So applying Pythagoras’ Theorem to the triangle ABK , equality of the third side is enforced.

Case 2) The median involved in the regularity condition is relative to one of the ab initio equal sides (Fig 21.b). This requires the mass-weighted triangle ABL to have sides in $1 : 1 : \frac{1}{2}$ ratio. Thus removing the mass-weighting, ABL ’s sides are in ratio $1 : \frac{\sqrt{3}}{2} : \frac{1}{2}$, by which we recognize it to be the ‘set square triangle’ with $\frac{\pi}{6}, \frac{\pi}{3}, \frac{\pi}{2}$ angles. We then note this means that a second median is perpendicular to its corresponding side, so it is twofold isosceles and thus threefold isosceles: equilateral. Alternatively, we know it is isosceles with $\frac{\pi}{3}$ angle included between its equal sides, so its remaining angles are $(\pi - \pi/3)/2 = \pi/3$, so it is equiangular and thus equilateral. \square

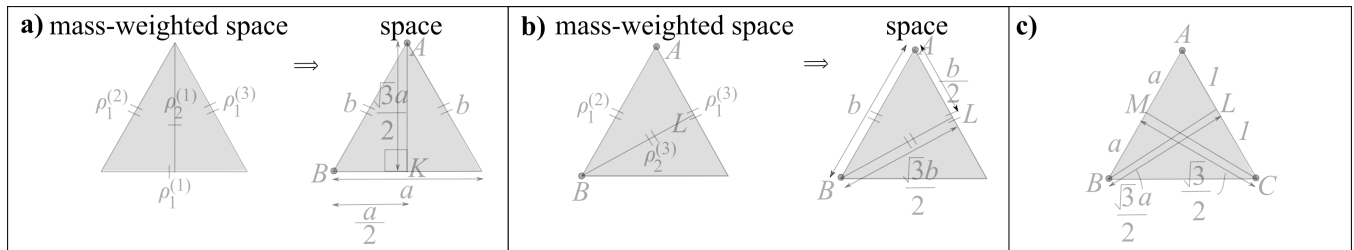


Figure 21: a) and b) are the two cases in the derivation of the equiregularity criterion for equilaterality in Proposition 1. c) gives Proposition 1’s set-up.

Proof of Proposition 1 In space, we have the data in Fig 21.c) Then $\triangle ALB$ is similar to $\triangle AMC$ by r - α (non-included), since the angle at A is shared and

$$\frac{LB}{AL} = \frac{\sqrt{3}}{2} = \frac{MC}{AM} \quad (168)$$

This means that

$$\frac{1}{a} = \frac{AM}{AL} = \frac{MC}{LB} = \frac{2a}{2} = a . \quad (169)$$

So, with $a \geq 0$ since it is a distance, $a = 1$. Thus $\triangle ABC$ is isosceles. But $\triangle ABC$ is certainly also regular (in either cluster it is not currently proven to be isosceles in). Moreover, we proved in Proposition 2.ii) that this condition implies equilaterality. \square

Definition 3 A triangle is *aregular* if it is not regular with respect to any clustering.

Remark 9 Note the parallel between equiregularity, regularity and aregularity, on the one hand, and equilaterality, isosceleness and scaleness on the other hand (see also Fig 20 in this regard).

Definition 4 A triangle is *tall* – denoted T – with respect to a given cluster if the inequality

$$l_1 < l_2 \Leftrightarrow \rho_1 < \rho_2 \quad (170)$$

holds. It is *flat* – denoted F – if the inequality

$$l_1 > l_2 \Leftrightarrow \rho_1 > \rho_2 \quad (171)$$

holds instead.

Remark 10 Barbour calls very tall configurations ‘*needles*’, while Kendall refers collectively to near-collinear configurations uniformly (bereft of distinct two-tail quantification of tall or flat content) as ‘*splinters*’ [43]. This leaves us needing a specifically very flat (including highly bilaterally symmetric) conceptual name: *pickaxe heads* (paralleling [90, 93], which also use *spear head* in place of ‘*needle*’.) See Fig 22.a) for the diversity of types of splinter, and Fig 22.b) for where these are located in the shape sphere. Kendall furthermore devised [43, 62] statistical tests for splinters as configurations of approximately-collinear triples of points, by which his treatment of splinters is a valuable quantitative prototype of Shape Statistics.

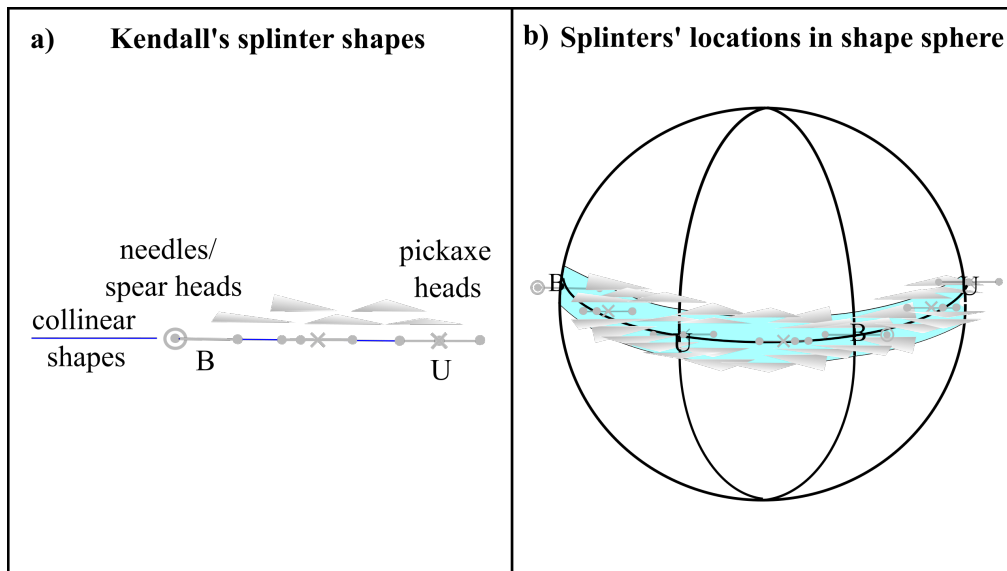


Figure 22: a) Types of splinter shapes, and b) where they are to be found in the triangleland shape sphere.

Remark 11 The halfway shape H for (3, 2) corresponds to

$$H = C \cap R . \quad (172)$$

This notion moreover indeed corresponds to Part I's (3, 1) notion of H shape.

Remark 12 See Fig 23 for a topological-level diagram of how this subsection's notions fit together.

12.4 Jacobian recharacterization of right, acute and obtuse

While we have already characterized rightness in Lagrangian terms, it turns out to admit a shape-theoretically useful Jacobian reformulation as follows.

Proposition 1 Right triangles are those for which

$$\frac{R_2}{R_1} = \frac{1}{2} \Leftrightarrow \frac{\rho_2}{\rho_1} = \frac{1}{\sqrt{3}} \Leftrightarrow \frac{l_2}{l_1} = \frac{1}{3} . \quad (173)$$

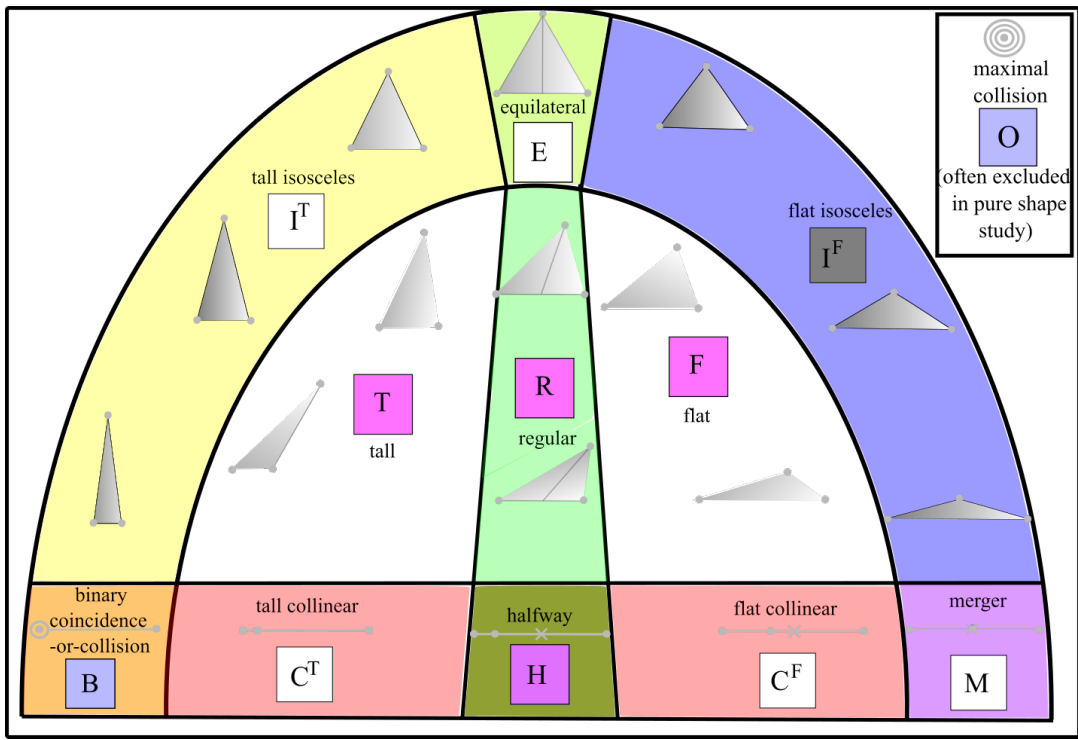


Figure 23: Shape-space-topological-manifold-level diagram for combined metric Lagrangian-and-Jacobian relative separation shapes-in-space. In Sec 15, we justify that this combination further merits the further name of Hopf structure.

Proof The angle subtended by a diameter is right. Reformulate as the median protruding from the right angle having the same length as half of the opposite base. This is in plain rather than mass-unweighted space, giving the first equation. The second then follows from mass weighting as per (I.34), and the third by squaring. \square

Remark 1 The second sentence is principle 5 of Chapter 5 of [28]; Proposition 1 boils down to pinning a Jacobian interpretation on this result.

Corollary 1 Acuteness and obtuseness are then characterized in Jacobian terms by the following inequalities:

$$\frac{R_2}{R_1} > \frac{1}{2} \Leftrightarrow \frac{\rho_2}{\rho_1} > \frac{1}{\sqrt{3}} \Leftrightarrow \frac{l_2}{l_1} = \frac{1}{3}, \quad (174)$$

and

$$\frac{R_2}{R_1} < \frac{1}{2} \Leftrightarrow \frac{\rho_2}{\rho_1} < \frac{1}{\sqrt{3}} \Leftrightarrow \frac{l_2}{l_1} = \frac{1}{3}, \quad (175)$$

respectively.

Remark 2 B is a limiting case of rightness, as one of the other angles becomes arbitrarily acute.

Remark 3 There is also a special right-and-regular triangle, which we denote by

$$R^\perp = \perp \cap R; \quad (176)$$

details of this shape can be found in Fig 24.

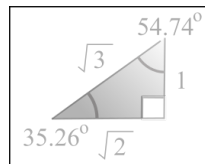


Figure 24: The right-and-regular triangle R^\perp . It has no uniformities of any kind.

Remark 8 Combining the right and regular decor, we have the final topological picture of shape space structure in Fig 25.

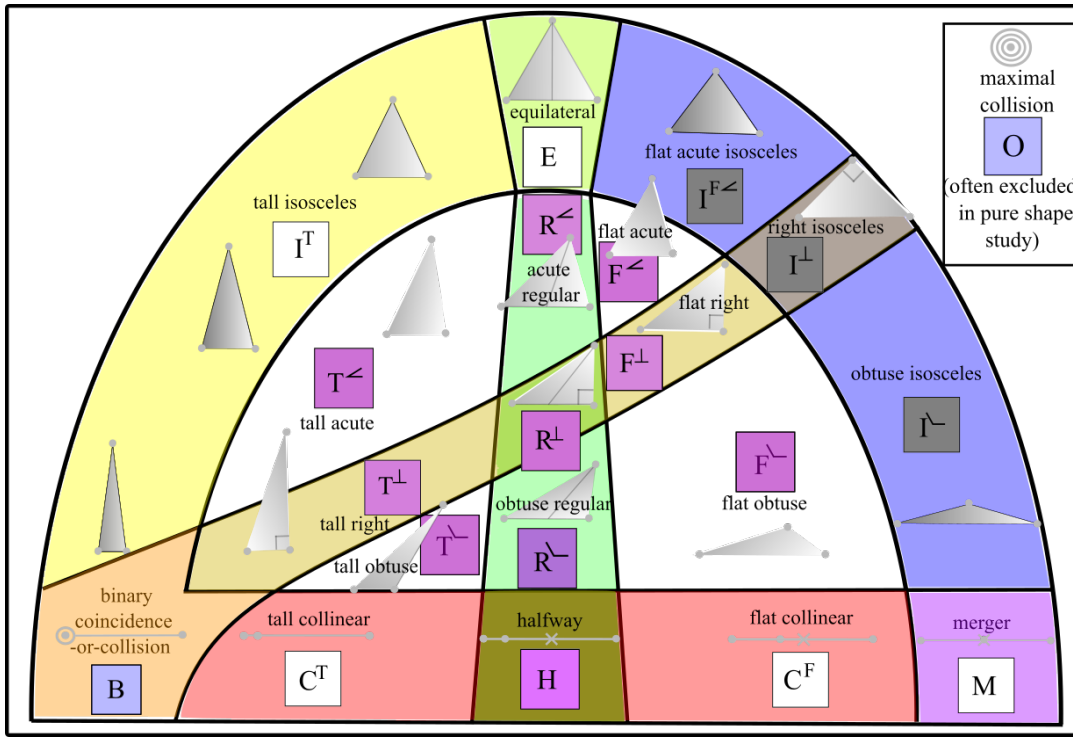


Figure 25: Shape-space-topological-manifold-level diagram of the full metric Jacobian-level shapes-in-space.

13 Jacobi-level analysis of shape space

Remark 1 The R's form 3 bimeridians which intersect E (and \bar{E}). Thus they intersect the three bimeridians of isoscelesness I there as well (Fig 26). By symmetry, the 3 R bimeridians are at $\frac{\pi}{3}$ to each other. They are also midway between the I bimeridians. Thus we have a total of six significant bimeridians through E at $\frac{\pi}{6}$ to each other.

Remark 2 Each clustering choice's bimeridian of regularity R separates the shape sphere into hemispheres of tall and flat triangles (relative to the same clustering).

Proposition 2 The Jacobi-uniform (and Jacobi-symmetric) structure consists of the R bimeridians alongside the I bimeridians (Fig 58).

Remark 3 This forms the same structure as the Lagrangian uniformity structure, except that it is at $\frac{\pi}{6}$ as Lagrange uniformity.

Remark 4 Values at which B and M are that \mathcal{V} sends the non-axial M's to 1 (and the nonaxial B's to 3), used in [125].

Proposition 3 i) The full Lagrange–Jacobi uniformity structure (Fig 29.1) is the orange of 12 segments, alias Zodiac split of the sky.

ii) The full Lagrange–Jacobi structure is the orange of twelve segments cut perpendicularly in half, with three additional cap-circles of rightness which kiss pairwise at the 3 B points.

Remark 5 Together, these intersecting arcs form the topology of the disc with eleven punctures (Appendix B). These intersecting arcs also provide the 'orange of 12 segments' tessellation (not cut in half).

Remark 6 The above discussion has moreover established why there are two notions of isoscelesness split by E: these are *tall isosceles* I^T versus flat isosceles triangles I^F . In this way, regularness R is needed even to finish explaining the features of the shape space distribution of the equilateral E, isosceles I, and scalene S triangles.

Proposition 1 The equilateral triangle E is uniquely characterized in Leibniz space as being

$$E = I \cap R . \tag{177}$$

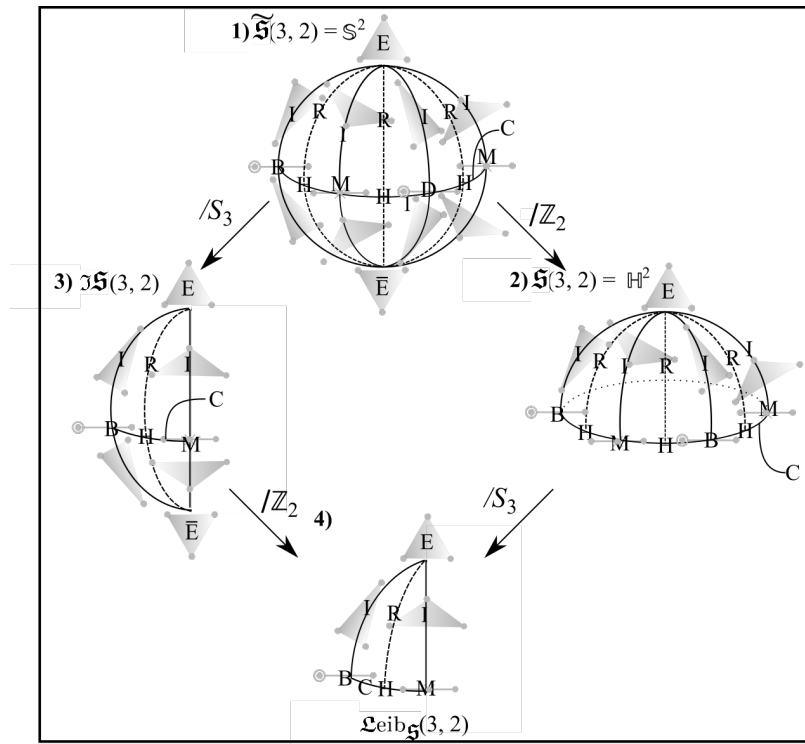


Figure 26: Triangleland configuration spaces at the metric level.

1) The metric-level shape sphere, now including the Hopf equal status collinear C , isosceles I and regular R shapes. The overall pattern is now that of a 12-segmented orange cut in half perpendicular to its segments. The whole and cut-in-half k -segment oranges are the ‘unexceptional’ tessellations of the sphere [34]. Among these, the orange of 12 segments admits the more vivid description as the Zodiac subdivision of the night sky, and this cut in half is the Zodiac split into northern and southern skies.

2), 3) and 4) then give the mirror image identified shape hemisphere, indistinguishable labels lune of width $\frac{\pi}{3}$, and Kendall’s spherical blackboard alias Leibniz space $\mathfrak{Leib}_{\mathfrak{S}}(3, 2)$. The C, I, R decor for these form the northern Zodiac, two star signs’ worth of Zodiac, and two star sign’s worth of northern Zodiac respectively.

Remark 7 Splinters lie near the arc of equator of collinearity, whereas needles can be found at the B end of this and pickaxe heads at the opposite M end.

Remark 8 Together, the Lagrangian and Jacobian separation structure form the topology of the disc with 11 points removed (consult Figs 54 and Fig 58) and are the basis of the ‘orange of 6 segments’ tessellation. The joint uniformity structure is the same minus the coincidence-or-collision points in shape space, which is topologically the same as the symmetry structure. The Lagrangian and Jacobian separation structure alongside collinearity –has the of the disc with 22 points removed (c.f. the same figures). and corresponds to the ‘6-segmented orange cut in half’ tessellation. Note that motivation for considering Lagrangian and Jacobian separations and collinearity together (or pairs thereof) will be greatly enhanced in Sec 15 where these are jointly identified as the Hopf structure.

Remark 9 This is a good point at which to recap that Sec 11.4 contained a shape space level result, namely that diagonalizing the Heron map yields the shape sphere.

13.1 Maximum area per unit moment of inertia plotted over shape space

Proposition 1 i) At the level of shape space, for mirror image identified versions,

$$area_{\max} \text{ is at the equilateral point } E, \quad (178)$$

and

$$area_{\min} \text{ is shared by the whole collinearity arc } C. \quad (179)$$

ii) For the mirror image distinct versions, for the unsigned version of $area$,

$$area_{\max} \text{ is at the equilateral points } E \text{ and } \bar{E}, \quad (180)$$

and its minimum is as above. For the signed version, (178) holds and $area_{\min}$ is at \bar{E} .

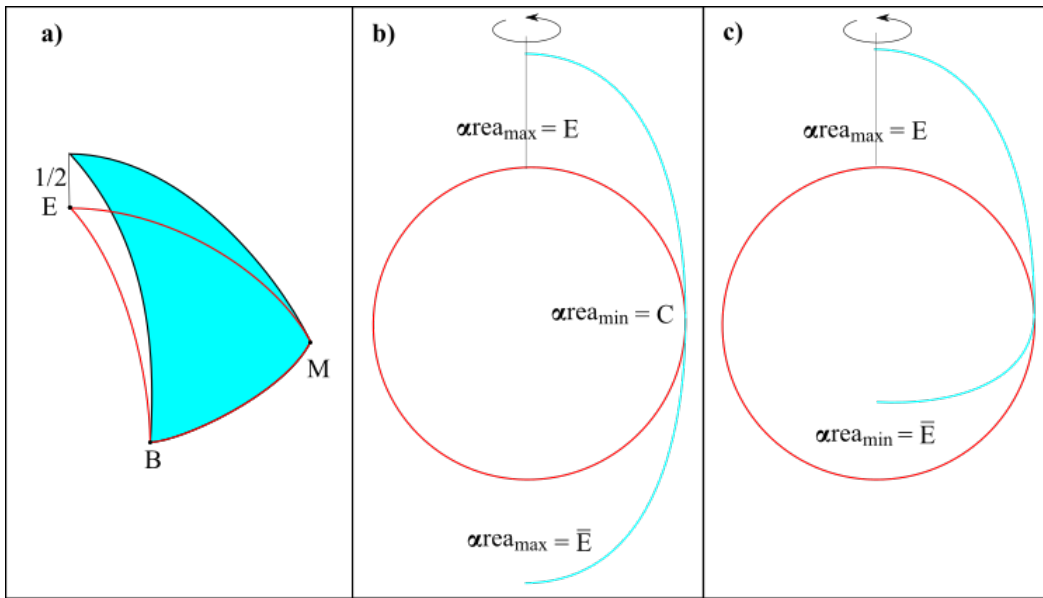


Figure 27: $\alpha_{rea_{max}}$ is the corresponding surface of revolution about the E axis a) on Leibniz space, and b), c) on the shape sphere in the unsigned and signed cases respectively.

Remark 1 This is axisymmetric, as is most easily seen in the EM-axis system:

$$(\text{normalized area}) = \cos \tilde{\Theta} , \quad (181)$$

and Fig 27.

13.2 Completing the main axis systems

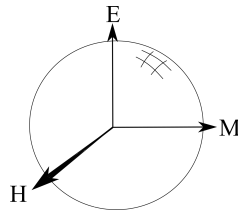


Figure 28: EUH axis system.

Remark 1 $E\bar{E}$ and MB are natural candidates for Cartesian axes for an ambient \mathbb{R}^3 for the triangleland shape sphere. While three different clustering's MB axes are available, only one can be used in any given axis system since they are not perpendicular (being rather at $\frac{2\pi}{3}$ to each other). On the other hand, $E\bar{E}$ is perpendicular to all the UB axes. The final perpendicular direction picks out a HH axis (Fig 28). The incipient Jacobi coordinates pick out the underlying cluster's BM axis as its principal axis, but this axis system can be relabelled so that the unique and more natural $E\bar{E}$ axis is the principal axis.

Remark 2 Following up Sec 10.3, the triangle can moreover be explicitly solved in a straightforward manner in terms of shape space spherical polar data Θ, Φ with UB as principal axis, by using the stereographic–azimuthal relation (I.174) in (I.172). The further passage to shape space spherical data with $E\bar{E}$ principal axis remains analytic, albeit with somewhat more elaborate formulae.

13.3 Spherical, Legendre and parabolic-type variables

Remark 1 Let us first recollect that the azimuthal spherical angle Θ is related to the mass-weighted relative Jacobi separations ratio

$$\mathcal{R} = \frac{\rho_2}{\rho_1} \quad (182)$$

by

$$\mathcal{R} = \tan \frac{\Theta}{2}. \quad (183)$$

In shape space geometry terms, \mathcal{R} is moreover the stereographic radius.

Definition 1 Another useful variable in the study of spherical geometry is the *Legendre variable* [13]; this features for instance in simplifying the azimuthal part of the (now triangle-land shape) spherical harmonics equation [79, 89]. The shape sphere realization of this relative to the UEH axis system is

$$\mathcal{X} := \cos \Theta = \text{ellip}. \quad (184)$$

Lemma 1 Thus its relation to \mathcal{R} and to the ρ_i is

$$\text{ellip} = \mathcal{X} = \frac{1 - \mathcal{R}^2}{1 + \mathcal{R}^2} = \frac{\rho_1^2 - \rho_2^2}{\rho_1^2 + \rho_2^2}. \quad (185)$$

The first of these forms moreover inverts to

$$\mathcal{R} = \sqrt{\frac{1 - \mathcal{X}}{1 + \mathcal{X}}} = \sqrt{\frac{1 - \text{ellip}}{1 + \text{ellip}}}. \quad (186)$$

Definition 2 The Legendre variable corresponding to the EUH axis system is

$$\tilde{\mathcal{X}} := \cos \tilde{\Theta} = \tau. \quad (187)$$

Remark 2 While this has the added virtues of being democratic and closely related to the intuitive area variable, its link to the relative variables is less direct.

Remark 3 At the level of relational space, each of (ℓ, Θ, Φ) and $(\ell, \tilde{\Theta}, \tilde{\Phi})$ constitute spherical polar coordinates.

Remark 4 The incipient relational coordinates (ρ_1, ρ_2, Φ) of Fig I.19.a), on the other hand, turn out to be closely related to *parabolic coordinates* [14]:

$$(\xi_1, \xi_2, \Phi) := (\sqrt{2}\rho_1, \sqrt{2}\rho_2, \Phi). \quad (188)$$

This is the way that the base-and-apex alias side-and-corresponding-median split is encoded into the mathematics of triangle-land.

13.4 Solving the triangle in terms of shape space spherical polar data

From (107),

$$\frac{b_{\pm}}{a} = \sqrt{\frac{2 - \cos \Theta \pm \sqrt{3} \sin \Theta \cos \Phi}{1 + \cos \Theta}}, \quad (189)$$

whereas from (112),

$$\cot \gamma_{\pm} = \frac{1}{\sqrt{3}} \operatorname{cosec} \Phi \cot \frac{\Theta}{2} \pm \cot \Phi \quad \text{and} \quad (190)$$

$$\cot \alpha = \frac{1}{2} \operatorname{cosec} \Phi \left(\sqrt{3} \tan \frac{\Theta}{2} - \frac{1}{\sqrt{3}} \cot \frac{\Theta}{2} \right) = \frac{1 - 2 \cos \Theta}{\sqrt{3} \sin \Theta \sin \Phi}. \quad (191)$$

13.5 Hopf-level count of qualitative types

We firstly consider this without rightness, since this case will later become geometrically significant as the Hopf structure (Sec 15).

Remark 1 This has $V = 4$ types of special vertices: E, B, M, and H.

Remark 2 This also has $E = 5$ edges: I^T, I^F as before, a new R and the C^T, C^F subdivision of the M arc.

Remark 3 Finally, there are now $F = 2$ faces: the tall T and flat F subdivision of the scalene triangles S.

Remark 4 These vertices, edges and faces can be located, and counted off, as per Fig 29.b).

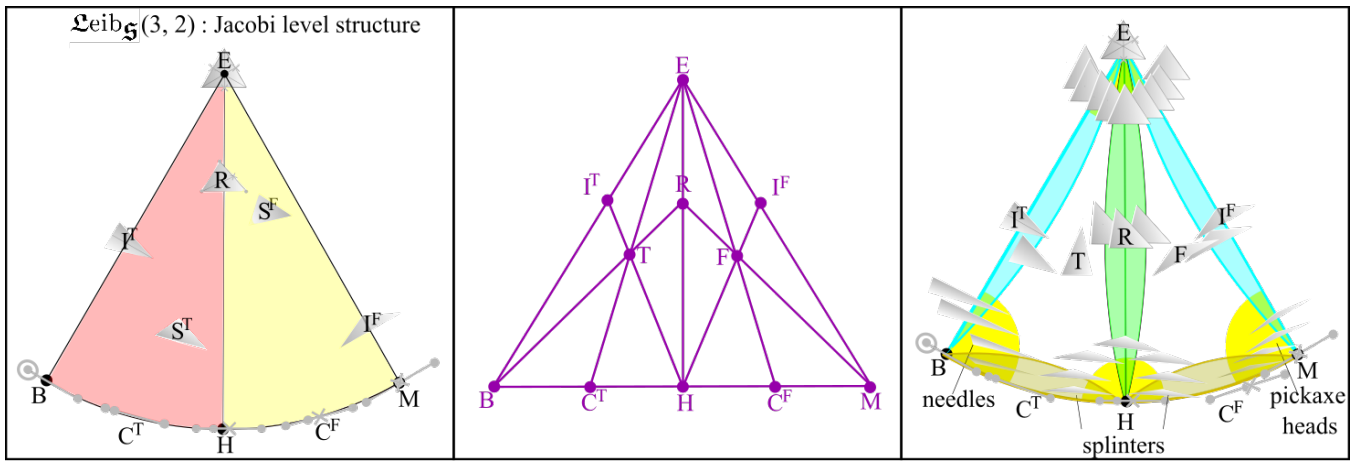


Figure 29: a) Metric-level detail of the shape space $\mathfrak{Leib}_S(3, 2)$ marking what will be identified as the Hopf-level metric shapes-in-space.
 b) Corresponding adjacency graph.
 c) Corresponding exact and approximate qualitative types.

shape space	$V = G $	$E = e(G)$	F	χ	p	Q	Q_{approx}	Q_{total}	Q_{Approx}	Q_{Total}
$\mathfrak{Leib}_S(4, 1)$	4	5	2	1	4	11	22	34	33	45
$\mathfrak{S}(4, 1)$	5	8	4	1	4	17	40	64	57	81
$\mathfrak{S}(4, 1)$	13	24	12	1	12	49	120	192	169	241
$\mathfrak{S}(4, 1)$	14	36	24	2	0	74	216	360	290	434

Figure 30: Number of qualitative types including the full Jacobian decor. Note that the first and fourth of these are the same as for the full Lagrangian decor, due to underlying isomorphic graphs. The second row's graph is isomorphic to the 4-wheel, W_4 .

Remark 5 Thus the number of exact qualitative types is

$$Q := V + E + F = 4 + 5 + 2 = 11 . \quad (192)$$

Remark 6 The adjacency graph 29.b) has $V(\text{Adj}) = Q = 11$ and $E(\text{Adj}) = 12$ by being isomorphic to Sec 9's graph.

Remark 7 See Figs 54–56 for an end-summary of special arcs and special points among the (3, 2) shapes. See Fig 30 for further counts of qualitative types in the four (3, 2) shape spaces, as exhibited in Fig 37 in the case of Leibniz space.

13.6 Centre of Mass rigidity in triangles

Hierarchical excess is interestingly trivial for triangle-land; see Part IV for its further nontriviality for quadrilateral-land.

Theorem 0 (Median Concurrence Theorem.) A triangle's three medians meet at a point.

Remark 1 This is elementary geometry, and also clear in the context of hanging triangles from each vertex. The concurrence point is the total CoM. While perhaps more often stated for triangular laminae, this result also holds in the constellational context of equal-mass points at each vertex.

Remark 2 This takes the form of the below constellation clumping hierarchy reinterpretation (see also Fig 32) of the following geometrical result already known to Euclid as a basic consequence of the Parallel Postulate.

Theorem 1 For any triangle figure in general position (rather than collinear or with coincidences), the midpoints of the sides form a similar triangle to that of the points, reflected and of half the size.

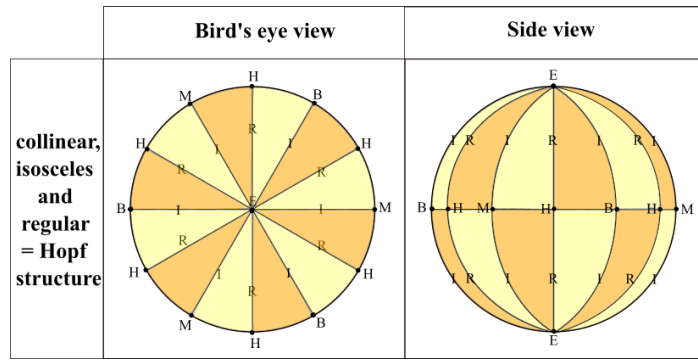


Figure 31: The Hopf structure's 12-segment orange cut in half, alias Zodiac split into northern and southern skies. The bird's eye view of this presents a clock face.

Theorem 2 The total centre of mass of three point masses is at the intersection of the three medians of the triangle formed by the points.

Theorem 3 The 2-particle CoMs form a similar triangle, reflected, of half the size. The total CoM is then at the common centroid of these two similar triangles.

Remark 3 This is a rigidity result: it says that there is no capacity for extra coincidences in CoM hierarchy for 3 particles in nondegenerate positions in $2-d$. For degenerate – collinear – shapes, however, $U(3, 1)$ offers the only way out.

Remark 4 Like $(3, 1)$, triangleland still only has one M notion corresponding to one M-point. But this is no longer aligned with the maximal U. So we need to discern between these two simplifying features.

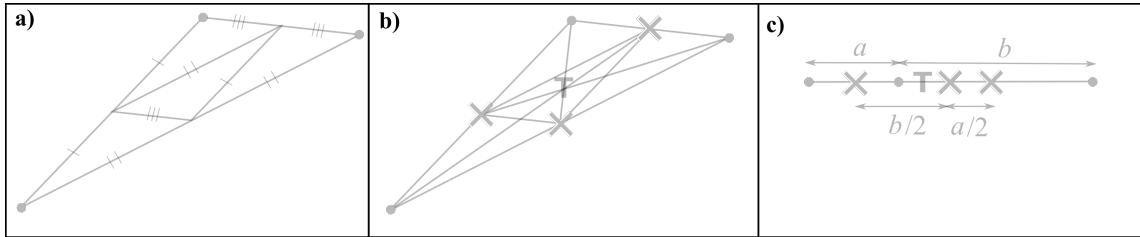


Figure 32: a) A theorem of Euclid.

b) Its slight extension and reformulation in CoM terms.

c) The collinear limit of this then recovers the $(3, 1)$ CoM hierarchy rigidity result, by which there is just one M shape for $(3, 1)$. This recovers Part I's result (previously featuring in Fig I.34).

Remark 5 We now recognize the $(3, 1)$ result of Fig I.34. While this theorem is usually stated for a general position triangle, it also holds for collineations and for coincidences-or-collisions.

Remark 6 We already know (from Part I) that for triangleland, parallelism always reduces to collinearity. Moreover, the only a priori distinct pure-Jacobi possibilities – self- or mutual base–median collinearity and median–median mutual collinearity – just reduce to the usual notion of collinearity. Part IV's quadrilaterals however suffice for some of these other cases to become nontrivial.

Remark 6 Secondly, once collinear, T can coincide with a P. If this happens, it must additionally coincide with an X, according to 'if particle 3 is at $\text{CoM}(12)$, then $\text{CoM}(123)$ coincides with these'. So constellations of 3 possess precisely one merger configuration, which is collinear and a fortiori M.

Remark 7 A further useful $2-d$ insight is to look for not just coincidences of particles and CoMs, but also for collineations of such (and eventually for right angles between such collineations).

Remark 8 Geometry's side midpoints are rephrased as the equal-masses 3-body problem's binary centres of mass. By this, another form of Theorem 1 is as follows.

Theorem 1' the binary centres of mass of any 3-point constellation form a similar constellation.

This is to be augmented as follows by the simple observation of where the total CoM is, and consequent collineations.

Theorem 1'' The binary centres of mass of any 3 point constellation form a similar constellation, with the centres of the two coincident and giving the position of the total centre of mass. Thus any constellation in G has a) three PXP collineations, b) three PTP collineations and c) three XTX collineations. All of b) and c) moreover intersect at T, and the angles between the three PP's are the same as those between the three XX's by Theorem 1.

This means that none of these features are remarkable when examining more special triangles such as isosceles, equilateral, right or regular, since *any* triangle has these features.

Remark 9 these coincidences determine where all the X's and the T are in relation to the three P's. This leaves no room for any excess clustering.

13.7 Rightness, obtuseness and acuteness in shape space

We now address the question of where in the shape sphere the right triangles are located.

Theorem 1 [54, 100, 112] The right triangles form three equal cap-spheres, each with azimuthal coordinate $\frac{\pi}{3}$ about the corresponding U point. These kiss at each B point.

Proof Begin with Fig 14.c)'s 1 : 2 ratio. Reinterpret the hypotenuse as R_1 and the corresponding median as R_2 , to obtain (173)'s Jacobi-magnitude and mass-weighted Jacobi magnitude ratios. Combining with the definition (182) of \mathcal{R} and its relation to Θ (183), this gives

$$\tan \frac{\Theta}{2} = \mathcal{R} = \frac{1}{\sqrt{3}}. \quad (193)$$

Thus, inverting,

$$\Theta = 2 \arctan \frac{1}{\sqrt{3}} = 2 \times \frac{\pi}{6} = \frac{\pi}{3}. \quad (194)$$

This is sketched in Fig 33.a) for one cluster choice's cap-circle of rightness. Repeat for each of the three clusters to obtain three cap-circles. Each is centred about the corresponding U-point pole, and kisses the other two at the two B points which are not antipodal to that U-point: *kissing cap-circles of rightness* as viewed in Fig 33.b-e) from a variety of directions. \square

Remark 1 In terms of the useful variable \mathcal{V} , the rightness condition comes out in the normalized form $\mathcal{V} = 1$; this geometrically underlies why \mathcal{V} is a useful variable.

Remark 2 The regions outside of these caps are acute, as seen e.g. from the observation that the equilateral triangles E residing at the poles are outside of these caps and are acute, and then applying a continuity argument. Conversely, the interiors of the caps are the obtuse triangles, so we term the caps themselves the *kissing caps of obtuseness*. There being three caps is commensurate with there being three ways a labelled triangle can be obtuse.

Remark 3 This cycle of pairwise-kissing circles can be deformed at the topological level by lengthening one attachment point to make the 3-finger knuckleduster. In turn, this can be deformed by dragging one of the lengthening's endpoints across to the same circle as the other endpoint. This forms the 4-bouquet: a topologically standard structure within the scope of Fig 57. This figure moreover shows this to be the deformation retract of the genus-2 surface. Alternatively, one can pass to the disc with 4 punctures and furthermore to the sphere with 5 punctures (both of these are also in Fig 57). On these grounds, the set of rightness has a well-understood general and algebraic topology.

Remark 4 Overall, the shape sphere is split into three lunes of width $\frac{2\pi}{3}$, 1 per cluster with equator-centred caps cutting each into three. Here clockwise and anticlockwise obtuse triangles are back-to-back about the equator with clockwise and anticlockwise acute disconnected from each other.

Remark 5 Noting the tall isosceles lines (Fig 10), the acute regions of the shape sphere are also tripartitioned.

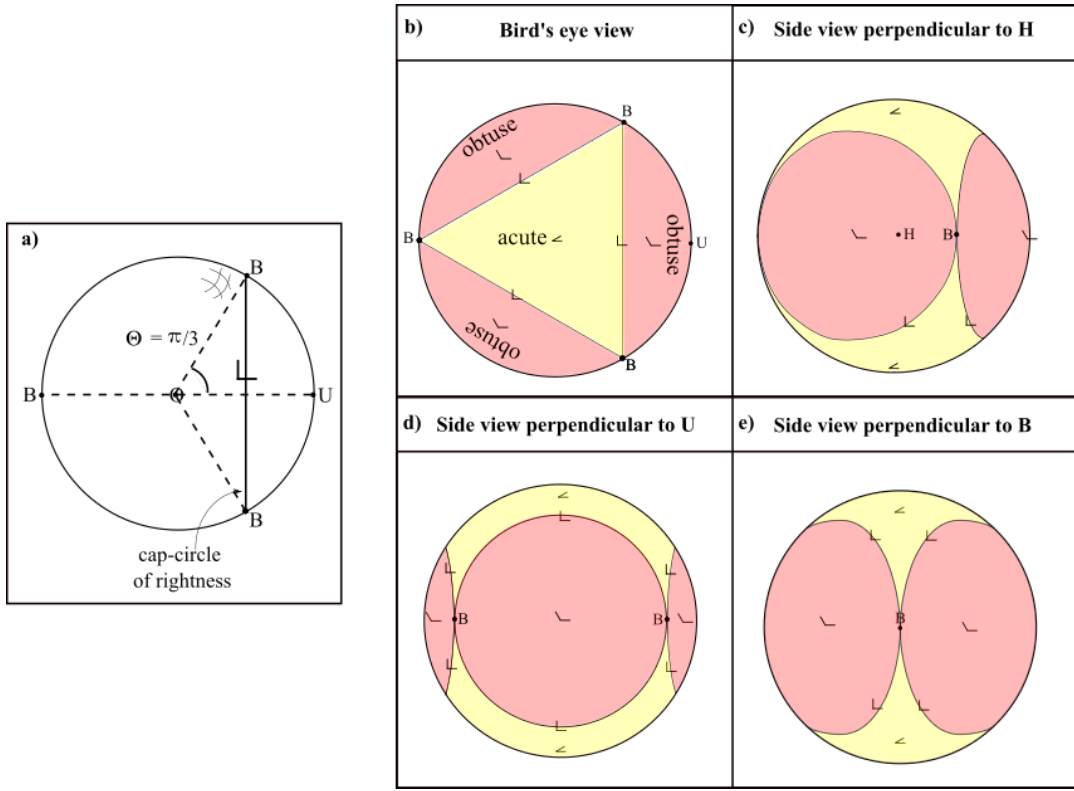


Figure 33: a) A given labelling of right triangles corresponds as indicated to a cap-circle of constant azimuthal value $\frac{\pi}{3}$.
b)-e) Kissing cap-circles of rightness, bounding kissing caps of obtuseness (shaded red), as viewed from various directions.

Remark 6 See row 1 of Fig 17 for the shape space decorated with the circles of rightness only, and rows 2 and 3 for the inter-relation between these and the meridians of isoscelesness and the equator of collinearity.

13.8 Full Jacobi analysis of qualitative types for triangles

We now include rightness so as to analyze the qualitative types for the full Jacobian structure. This combines the right and regular structure (Fig 34).

Remark 1 This case has $V = 6$ vertices: E, B, M, H, I^\perp and R^\perp .

Remark 2 It also has $E = 9$ edges: I^T, C^T, C^F as before, a further subdivision $I^{F<}, I^{F\setminus}$ of I^F , a further subdivision $R^{<}, R^{\setminus}$ of R , and new edges T^\perp and F^\perp .

Remark 3 It finally has $F = 4$ faces: the (tall and flat) \times (acute and obtuse) quartering of the scalene triangles, giving $T^{<}, F^{<}, T^{\setminus}$ and F^{\setminus} .

Remark 4 These vertices, edges and faces can be located, and counted off, as per Fig 36.a).

Remark 5 Thus there is a total of

$$Q := V + E + F = 6 + 9 + 4 = 19 . \quad (195)$$

exact qualitative types in Leibniz space with full Jacobi decor.

Remark 6 In the adjacency graph of Fig 36.b), $V(\text{Adj}) = Q = 19$ and $E(\text{Adj}) = 44$. This graph is moreover three 6-wheels W_6 and one 8-wheel W_8 joined cyclically, with one shared central vertex and four pairs of shared vertices. Thus

$$E(\text{Adj}) = 3 \times 12 + 16 - 4 \times 2 = 44 . \quad (196)$$

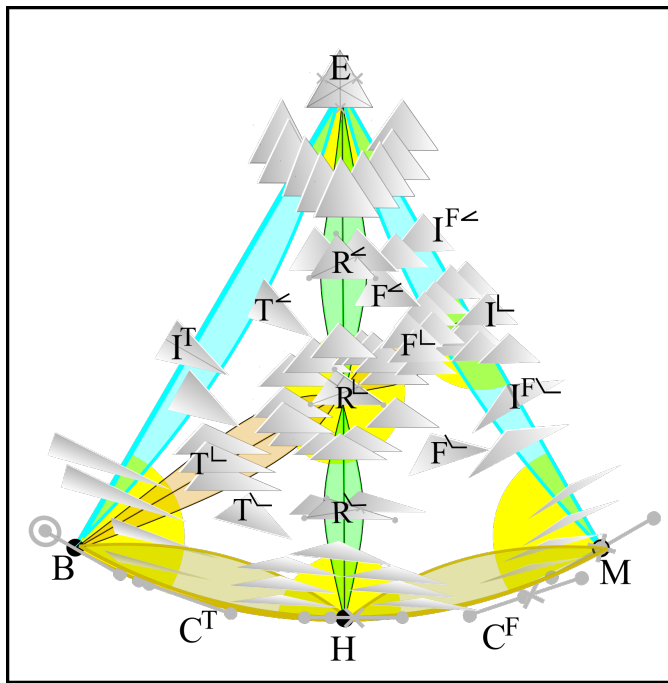


Figure 37: Exact and approximate qualitative types of triangles at the full Jacobian level of structure.

13.9 Shape space centres

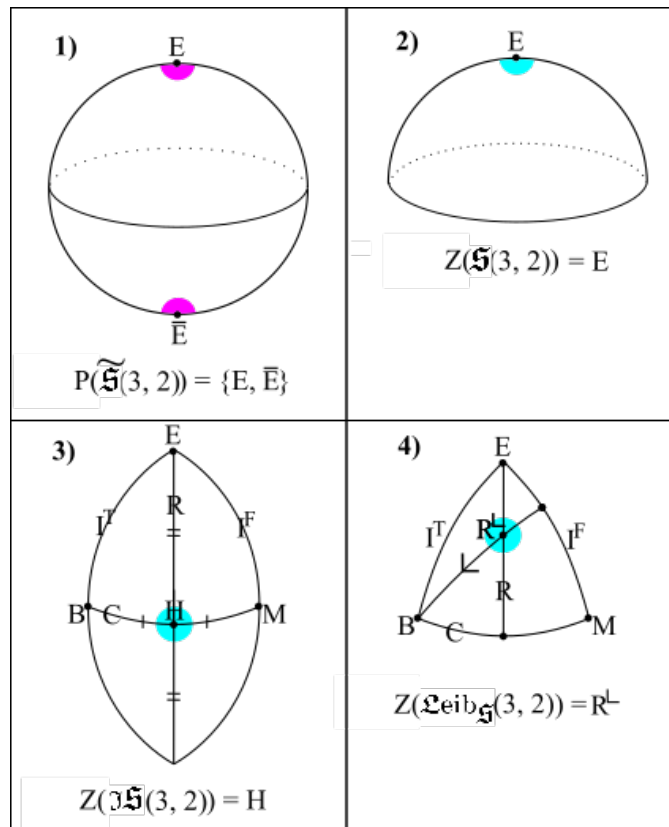


Figure 38: Shape space centres Z for the various trianglelands; P denotes poles.

Observation 1 $\mathfrak{F}(3, 2)$ has a single centre, $Z(\mathfrak{F}(3, 2)) = E$ (Fig 38.2).

Observation 2 On the other hand, $\tilde{\mathfrak{F}}(3, 2)$ has two centres: the equilateral triangles at the poles (Fig 38.1). Having two centres is an indication of being a double cover.

Observation 3 $H = Z(\mathfrak{J}\mathfrak{F}(3, 2))$ is the indisputable centre of $\mathfrak{J}\mathfrak{F}(3, 2)$, due to this possessing two perpendicular lines of symmetry, R and C, which intersect at H (Fig 38.3).

Observation 4 In $\mathfrak{L}\text{eib}_{\mathfrak{F}}(3, 2)$, however, E is a vertex. $\mathfrak{L}\text{eib}_{\mathfrak{F}}(3, 2)$ is moreover an isosceles spherical triangle, so its notions of centre must lie on its line of symmetry, the semimeridian R. The point H – also on the R meridian – however features just as an edge midpoint for $\mathfrak{L}\text{eib}_{\mathfrak{F}}(3, 2)$, so it is not available as a shape-theoretic centre for $\mathfrak{L}\text{eib}_{\mathfrak{F}}(3, 2)$. Thus E and H are not available as a notion of centre. We then suggest the intersection of \perp and R to be a shape theoretically significant notion of centre (Fig 38.4).

13.10 The maximal angle flow

The current treatise's first new result is that the maximal angle curves on the shape sphere are underlied by the following constant-angle curves.

Theorem 2 The curves of constant angle

$$\alpha \neq \frac{\pi}{2} \tag{197}$$

– the angle defined in Fig 4 – are given by

$$\Phi = \arcsin\left(\frac{1 - 2 \cos \Theta}{\sqrt{3} k \sin \Theta}\right) = \arcsin\left(\frac{1 - 2 \mathcal{X}}{\sqrt{3} k \sqrt{1 - \mathcal{X}^2}}\right). \tag{198}$$

where

$$k := \cot \alpha. \tag{199}$$

(See [115] for a proof.)

Remark 1 We sketch and interpret the maximal- α curves that follow from these constant- α curves in Fig 39. Note that the kissing cap-circles of rightness recur within this flow as a separatrix. See [115] for further analysis and discussion of this flow.

14 Some new results concerning random triangles

14.1 Probability that a triangle is obtuse

Corollary 1

$$\text{Prob}(\text{obtuse}) = \frac{3}{4}, \text{ so, complementarily } \text{Prob}(\text{acute}) = \frac{1}{4}. \tag{200}$$

Proof Each cap of obtuseness contributes an area (or more basically, surface of revolution) integral⁶

$$\int_{\Phi=0}^{2\pi} \int_{\Theta=0}^{\frac{\pi}{3}} \sin \Theta \, d\Theta \, d\Phi = 2\pi \int_{\Theta=0}^{\frac{\pi}{3}} \sin \Theta \, d\Theta = 2\pi [-\cos \Theta]_{\Theta=0}^{\frac{\pi}{3}} = 2\pi \left(-\frac{1}{2} + 1\right) = \pi. \tag{201}$$

Thus, between them, the three caps of obtuseness contribute an area of 3π . On the other hand, the area of the whole 2-sphere is 4π , so

$$\text{Prob}(\text{obtuse}) = \frac{3\pi}{4\pi} = \frac{3}{4}. \tag{202}$$

Finally, complementarily

$$\text{Prob}(\text{acute}) = 1 - \text{Prob}(\text{obtuse}) = 1 - \frac{3}{4} = \frac{1}{4}. \square \tag{203}$$

Remark 1 This answer is in the context of interpreting the question's probability distribution to be the *uniform* one on the corresponding shape space, as equipped with the standard spherical metric that Kendall [38, 43, 62] showed to be natural thereupon. The uniqueness of this metric is furtherly intuitively obvious from its being induced as a

⁶Archimedes gave an even more basic derivation for the area of a spherical cap, by which Calculus could be avoided altogether in this derivation.

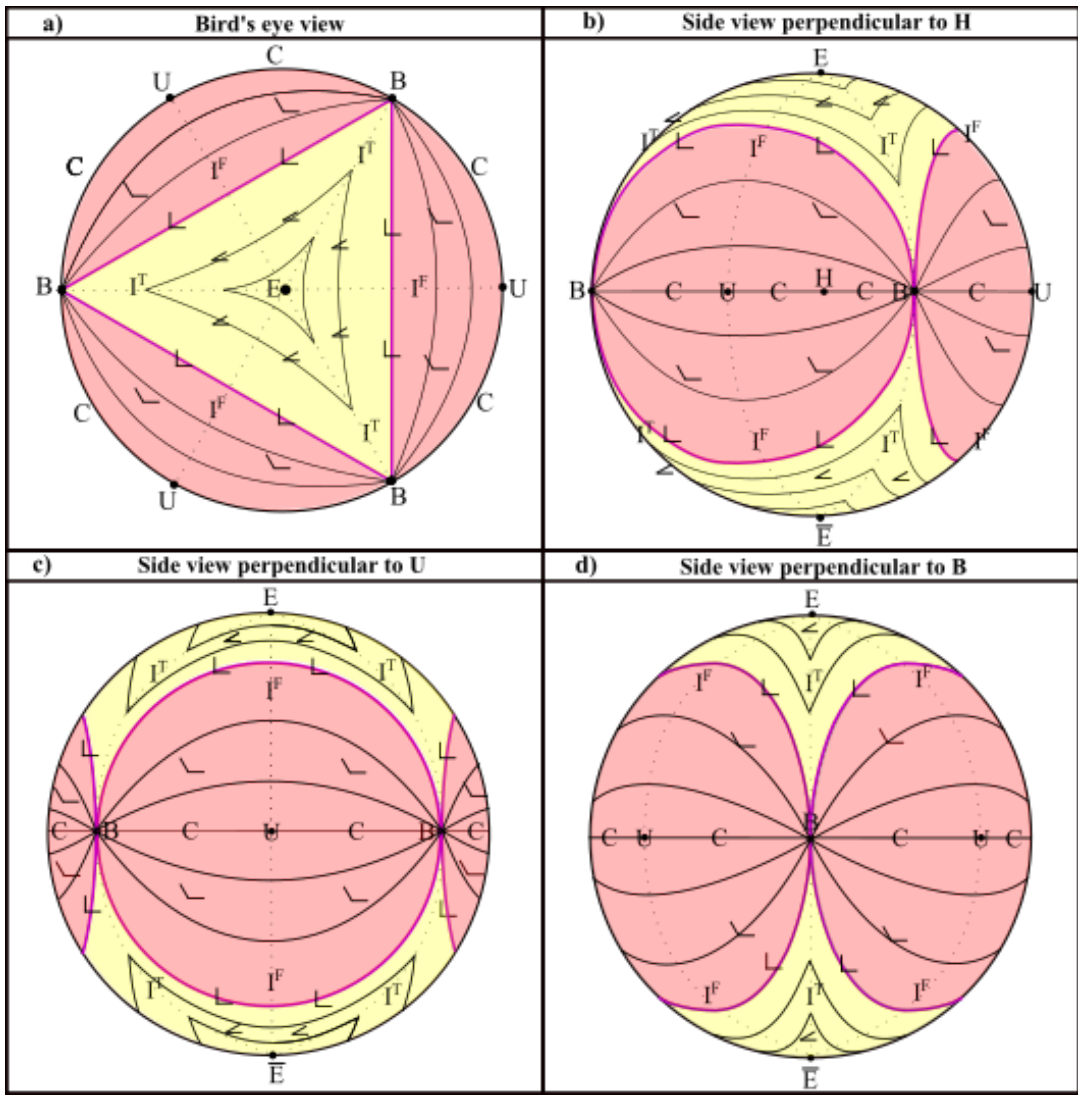


Figure 39: The maximal angle flow over the shape sphere of triangles as seen from various directions. The kissing cap-circles of rightness separatrix is highlighted in indigo, with the two qualitatively different types of region separated by this shaded in red and yellow. The dotted lines indicate alignments of cusps and of stationary points.

quotient of a simpler structure (position space or relative space: flat spaces), or from its arising correspondingly by reduction of the corresponding mechanical actions.

Also note that $\frac{3}{4}$ is in fact one [49, 50] of the more common answers to Lewis Carroll's pillow problem, now obtained moreover on shape-theoretic premises. Small [54] and Edelman and Strang [100] obtained this result using Kendall's Shape Theory, while [112] gave a simplified proof along the lines provided above. In conjunction with various elementary derivations of Kendall's shape sphere [112, 132], this reduces the shape-theoretic answer to Lewis Carroll's pillow problem to just elementary algebra and (pre)calculus. This renders it open, both to anybody studying STEM subjects at University (or even High School in many countries) and also to considerable generalization to a whole class of geometrical problems, of which [112], the current treatise and [124] provide the first few.

Remark 3 See also [49, 50] for various other answers' values for Prob(Obtuse), and a general principle behind the methods which share the answer $3/4$ being called for. Shape Theory as per above surely provides a principle, though whether *all* known methods which yield $3/4$ can be shown to follow from this shape-theoretic principle is left as a good topic for a further paper.

14.2 Probability that an isosceles triangle is obtuse

Example 1) Let us next pose and solve a further pillow problem variant that requires no further definitions,

$$\text{Prob}(\text{Obtuse} \mid \text{Isosceles}) = \frac{\text{length}(I^{\angle})}{\text{length}(I)} = \frac{\frac{\pi}{3}}{2 \times \frac{\pi}{2}} = \frac{1}{3}, \quad (204)$$

using that I^{\perp} is $\frac{\pi}{3}$ along the I^F semi-meridian. Then complementarily

$$\text{Prob}(\text{Acute} \mid \text{Isosceles}) = 1 - \text{Prob}(\text{Obtuse} \mid \text{Isosceles}) = \frac{2}{3}. \quad (205)$$

14.3 Probability that a tall triangle is obtuse, and related examples

Remark 1 It is clear in shape space from the bimeridians of regularity running along the line of reflection symmetry of the minimum cell in shape space (the 1/6th hemisphere bounded by arcs of isoscelesness and collinearity) that

$$\text{Prob}(\text{Flat}) = \frac{1}{2} = \text{Prob}(\text{Tall}). \quad (206)$$

So introducing tallness and flatness *by themselves* do not prompt further interesting variants of the pillow problem. Statements combining tallness or flatness with isoscelesness or with acuteness and obtuseness, however, do make for interesting variants, as follows.

Remark 2 Given that we know $\text{Prob}(\text{Obtuse})$ and $\text{Prob}(\text{Flat})$, the following four probabilities have only one degree of freedom between them, so they form a connected quadruple of pillow problems, as follows.

What are $\text{Prob}(\text{Acute and Tall})$, $\text{Prob}(\text{Acute and Flat})$, $\text{Prob}(\text{Obtuse and Tall})$, and $\text{Prob}(\text{Obtuse and Flat})$?

Remark 3 Upon evaluating these, we can furthermore answer conditioned questions along the following lines.

What are $\text{Prob}(\text{Acute} \mid \text{Flat})$, $\text{Prob}(\text{Acute} \mid \text{Tall})$, $\text{Prob}(\text{Obtuse} \mid \text{Flat})$ and $\text{Prob}(\text{Obtuse} \mid \text{Tall})$?

Conditioning conversely, what are $\text{Prob}(\text{Flat} \mid \text{Acute})$, $\text{Prob}(\text{Flat} \mid \text{Obtuse})$, $\text{Prob}(\text{Tall} \mid \text{Acute})$ and $\text{Prob}(\text{Tall} \mid \text{Obtuse})$?

Remark 4 Finally, we also consider the complementary pairs $\text{Prob}(\text{Isosceles is Flat})$ and $\text{Prob}(\text{Isosceles is Tall})$, $\text{Prob}(\text{Right is Flat})$ and $\text{Prob}(\text{Right is Tall})$, and $\text{Prob}(\text{Regular is Obtuse})$ and $\text{Prob}(\text{Regular is Acute})$.

These are all questions concerning generic triangles, meaning they correspond to regions whose configuration space dimension is maximal, i.e. not lying on C , I , R or \perp .

Remark 5 Our treatment makes use of the *departure from independence*

$$\delta(A, B) := \text{Prob}(A) \text{Prob}(B) - \text{Prob}(A \cap B) \quad (207)$$

of random variables A and B . For our 2×2 -value discrete bivariate joint distributions, this takes a single value, so we can simplify notation from $\delta(A, B)$ to just δ . Formulated in terms of this value, the four probabilities in question are cast in a symmetric form.

Example 1 [112] showed that

$$\delta = 3 \left(\frac{1}{8} - \frac{1}{\pi} \left(\arcsin \sqrt{\frac{2}{3}} - \frac{1}{2} \arcsin \frac{1}{3} \right) \right) \approx 0.0505. \quad (208)$$

In terms of this, moreover,

$$\text{Prob}(F^{\angle}) = \frac{1}{8} - \delta \approx 0.1755, \quad \text{Prob}(T^{\angle}) = \frac{1}{8} + \delta \approx 0.0745, \quad (209)$$

$$\text{Prob}(F^{\setminus}) = \frac{3}{8} + \delta \approx 0.4255, \quad \text{Prob}(T^{\setminus}) = \frac{3}{8} - \delta \approx 0.3245. \quad (210)$$

So $\text{Prob}(T^{\setminus})$ is the most probable and $\text{Prob}(T^{\angle})$ is the least probable, in approximately a 6 : 1 ratio.

Example 1) [112]

$$\text{Prob}(\angle | F) = \frac{1}{4} - 2\delta \approx 0.149, \quad \text{Prob}(\setminus | F) = \frac{3}{4} + 2\delta \approx 0.851, \quad (211)$$

$$\text{Prob}(\angle | T) = \frac{1}{4} + 2\delta \approx 0.351, \quad \text{Prob}(\setminus | T) = \frac{3}{4} - 2\delta \approx 0.649, \quad (212)$$

and

$$\text{Prob}(F | \angle) = \frac{1}{2} - 4\delta \approx 0.298, \quad \text{Prob}(T | \angle) = \frac{1}{2} + 4\delta \approx 0.702, \quad (213)$$

$$\text{Prob}(F | \setminus) = \frac{1}{2} + \frac{4}{3}\delta \approx 0.567, \quad \text{Prob}(T | \setminus) = \frac{1}{2} - \frac{4}{3}\delta \approx 0.433. \quad (214)$$

14.4 Solution of further restricted pillow problem variants

By ‘restricted’, we mean non-generic. The cases considered in particular concern assuming a property that is restricted to lie on an arc (or collection of arcs) on the shape sphere.

Example 1) [112]

$$\text{Prob}(F | \perp) = \frac{\text{length}(F^\perp)}{\text{length}(\perp)} = \frac{2}{\pi} \arcsin \frac{1}{3} \approx 0.2163, \quad \text{and} \quad (215)$$

$$\text{Prob}(T | \perp) = 1 - \text{Prob}(\text{Flat} | \perp) = \frac{\pi - 2 \arcsin \frac{1}{3}}{\pi} \approx 0.7837. \quad (216)$$

$$\text{Prob}(F | C) = \frac{1}{2} = \text{Prob}(T | C) \quad (217)$$

is obvious by reflection symmetry.

Example 2 [112],

$$\text{Prob}(\angle | R) = \frac{\text{length}(R^\angle)}{\text{length}(R)} = \frac{2}{\pi} \arcsin \frac{1}{\sqrt{3}} \approx 0.3918. \quad (218)$$

Complementarily,

$$\text{Prob}(\setminus | R) = 1 - \text{Prob}(\angle | R) = \frac{\pi - 2 \arcsin \frac{1}{\sqrt{3}}}{\pi} \approx 0.6082. \quad (219)$$

14.5 Probability that a triangle is Fermat-acute

$$\alpha_{\max} = \frac{2\pi}{3} \quad (220)$$

is a meaningful critical value as regards Fermat’s problem (Fig 40.a) of which point F minimizes the total distance from itself to a triangle’s three vertices (Fig 40). This is a critical value for Fermat’s problem because for

$$\alpha_{\max} \geq \frac{2\pi}{3}, \quad (221)$$

the Fermat (alias Torricelli) point F is just at the obtuse angle’s vertex (Fig 40.b), whereas for

$$\alpha_{\max} < \frac{2\pi}{3}, \quad (222)$$

the Fermat point F is a nontrivial point in the interior of the triangle (Fig 40.c). These are clearly qualitatively different regimes. On these grounds, we make the following definitions.

Corollary 1 [115] For each cluster i)

$$\text{Area} = 2 \left| \int_{\mathcal{X}=0}^{1/2} d\mathcal{X} \arcsin \left(\frac{1 - 2\mathcal{X}}{\sqrt{3}k\sqrt{1 - \mathcal{X}^2}} \right) \right| \stackrel{\text{Fermat case}}{=} 2 \left| \int_{\mathcal{X}=0}^{1/2} d\mathcal{X} \arcsin \left(\frac{2\mathcal{X} - 1}{\sqrt{1 - \mathcal{X}^2}} \right) \right|. \quad (223)$$

This can moreover be evaluated using Maple [111].

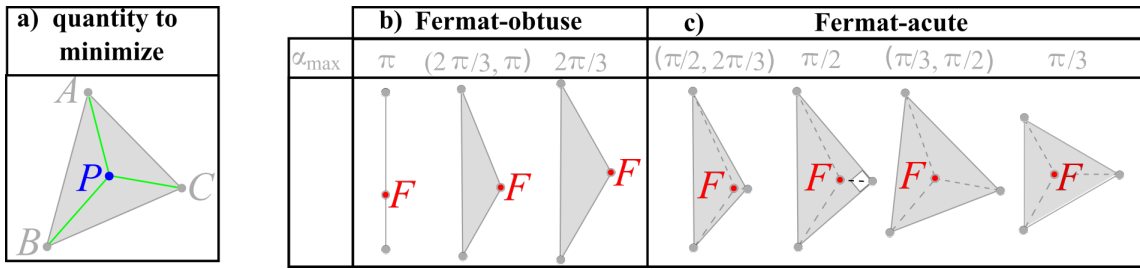


Figure 40: a) Fermat's problem is, given a triangle ABC , to find the position of the point P (in blue) such that the sum of the lengths (in green) from it to the three vertices is minimized. b) This is solved by the Fermat point F (in red), which is moreover just at the obtuse vertex for triangles with $\alpha_{\max} \geq \frac{2\pi}{3}$, which we term Fermat-obtuse. c) On the other hand, the Fermat point F has a nontrivial position for triangles with $\alpha_{\max} < \frac{2\pi}{3}$. In this case, F is such that the vertices are spread out at $2\frac{\pi}{3}$ from each other relative to F , as indicated by the dashed lines. Moreover, for $\alpha_{\max} = \frac{\pi}{3}$, the position of F reduces to just that of the centre of symmetry of the equilateral triangle.

Remark 1 Furthermore, once again normalizing by the total area of the sphere,

$$\text{Prob}(\alpha\text{-obtuse}) = \frac{3 \text{Area}}{4\pi} . \quad (224)$$

Thus

$$\text{Prob}(\text{Fermat-obtuse}) = 0.1394 . \quad (225)$$

Complementarily,

$$\text{Prob}(\alpha\text{-acute}) = 1 - \text{Prob}(\alpha\text{-obtuse}) = \frac{4\pi - 3 \text{Area}}{4\pi} , \quad (226)$$

So

$$\text{Prob}(\text{Fermat-acute}) = 0.8606 , \quad (227)$$

which is the quantity of particular interest due to its correspondence to the triangles whose Fermat points are nontrivially positioned.

15 The Hopf map in the shape-theoretic context

Structure 1 There is a Hopf map from the 3-sphere to the 2-sphere (I.180), which is moreover realized by the reduction from the preshape 3-sphere to the shape sphere. Indeed, this provides a derivation that the triangleland shape space is a sphere.

Remark 1 On the one hand, it is immediately clear in 1- d how to represent $\mathbb{S}^{n-1} = \mathfrak{S}(N, 1) = \mathfrak{P}(N, 1)$ within $\mathcal{R}(N, 1) = \mathfrak{r}(N, 1) = \mathbb{R}^n$. On the other hand, for 3 points-or-particles in $d \geq 2$, such representation is more complicated. While there is a flat relative space $\mathfrak{r}(3, 2)$, this is \mathbb{R}^4 rather than \mathbb{R}^3 . This does not yet account for how to embed a 2-sphere in a flat 4-space in an *equable manner*, i.e. making equal use of each component of $\underline{\rho}_1$ and $\underline{\rho}_2$. One geometrical way of arriving at this answer to this is to concatenate the Hopf map of spheres \mathcal{H}_S with the obvious codimension-1 embeddings of \mathbb{S}^2 and \mathbb{S}^3 :

$$\mathbb{R}^4 \xrightarrow{\text{unit sphere map}} \mathbb{S}^3 \xrightarrow{\text{Hopf fibration (I.159)}} \mathbb{S}^2 \xrightarrow{\text{embedding map}} \mathbb{R}^3 . \quad (228)$$

This forms the ‘extended Hopf map of Cartesian directions’ \mathcal{H}_C .

Remark 2 A somewhat more elegant reformulation: the ‘Hopf Cartesian coordinates map’, \mathcal{H}_C is related to the Hopf spheres map \mathcal{H}_S by the composition of maps

$$\mathcal{H}_C = U_3 \circ \mathcal{H}_S \circ C_2 , \quad (229)$$

as per Fig 41.



Figure 41: a) Hopf map \mathcal{H}_S from \mathbb{S}^3 to \mathbb{S}^2 , including also mapping the natural ambient \mathbb{R}^4 for the \mathbb{S}^3 to a less obviously realized natural ambient \mathbb{R}^3 for the \mathbb{S}^2 by the Hopf Cartesian map \mathcal{H}_C . U_k are here unit vector maps to the k -sphere, and C_k are cone maps from the k -sphere. b) Its shape-theoretic implementation.

Remark 3 As already outlined in Part I, \mathcal{H}_S is realized by the reduction from the preshape 3-sphere to the shape sphere. This and the accompanying metric-level calculation indeed constitutes an elegant derivation that the (3, 2) shape space is a sphere, i.e. of the special case of Kendall’s Theorem that the current Part III of this treatise is built around.

Remark 4 As also already outlined in Part I, this unit sphere map is realized by the reduction of relative space to preshape space, and this embedding map by the coning of the shape space to produce the relational space. This indeed constitutes an elegant derivation that the (3, 2) relational space is topologically \mathbb{R}^3 , though now the metric part of the calculation reveals that this does not carry the flat metric. It is conformally flat (if the maximal collision is excised, since the conformal transformation in question is invalid there).

Structure 2 In this shape-theoretic setting, and with respect to a choice of clustering to define the relative Jacobi coordinates underpinning the $\underline{\rho}_i$, Θ and Φ , the extended Hopf map takes the form given in Fig 42.

Exercise 1 These can be readily checked to obey

$$Hopf_x^2 + Hopf_y^2 + Hopf_z^2 = \iota^2 = (\rho_1^2 + \rho_2^2)^2 = (\rho_{1x}^2 + \rho_{1y}^2 + \rho_{2x}^2 + \rho_{2y}^2)^2 . \quad (230)$$

Structure 3 There is moreover a unit Cartesian direction version of this obtained by dividing each term by ι . Using unit relative Jacobi coordinates, this gives Fig 43.

Exercise 2 The counterpart of (230) now readily gives the on-2-sphere condition

$$hopf_x^2 + hopf_y^2 + hopf_z^2 = 1 . \quad (231)$$

Lemma 1 In terms of the shape-theoretic stereographic radius coordinate

$$hopf_z = \frac{1 - \mathcal{R}^2}{1 + \mathcal{R}^2} , \quad (232)$$

relational space coordinates			relative space coordinates
spherical polar and Cartesian coordinates		parabolic-type coordinates	
E-centred coordinates	B-centred coordinates		
$l \cos \tilde{\Theta} =: \widetilde{Hopf}_z$	$Hopf_x := l \sin \Theta \cos \Phi$	$= 2 \rho_1 \rho_2 \cos \Phi$	$= 2(\rho_1 \times \rho_2)_3$
$l \sin \tilde{\Theta} \sin \tilde{\Phi} =: \widetilde{Hopf}_y$	$Hopf_y := l \sin \Theta \sin \Phi$	$= 2 \rho_1 \rho_2 \sin \Phi$	$= 2 \rho_1 \cdot \rho_2$
$l \sin \tilde{\Theta} \cos \tilde{\Phi} =: \widetilde{Hopf}_x$	$Hopf_z := l \cos \Theta$	$=$	$\rho_1^2 - \rho_2^2$

Figure 42: Here each equation's first forward equality just recasts the Hopf Cartesian coordinates in standard spherical polar coordinates, with the moment of inertia $l = \rho^2$ playing the role of radius. Each equation's second forward equality amounts to the shape-theoretic relations between the ρ_i and l , Θ and Φ . The third forward equality, when present, just incorporates standard basic formulae for dot and cross products. To get parabolic coordinates, just use $\xi_i = \sqrt{2} \rho_i$. Thus Hopf and parabolic coordinates are very closely related. The remaining conceptual leap is to regard the ξ_i as magnitudes of 2 - d vectors, thus passing from relating three squares to the square of two squares to the square of four squares in (230). The first backward equality is a switch of which axis is primary, with the second backward equality then giving the corresponding expression in tilded spherical polar coordinates.

shape space coordinates			preshape space coordinates
spherical and unit Cartesian coordinates		unit parabolic-type coordinates	
E-centred coordinates	B-centred coordinates		
$\cos \tilde{\Theta} =: \widetilde{hopf}_z$	$hopf_x := \sin \Theta \cos \Phi$	$= 2 \nu_1 \nu_2 \cos \Phi$	$= 2\{\nu_1 \times \nu_2\}_3$
$\sin \tilde{\Theta} \sin \tilde{\Phi} =: \widetilde{hopf}_y$	$hopf_y := \sin \Theta \sin \Phi$	$= 2 \nu_1 \nu_2 \sin \Phi$	$= 2 \nu_1 \cdot \nu_2$
$\sin \tilde{\Theta} \cos \tilde{\Phi} =: \widetilde{hopf}_x$	$hopf_z := \cos \Theta$	$=$	$\nu_2^2 - \nu_1^2$

Figure 43: Moment of inertia normalized version of the previous, giving shape variables.

$$hopf_x = \frac{2 \mathcal{R} \cos \Phi}{1 + \mathcal{R}^2}, \quad (233)$$

$$hopf_y = \frac{2 \mathcal{R} \sin \Phi}{1 + \mathcal{R}^2}. \quad (234)$$

Proof Use (I.174) and (92) in rows 1 and 2 of Fig 43. The first of these is also a repackaging of (185). \square

Exercise 3 The reader can furthermore check that these three expressions indeed square to 1.

End-Comment 1 This subsection is well-known and applied in Molecular Physics [55], but has received little attention in Shape Statistics.

15.1 Mirror image identified and indistinguishable versions

Structure 1 The $\mathcal{R}(3, 2)$ case was considered by physicist Alex Dragt in the 1960's [24] in the Molecular Physics literature (see also [18], and [40, 41, 55, 60] for some applications). In this case, $\Phi = 0$ to π or $\tilde{\Theta} = 0$ to $\frac{\pi}{2}$. This case has the advantage of being obligatory in 3 - d to the Hopf case itself being disallowed.

Remark 1 This subsection's Hopf quantities are well-known and applied in Molecular Physics (often under the name of 'Dragt coordinates', but has received little attention in Shape Statistics. The remaining subsections gives further shape-theoretic interpretation and a start on useful applications.

Structure 2 The $\mathcal{J}\mathcal{R}$ case of Hopf-type map is new to the current Part. Here $\tilde{\Phi} = 0$ to $\frac{\pi}{3}$ or $\Phi = 0$ to π and $\Theta = 0$ to $\frac{\pi}{3}$.

Structure 3 The $\mathfrak{L}eib_{\mathfrak{R}}(3, 2)$ case of Hopf-type map – corresponding to Kendall's spherical blackboard from the Shape Statistics literature – is also new to the current treatise. Here, $\tilde{\Phi} = 0$ to $\frac{\pi}{3}$ or $\Phi = 0$ to π and $\Theta = 0$ to $\frac{\pi}{3}$.

This section's Hopf quantities furthermore admit the following lucid shape-theoretic interpretation [79, 89, 108].

15.2 Shape theoretic interpretation of the Hopf-type quantities. I. Tetra-area

Remark 1 $hopf_x$'s shape-theoretic true name is mass weighted 'tetra-area' (per unit moment of inertia), τ . This is moreover a quantifier of noncollinearity, i.e. departure from collinearity.

Remark 2 In shape space, the plane through the origin that is perpendicular to the $\tau = E\bar{E}$ axis is indeed the plane of collinearity, C.

Remark 3 Interpretation using the Heron form in the square root, zero area results from zero semi-perimeter: O, or from semi-perimeter being equal to a side, without loss of generality a :

$$a = s = \frac{a+b+c}{2} \Leftrightarrow a = b+c \Leftrightarrow (\text{triangle inequality is saturated}) \Leftrightarrow \text{degenerate} . \quad (235)$$

Sec 8 showed how Jacobi coordinates cast the similar medians counterpart of Heron's formula in identical functional form.

Remark 4 τ is moreover clustering-independent, i.e. democracy-invariant in the Jacobian sense.

Remark 5 τ is a signed quantifier, with clockwise and anticlockwise configurations contributing positive and negative signs, as per inequalities (147) and (148).

Remark 6 One can moreover define an unsigned version, $|\tau|$, which is insensitive to the clockwise-anticlockwise distinction. The identification $|\tau|$ gives another way of ascertaining that, firstly, the equilateral triangles E and \bar{E} maximize and minimize τ respectively. Secondly, that $|\tau|$ is co-maximized by E and \bar{E} and jointly minimized by the collinear shapes C.

15.3 Shape theoretic interpretation of the Hopf-type quantities. II. Ellipticity

Interpretation 1 The ellipticity $ellip$ is the difference of the two 'normalized' partial moments of inertia involved in the clustering in question: that of the base and that of the median.

Remark 1 In terms of the sides of the triangle,

$$\epsilon llip = \frac{a^2 + b^2 - 2c^2}{3} , \quad (236)$$

whereas, in terms of the side-ratios of the triangle,

$$ellip = \frac{a^2 + b^2 - 2c^2}{a^2 + b^2 + c^2} . \quad (237)$$

These formulae single out the base side of the cluster, so $ellip$ is a cluster-dependent quantity.

Interpretation 2 $ellip$ is a Heron map eigenvector and Cartesian axis direction in relational space.

Interpretation 3 The further intuitive reformulations

$$\epsilon llip = \frac{a^2 + b^2 + c^2}{3} - c^2 = l - c^2 = \langle \text{side}^2 \rangle - (c\text{-side})^2 , \quad \text{and} \quad (238)$$

$$ellip = 1 - \frac{(c\text{-side})^2}{\langle \text{side}^2 \rangle} = \frac{\langle \text{side}^2 \rangle - (c\text{-side})^2}{\langle \text{side}^2 \rangle} , \quad (239)$$

are in terms of what is conceptually a *contrast* object, from the point of view that the democratic average 'is the norm' and thus to be used to normalize. In this way, the Hopf bundle structure provides a natural and significant contrast variable.

Remark 3 Setting $a = b = c$, the numerator is zero for the equilateral triangle, E, but it is not unique as a such.

Interpretation 4 The plane through the origin that is perpendicular to the $ellip = MB$ axis is indeed the plane of regularity, R. Thus $ellip$ is a measure of departure from regularity, R (hence regularity's 'circular' alias in Sec 12.3). $ellip$ is thus conceptually an anisotropy, more concretely a partial moments of inertia or Jacobi anisotropy.

Remark 5 \textit{ellip} is also a signed quantifier, in that it distinguishes between tall and flat departures from regularity (Fig 6.1).

$$\textit{ellip} > 0 \text{ is flat , and} \quad (240)$$

$$\textit{ellip} < 0 \text{ is tall .} \quad (241)$$

Remark 6 One can moreover define an unsigned version, $|\textit{ellip}|$, which is insensitive to the tallness-flatness distinction, by using $|a^2 + b^2 - 2c^2|$ in place of $a^2 + b^2 - 2c^2$.

Remark 7 \textit{ellip} is minimal for B and maximal for M, whereas $|\textit{ellip}|$ is co-maximal for B and M shapes and jointly minimal for all regular triangles, R.

15.4 Shape theoretic interpretation of the Hopf-type quantities. III. Anisoscelesness

Interpretation 1 $\alpha\textit{niso}$ is a a quantifier of ‘anisoscelesness’ departure from being isosceles.

Remark 1 In terms of the sides of the triangle,

$$\alpha\textit{niso} = \frac{a^2 - b^2}{\sqrt{3}} , \quad (242)$$

whereas, in terms of the side-ratios of the triangle,

$$\alpha\textit{niso} = \frac{\sqrt{3}(a^2 - b^2)}{a^2 + b^2 + c^2} = \frac{a^2 - b^2}{\sqrt{3}\langle \textit{side}^2 \rangle} . \quad (243)$$

This is clearly a clustering-dependent notion.

Remark 2 Anisoscelesness compares the remaining 2 sides of the cluster, in which way it is a measure of ‘contents inhomogeneity’ [78, 110] within the given cluster.

Remark 3 $a = b$ – the basic isoscelesness condition – indeed returns zero anisoscelesness.

$$\alpha\textit{niso} = 0 \text{ for isosceles triangles .} \quad (244)$$

Remark 4 The plane through the origin that is perpendicular to the $\alpha\textit{niso} = \text{HH}$ axis is indeed the plane of isoscelesness, I.

Interpretation 2 $\alpha\textit{niso}$ is also a Heron map eigenvector and Cartesian axis direction in relational space.

Remark 5 $\alpha\textit{niso}$ is a signed quantifier, in that it distinguishes between left-leaning and right-leaning deviations from isoscelesness (Fig 6.1).

$$\alpha\textit{niso} < 0 \text{ is right-leaning ,} \quad (245)$$

and

$$\alpha\textit{niso} > 0 \text{ is left-leaning .} \quad (246)$$

Remark 6 One can moreover define an unsigned version, $|\alpha\textit{niso}|$, by using $|a^2 - b^2|$ instead of $a^2 - b^2$; this is insensitive to the left-or-right leaning distinction.

Remark 7 $\alpha\textit{niso}$ is maximal and minimal for H shapes, whereas $|\alpha\textit{niso}|$ is maximal for H shapes and jointly minimal for all isosceles triangles I.

15.5 Comment on the previous three subsections’ structural similarnesses

Structural Parallel 1 Each concerns an axis perpendicular to a plane through the relational space origin 0, with moreover the three of them being mutually perpendicular, i.e. forming a Cartesian axis system.

Structural Parallel 2 Each plane divides the shape sphere into two meaningful hemispheres (Fig 44) characterized by geometrical inequalities.

Structural Parallel 3 Each axis passes through two antipodal points on the shape sphere. These maximize the maximize-and-minimize the signed version of the quantifier and co-maximize the normed version, which is in turn jointly minimized on the perpendicular plane through the origin.

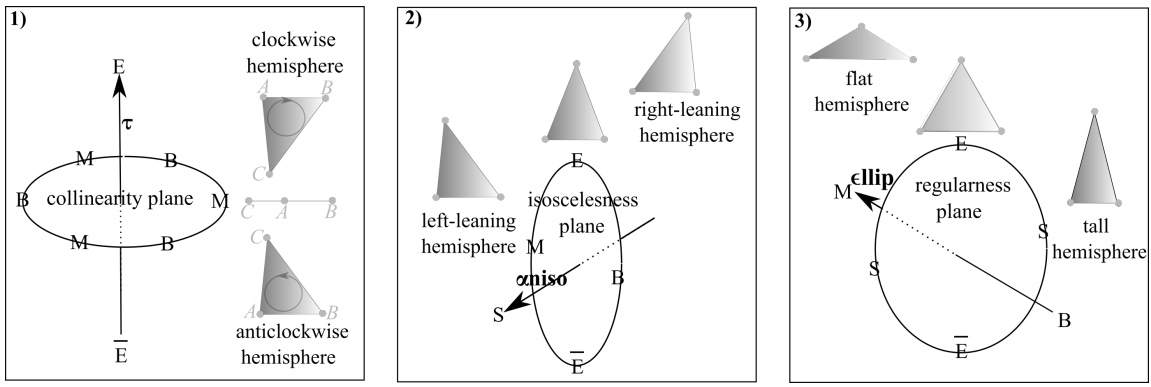


Figure 44: 1) Collinear shapes separate hemispheres of clockwise and anticlockwise triangles.

2) Isosceles triangles separate hemispheres of left-leaning and right-leaning triangles.

3) Regular triangles separate hemispheres of tall and flat triangles.

Difference/Primality 1 There is a difference in the labelled case (but not the unlabelled case) as regards one pair of axes coming with three possible clustering choices, while the other $-\tau-$ is always the same: clustering-democratic.

Structural Parallel 4 The three Hopf quantities in question moreover enter much further bundle mathematics as per below. Due to this, *ellip*, *aniso* and τ are a very geometrically structured and meaningful triple to consider. This justifies the combination of features exposited in Secs 12.3 and 13.5.

Application 1 One can also arrive at the BM, $E\bar{E}$ and HH axis system – in some order – by considering the three Hopf quantities *ellip*, τ along $E\bar{E}$ and *aniso*. Hopf’s fibre bundle mathematics moreover ascribes *equal status* to collinearity C, isoscelesness I, and regularity R, so it does not source a reason for picking principal, second and third axes. Selection principles for these are, rather, the above democratic principle for $E\bar{E}$ and the next subsection’s arguments for BM.

15.6 τ versus *ellip*’s claims to primality

Difference/Primality 1 τ , unlike *ellip* and *aniso*, is a ‘democracy invariant’. This is attained by all three clustering choices sharing one of the Cartesian axes picked out by the corresponding Hopf map (their other axes all lying at $\frac{\pi}{6}$ to each other in the common plane of collinearity).

Remark 1 As formulated above, *aniso* is a pure ratio of relative separations. Sec 3.3’s isosceles–isoangular duality moreover indicates that it can be rephrased in relative angle terms: it is a mixed angles and length ratios notion of anisotropy. *ellip* is also a function of pure ratio of relative separations. However, on this occasion, it cannot be rephrased in angular terms; it is a pure-ratio anisotropy.

Another point of view is to use the spherical angles that are most directly interpreted in shape-in-space terms: the untilded Θ and Φ . From their definitions I.(171-172) it is clear that

$$\Theta \text{ is pure ratio of relative separations} \quad (247)$$

and

$$\Phi \text{ is pure relative angle} . \quad (248)$$

Then, concatenating *ellip*’s definition and the third row of Fig 43,

$$ellip = \cos \Theta = \text{pure ratio of relative separations} . \quad (249)$$

The first equality here moreover means that *ellip* plays the mathematical role of Legendre variable, as per eq. (184). In the tilded variables, however, it is τ that plays this role, as per eq. (187)

In contrast, both *aniso* and τ provide mixed (ratio of relative separations) and (relative angle) information. On the one hand, the ‘ratio of relative separations’ information in both of these of these is a factor of

$$\sin \Theta = \sqrt{1 - \cos^2 \Theta} = \sqrt{1 - ellip^2} = \sqrt{aniso^2 + \tau^2} . \quad (250)$$

Here the second equality follows from (249) and the third from (141). On the other hand, the relative angle information is in the $\cos \Phi$ and $\sin \Phi$ factors respectively. This can moreover be envisaged as a parametrization of the corresponding perpendicular circle of regularity, R .

Difference/Primality 2 the $\textit{ellip} = \text{MB}$ axis corresponds to *irreducibly* (pure ratio of relative separation) information. BM 's claim to be principal axis is rooted on this, having the simplest shape-in-space to shape space map, its involvement in the relative Jacobi coordinates, and its irreducibly signed nature explained next below.

Difference/Primality 3 While mirror image identification and particle indistinguishability can do away with clockwise versus anticlockwise and left- versus right-leaning triangles, \textit{ellip} 's two signs correspond to inherently different shapes: tall versus flat triangles.

End-Point 1 So $\textit{ellip} = \text{MB}$ axis primality is also strongly supported, especially for label-indistinguishable modelling for which the objection of there being three clustering choices for $\textit{ellip} = \text{MB}$ axis evaporates. Given that spheres are $2-d$ and so require two coordinates, τ and \textit{ellip} havin the above privileges suggests using (231) to eliminate \textit{aniso} from intrinsic workings, so that these be in terms of τ and \textit{ellip} alone.

15.7 Partially angular reformulations of \textit{aniso} and τ

Proposition 1 A partially angular characterization of anisoscelesness is

$$\textit{aniso} = \frac{4 - 3 \textit{ellip}}{2\sqrt{3}} \frac{\cos^2 \gamma - \cos^2 \beta}{\sin^2 \gamma + \sin^2 \beta}. \quad (251)$$

Proof subtract the squared cosine form of the first and second equations in (108). \square

Remark 1 So $\beta = \gamma$ – the isoangularity characterization of isoscelesness – returns $\textit{aniso} = 0$; the other zeros lie outside the range of validity of the angles.

Remark 2 That (251)'s pure-ratio prefactor is not capable of generating any zeros is clear from

$$4 - 3 \textit{ellip} = \frac{1 + 3 \mathcal{R}^2 + 1}{1 + \mathcal{R}^2}, \quad (252)$$

which follows from (232).

Proposition 2 A partially angular characterization of tetra-area is

$$T = 2 a b \sin \gamma = \text{cycles}, \quad (253)$$

or their democratic average,

$$T = \frac{2}{3} (a b \sin \gamma + \text{cycles}). \quad (254)$$

The normalized mass-weighted form of this is

$$\tau = 2\sqrt{3} \frac{a b \sin \gamma}{a^2 + b^2 + c^2} = \text{cycles} = \kappa \frac{a b \sin \gamma + \text{cycles}}{a^2 + b^2 + c^2}. \quad (255)$$

Remark 3 The non-democratic form permits C and B case zeros to just be read off (zero angle, a zero side respectively).

Remark 4 Finally, there is no partially angular characterization of ellipticity, since this is a pure-ratio notion.

15.8 Further structural parallels

Remark 1 As regards tilded coordinates, the azimuthal angle $\tilde{\Theta}$ encodes area content via

$$\tau = \cos \tilde{\Theta}, \quad (256)$$

whereas its polar angle partner $\tilde{\Phi}$ is the mirror image identified (3, 1) shape space coordinate (Shape-Theoretic Aufbau Principle!).

Remark 2 While there is less use for HH-centric spherical coordinates, let us comment here that their azimuth is a pure function of anisoclesness and the polar angle parametrizes the isosceles-space circle.

Structural Parallel 5 The previous subsection's Remark 5 completes the general pattern of the principal axis having a pure quantity to its perpendicular plane having two mixed quantities and a coordinate that is conceptually complementary to the principal axis's azimuthal significance. I.e. (area content) plus (collinearity parametrization), versus (ellipticity content) plus (regularity parametrization), and versus (anisocseles content) plus (isoscelesness parametrization).

Structural Parallel 6 and Application 2 The Hopf map structure picks out three uniformity notions. I.e. a uniform angle notion: collinearity, a pure ratio uniformity notion: regularity, and a notion which is dual angle-separation uniformity: isoscelesness.

15.9 Further Linear Algebra, now of Hopf Quantities

Remark 1 Anisocselesness and ellipticity have the further interpretation of being the eigenvectors of the Heron map \underline{H} . [This follows from Sec 11.2 alongside the identification of x with anisocselesness and z with ellipticity.]

Remark 2 Due to \underline{H} and \underline{J} commuting with each other, these maps moreover share their eigenvectors.⁷ Anisocselesness and ellipticity are thus also eigenvectors of the sides-medians involution \underline{J} .

Structure 1 Let us further formulate anisocselesness and ellipticity in Linear Algebra terms as follows.

$$\alpha niso = \mathcal{A}_i s_i^2 = \mathcal{A}_i J_{ij} m_i^2 = -\mathcal{A}_i m_i^2 \quad (257)$$

and

$$\epsilon llip = \mathcal{E}_i s_i^2 = \mathcal{E}_i J_{ij} m_i^2 = -\mathcal{E}_i m_i^2 . \quad (258)$$

for vectors

$$\underline{\mathcal{A}} := \begin{pmatrix} 1 \\ -1 \\ 0 \end{pmatrix} \text{ and } \underline{\mathcal{E}} := \begin{pmatrix} 1 \\ 1 \\ -2 \end{pmatrix} . \quad (259)$$

Structure 2 Introduce furthermore \underline{E} and \underline{A} matrices for ellipticity squared and anisocselesness squared,

$$\epsilon llip^2 = E_{ij} s_i^2 s_j^2 \quad (260)$$

and

$$\alpha niso^2 = A_{ij} s_i^2 s_j^2 , \quad (261)$$

for

$$\underline{E} := \begin{pmatrix} 4 & -2 & -2 \\ 2 & 1 & 1 \\ 2 & 1 & 1 \end{pmatrix} , \text{ and } \underline{A} := \begin{pmatrix} 0 & 0 & 0 \\ 0 & 1 & -1 \\ 0 & -1 & 1 \end{pmatrix} . \quad (262)$$

Motivation for doing this for the squares is that it is these which are on a Hopf bundle-theoretic par with the Heron map \underline{H} of Sec 2. We then observe the following remarkable commutativity theorem.

Theorem 1 All three of the $Hopf^2$ quantities' matrices commute

i) with each other,

$$[\underline{H}, \underline{E}] = [\underline{H}, \underline{A}] = [\underline{E}, \underline{A}] = 0 , \quad \text{and} \quad (263)$$

ii) with the sides-median involution \underline{J} ,

$$[\underline{H}, \underline{J}] = [\underline{E}, \underline{J}] = [\underline{A}, \underline{J}] = 0 . \quad (264)$$

(See [113] for a proof.)

⁷Sharing of eigenvectors under these circumstances is well-known in Quantum Mechanics, under the name of 'complete set of commuting observables' (CSCO), and in Methods of Mathematical Physics.

Remark 3) A matrix form of the Hopf on-sphere condition is given by

$$\underline{H} + \underline{A} + \underline{E} = \frac{1}{9} \underline{I}. \quad (265)$$

Here, \underline{I} is the degenerate ‘all unit entries matrix’

$$\underline{I} := \begin{pmatrix} 1 & 1 & 1 \\ 1 & 1 & 1 \\ 1 & 1 & 1 \end{pmatrix}. \quad (266)$$

15.10 Hopf congruence and similarity conditions

Following on from Sec 3.5 and 5.2’s standard congruence and similarity conditions, and then Sec 10.3’s involving medians or Jacobi coordinates, we now provide Hopf congruence and similarity conditions for triangles.

Definition–Proposition 1: Hopf congruence condition 7) \mathcal{T} -*Ellip- \mathcal{A} niso* (for a given clustering choice’s *Ellip* and *\mathcal{A} niso*).

Definition–Proposition 2: Hopf similarity condition 7) τ -*ellip* (for a given clustering choice’s *ellip*).

Definition–Proposition 3: Hopf similarity condition 8) τ - *\mathcal{A} niso* (for a given clustering choice’s *\mathcal{A} niso*).

Definition–Proposition 4: Hopf similarity condition 9) *ellip- \mathcal{A} niso* (for a given clustering choice’s *ellip* and *\mathcal{A} niso*).

Remark 1 Among these Hopf similarity conditions, τ -*ellip* has further democracy and pure-ratio raisons d’être than the τ - *\mathcal{A} niso* and *ellip- \mathcal{A} niso* versions muster.

Remark 2 On the other hand, it is *ellip- \mathcal{A} niso* data which most readily interconverts with the standard side-angle and side-ratio variables, as per the next subsection.

15.11 Solving a triangle given Hopf data

Proposition 1 For Hopf relational data,

$$a = \sqrt{l + \text{Ellip}}, \quad b_{\pm} = \frac{1}{\sqrt{2}} \sqrt{2l - \text{Ellip} \pm \sqrt{3} \mathcal{A}niso}, \quad (267)$$

$$\cot \gamma_{\pm} = \frac{1}{\sqrt{3}} \sqrt{\frac{1 - \text{ellip}}{1 + \text{ellip}}} \operatorname{cosec} \Phi \pm \cot \Phi \quad \text{and} \quad \cot \alpha = \frac{1 - 2 \text{ellip}}{\sqrt{3} \sqrt{1 - \text{ellip}^2} \sin \Phi}. \quad (268)$$

Proof Let us first note that

$$\lambda l_1 + \mu l_2 = \frac{\lambda + \mu}{2} l - \frac{\mu - \lambda}{2} \text{Ellip}. \quad (269)$$

As a first instance of this,

$$\frac{l + \text{Ellip}}{2} = l_1 = \rho_1^2 = \mu_1 R_1^2 = \frac{1}{2} a^2, \quad (270)$$

from which the first equation follows.

The second equation follows from eq. 1 of (104)’s mass-weighted consequence of the cosine rule, definition (242) and subcase

$$3 l_2 + l_1 = 2l - \text{Ellip}, \quad (271)$$

of (269). The third equation follows likewise from (104).

The fourth equation follows from the first equation in (108) by use of definitions (242) and (236). The fifth follows likewise from the second equation in (108), and the sixth from (109) \square .

Proposition 2 For *ellip- α iso* Hopf similarity data,

$$\frac{b_{\pm}}{a} = \sqrt{\frac{2 - \text{ellip} \pm \sqrt{3} \alpha \text{iso}}{2(1 + \text{ellip})}} , \quad (272)$$

$$\cot \gamma_{\pm} = \frac{1}{\sqrt{3} \alpha \text{area}} (1 - \text{ellip}) \pm \alpha \text{iso} , \quad (273)$$

$$\cot \alpha = \frac{1 - 2 \text{ellip}}{\sqrt{3} \alpha \text{area}} . \quad (274)$$

15.12 Relational space application of the Hopf map to Shape Theory

Application 3 An ambient \mathbb{R}^3 can moreover be interpreted as relational space.

$$\mathcal{R}(3, 2) \stackrel{\text{topologically}}{=} \mathbb{R}^3 . \quad (275)$$

Remark 1 Relational space does not however admit the flat metric. For instance, the Ricci scalar is

$$\text{Ric} = \frac{6}{l} . \quad (276)$$

As well as indicating curvature, this moreover blows up at $l = 0$, i.e. at the maximal coincidence-or-collision O, showing this to be a singular metric geometry.

Remark 2 This metric is however conformally flat [c.f. eq. (I.186)] if one disregards the mathematically pathological O. Moreover, we would expect some features would then be lost, starting with the metric-level consequences of the curvature singularity at O.

Thus we disrecommend solely proceeding via ‘passing to’ a conformally flat representation for which the underlying conformal transformation, however, goes singular at precisely the point of main geometrical, topological and dynamical interest: O.

Remark 3 Mirror image identified configurations are singular for 2- and 3-*d* RPMs.

15.13 Hopf map for degenerate shapes

For collinear configurations, *Area* vanishes, whereas

$$\alpha \text{iso} = 2 \rho_1 \rho_2 \quad (277)$$

and *Ellip* is unaffected. One can readily check these obey the on-circle condition,

$$\alpha \text{iso}^2 + \text{ellip}^2 = 1 . \quad (278)$$

This amounts to

$$\alpha \text{iso} = \frac{2 \mathcal{R}}{1 + \mathcal{R}^2} = 2 \frac{\tan \frac{\Theta}{2}}{1 + \tan^2 \frac{\Theta}{2}} = \sin \Theta , \quad (279)$$

and consequently

$$\text{ellip} = \cos \Theta . \quad (280)$$

This inter-relates *ellip* and *αiso*, for collinear configurations, with Part I’s (3, 1) angular ratio variable.

15.14 Democratic ellipticity quantifier and inequalities satisfied by it

Definition 1 The democratic version of ellipticity is

$$\langle \text{ellip} \rangle := \mu_{\mathbb{Q}}^2 - \sigma_{\mathbb{Q}}^2 . \quad (281)$$

The corresponding pure-ratio quantity is, normalizing by

$$Z_{\text{T}} := \mu_{\mathbb{Q}}^2 + \sigma_{\mathbb{Q}}^2 = \frac{1}{3} \sum_i \left(\rho_1^{(i)2} + \rho_2^{(i)2} \right) , \quad (282)$$

$$\langle \epsilon lip \rangle := \frac{\langle \mathcal{E} lip \rangle}{Z_T} . \quad (283)$$

Remark 1 However, since $Z_1 = Z_2$ by (98), $\langle \mathcal{E} lip \rangle$ and thus $\langle \epsilon lip \rangle$ are zero. Thus democratic ellipticity in the immediate senses of the preceding Sec is a sterile concept.

Remark 2 This suggests seeking an alternative ellipticity quantifier whose democratic form remains shape-theoretically nontrivial. The obvious candidate for a such follows from considering the linear counterpart of the above construct, as follows.

Definition 2 The *linear ellipticity* is given by

$$\Lambda in \mathcal{E} lip := \rho_2 - \rho_1 . \quad (284)$$

Remark 3 $\Lambda in \mathcal{E} lip$'s zero corresponds to

$$2a^2 = b^2 + c^2 . \quad (285)$$

Thus equilaterality $a = b = c$ solves, but not uniquely [114].

Remark 4 The normalized version, $\lambda in \mathcal{E} lip$, turns out to have no extrema, its *extremal values* occurring at the ends of its allowed range: -1 for the binary coincidence-or-collision shape B and $+1$ for the uniform collinear configuration, U.

Structure 1 The democratic version of these are, firstly,

$$\langle \Lambda in \mathcal{E} lip \rangle := \mu_A - \sigma_A . \quad (286)$$

Secondly, normalizing by

$$F_T := \mu_A + \sigma_A = \frac{1}{3} \sum_i (\rho_1^{(i)} + \rho_1^{(i)}) , \quad (287)$$

where ‘T’ stands for total average: *all* Jacobi coordinates, corresponding to all mass-weighted sides *and* all mass-weighted medians,

$$\langle \lambda in \mathcal{E} lip \rangle := \frac{\langle \Lambda in \mathcal{E} lip \rangle}{F_T} = \frac{\mu - \sigma}{\mu + \sigma} = \frac{\Psi - 1}{\Psi + 1} . \quad (288)$$

Remark 5 See [114] for a determination of the zeros of this and [125] for its extremization.

Corollary 1

$$-\frac{2 - \sqrt{3}}{2 + \sqrt{3}} \leq \langle \lambda in \mathcal{E} lip \rangle \leq \frac{2 - \sqrt{3}}{2 + \sqrt{3}} . \quad (289)$$

Remark 7 This is symmetrically placed, as befits a two-tailed quantity. This result also prompts a renormalized re-issuing of the definition of linear ellipticity as follows, so that the range now be the standard 2-tailed one from -1 to $+1$.

$$\langle \widetilde{\lambda in \mathcal{E} lip} \rangle := \frac{2 + \sqrt{3}}{2 - \sqrt{3}} \frac{\mu - \sigma}{\mu + \sigma} = \frac{2 + \sqrt{3}}{2 - \sqrt{3}} \frac{\Psi - 1}{\Psi + 1} . \quad (290)$$

Remark 8 For the equilateral triangle E , $\langle \widetilde{\lambda in \mathcal{E} lip} \rangle = 0$. $\langle \widetilde{\lambda in \mathcal{E} lip} \rangle_{\max}$ is at the binary coincidence-or-collision B, whereas $\langle \widetilde{\lambda in \mathcal{E} lip} \rangle_{\min}$ is at the uniform collinear shape U. Among the splinters, these are (Fig 22.b) respectively, the extreme spear-head and the extreme pickaxe-heads. We finally have the following results [114].

Theorem 1

$$-1 \leq \langle \widetilde{\lambda in \mathcal{E} lip} \rangle \leq 1 . \quad (291)$$

Theorem 2

$$\frac{\mathcal{I} - 1}{\mathcal{I} + 1} \leq \frac{2 - \sqrt{3}}{2 + \sqrt{3}} \langle \widetilde{\lambda in \mathcal{E} lip} \rangle \leq \frac{1 - \mathcal{I} \mathcal{G}^3}{1 + \mathcal{I} \mathcal{G}^3} . \quad (292)$$

16 Configuration space automorphism groups

16.1 Graph automorphisms

Proposition 1 i)

$$Aut(\mathfrak{T}_{\text{op}}\widetilde{\mathfrak{S}}(3, 2)) = Aut(\mathfrak{T}_{\text{op}}\mathfrak{S}(3, 2)) = Aut(\text{claw graph with equal talons as per Fig 2.1}) = D_3 = S_3 . \quad (293)$$

ii)

$$Aut(\mathfrak{T}_{\text{op}}\mathfrak{L}_{\text{eib}}\mathfrak{S}(3, 2)) = Aut(\mathfrak{T}_{\text{op}}\mathfrak{J}\mathfrak{S}(3, 2)) = Aut(P_2 \text{ as labelled in Fig 2.2}) = \mathbb{Z}_2 . \quad (294)$$

iii) By the argument of Sec I.20.1, the above automorphism groups remain unchanged under $\mathfrak{S} \longrightarrow \mathcal{R}$.

16.2 Shape momenta

The remainder of this section is **Application 4** of the Hopf map, due to the Cartesian axes it provides being useful in discussing shape momenta and conserved quantities.

Remark 1 For triangleland in spherical coordinates, the momenta are

$$\mathcal{J} := p_{\Phi} = \text{hopf}_1 \pi_2^{\text{hopf}} - \text{hopf}_1 \pi_2^{\text{hopf}} . \quad (295)$$

Since Φ is a relative angle in space, this is a relative angular momentum in space (hence the notation \mathcal{J}).

On the other hand,

$$\text{Dil}_{\Delta} := p_{\Theta} \quad (296)$$

is indeed a relative dilational quantity since Θ is a function of a relative distance (length ratio).

16.3 Killing vectors and isometry group

Remark 1 Pure-shape triangleland has the maximal three Killing vectors, among which the ‘axial’ $\partial/\partial\Phi$ corresponds to invariance under change of relative angle. Scaled triangleland has three conformal Killing vectors. These do not include the three

$$\frac{\partial}{\partial \text{hopf}^i} \quad (297)$$

because of the origin’s topological and geometrical distinctiveness. It is rather the three

$$\text{hopf}^j \frac{\partial}{\partial \text{hopf}^i} - \text{hopf}^i \frac{\partial}{\partial \text{hopf}^j} \quad (298)$$

– $SO(3)$ quantities – which survive.

Remark 2 In the present context these are to be interpreted as follows [76]. One is the relative angular momentum

$$\mathcal{J} = \frac{l_1 l_2}{l} \dot{\Phi} = \frac{l_1 l_2}{l} (\dot{\theta}_2 - \dot{\theta}_1) = \frac{l_1 \Lambda_2 - l_2 \Lambda_1}{l} = \Lambda_2 - \Lambda_1 = \frac{1}{2}(\Lambda_2 - \Lambda_1) . \quad (299)$$

The θ_i here are polar relative Jacobi angles and the Λ_i are the corresponding partial angular momenta. The last expression can thus be interpreted as half of the difference between the two subsystems’ angular momenta.

Remark 3 The other two Killing vectors are mixed relative dilational and angular momenta. Such quantities have previously been termed *generalized angular momenta* by physicist Felix Smith [16], more descriptively *rational momenta* (conjugate to general ratio variables) by Anne Franzen and the Author [78], and finally *shape momenta* [90, 89] following discussions with Eduardo Serna. Hence we denote the three of them by

$$s_i = \epsilon_{ijk} \text{hopf}_j \pi_k^{\text{hopf}} , \quad (300)$$

and recover the pure relative angular momentum

$$\mathcal{J} := s_3 = \frac{\partial}{\partial \Phi} . \quad (301)$$

Proposition 1 All in all,

$$\text{Isom}(\mathfrak{S}(3, 2)) = SO(3) . \quad (302)$$

Consult Fig 45 for the mirror image identified, indistinguishable and Leibniz versions.

Remark 3 Finally note that the constant- Φ curves are furthermore privileged as Killing vector preserving curves. Such ‘adapted’ submanifolds privileged by Killing vector preservation will play a substantial role in the theory of planar quadrilateral shapes [124, 123].

	tilded	\mathfrak{I}	plain	\mathfrak{Leib}
$Isom(\mathfrak{GS}(3, 2))$ = $Sim(\mathfrak{GS}(3, 2))$	E	A	A	A
$Isom(\mathfrak{GR}(3, 2))$	E	A	A	A
$Sim(\mathfrak{GR}(3, 2))$	H	B	B	B

Figure 45: Table of pattern of isometry and similarity groups for (scale and) shape spaces for 3 points in 2-d.

17 Shape representatives

Structure 1 The Hopf map is moreover closely related to the Hopf fibre bundle a principal fibre bundle with \mathbb{S}^2 as base space, \mathbb{S}^3 as total space, and $\mathbb{S}^1 = U(1)$ as fibres and structure group.

Remark 1 This and the next section exploit this further feature.

Structure 2 Let us now label $\tilde{\mathfrak{S}}(3, 2)$, $\mathfrak{S}(3, 2)$, $\mathfrak{IS}(3, 2)$ and $\mathfrak{Leib}_{\mathfrak{S}}(3, 2)$ not with a representative as in Figs 47-48 but with what the entire space of representatives at that point is.

Proposition 1 In the case of the shape sphere, this is

$$SO(2) = U(1) \stackrel{m}{=} \mathbb{S}^1 \quad (303)$$

as its representative everywhere. This homogeneity of fibre objects permits a simple reformulation for the space of spaces of representatives, $\mathfrak{SSR}(\mathfrak{S}(3, 2))$, as follows.

$$\mathfrak{SSR}(\mathfrak{S}(3, 2)) = P(\mathbb{S}^2, \mathbb{S}^1) : \quad (304)$$

the principal bundle of the base space \mathbb{S}^2 and fibres = structure group $\mathbb{S}^1 = U(1)$.

Remark 2 This is of course the Hopf fibre bundle itself, since

$$\mathfrak{SSR}(\mathfrak{S}(3, 2)) \text{ is just another conception of preshape space } \mathfrak{p}(3, 2) \quad (305)$$

with

$$\mathfrak{p}(3, 2) = \mathbb{S}^3 \text{ viewed as the total space of the } P(\mathbb{S}^2, \mathbb{S}^1) \text{ Hopf bundle .} \quad (306)$$

Remark 3 A major issue with this result is that the particular mathematical niceness of preshape space being a fibre bundle does not generalize particularly far. This causes a number of ‘intuitions’ about the nature of Shape Theory obtained by studying these few particularly nice cases to unfortunately turn out to be atypical. Note firstly that the generalization which still does work out nicely is to the similarity N -a-gon, as exposted in Part IV.

Remark 4 What we show below is that mirror image identification and/or point indistinguishability partly spoil this result. This counts as a mathematical simplicity argument against studying these cases, but also, due to the inherent interest of these cases, as an argument to upgrade the mathematical methods used in Shape Theory to overcome this impasse.

Remark 5 As a final example, [123] shows a yet more substantial breakdown of this fibre bundle result in the case of affine shape spaces (even without mirror image identification or indistinguishable points).

Remark 6 Choice of representative is moreover a realization of gauge freedom, whereas space of representatives is the gauge orbit corresponding to each base point space.

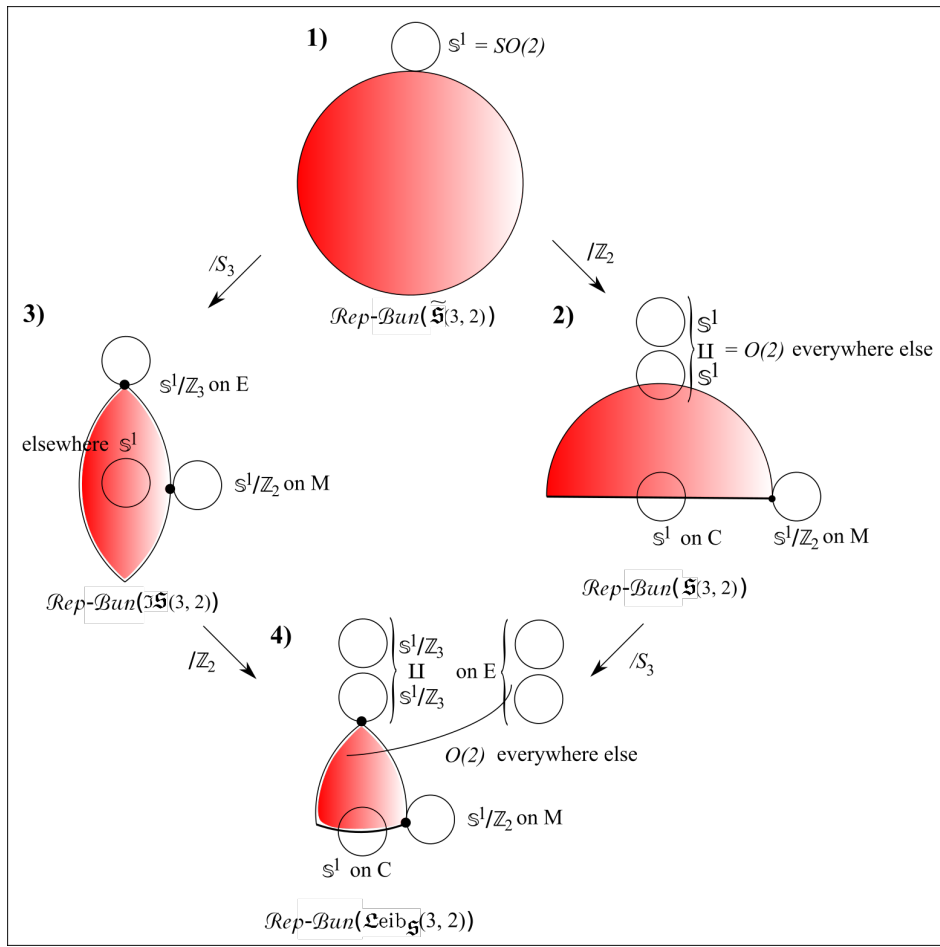


Figure 46: (3, 2) triangleland bundles of shape representatives.

17.1 Shape Theory requires general bundles

Proposition 1 For 2- d similarity shape theory, the space of spaces of representatives admits decomposition into a *bundle of representatives*:

$$\mathfrak{Sp}(N, 2) = \mathfrak{SSR}(\mathfrak{GS}(N, 2)) = \mathfrak{Rep}\text{-}\mathfrak{Bun}(\mathfrak{GS}(N, 2)) . \quad (307)$$

Remark 2 This is a *general bundle* and not usually more specifically a *fibre bundle*, since the attached objects can differ from point to point.⁸ For $\tilde{\mathfrak{p}}(N, 2)$ itself, this is, exceptionally, a fibre bundle as well. The point of this generalization is, rather, covering how $\mathfrak{p}(N, 2)$, $\mathfrak{Ip}(N, 2)$ and $\mathfrak{Leib}_{\mathfrak{p}}(N, 2)$ decompose as regards the corresponding base shape space and the corresponding spaces of representatives.

Proposition 2

$$\tilde{\mathfrak{p}}(3, 2) = \mathfrak{Rep}\text{-}\mathfrak{Bun}(\tilde{\mathfrak{S}}(3, 2)) = P(\mathbb{S}^2, \mathbb{S}^1) = \text{Hopf fibration of } \mathbb{S}^3 . \quad (308)$$

$$\mathfrak{p}(3, 2) = \mathfrak{Rep}\text{-}\mathfrak{Bun}(\mathfrak{S}(3, 2)) , \quad (309)$$

$$\mathfrak{Ip}(3, 2) = \mathfrak{Rep}\text{-}\mathfrak{Bun}(\mathfrak{IS}(3, 2)) \text{ and} \quad (310)$$

$$\mathfrak{Leib}_{\mathfrak{p}}(3, 2) = \mathfrak{Rep}\text{-}\mathfrak{Bun}(\mathfrak{Leib}_{\mathfrak{S}}(3, 2)) \quad (311)$$

are as per Fig 46.2)-4) respectively.

Remark 3 Now not only C is distinguished by stratification, but also E and $M = U(3, 1)$ are as well. This further justifies interest in $M = U(3, 1)$.

Remark 4 These strata arise as follows. The relevant master group is now $O(2)$, which $SO(2)$ as a nontrivial subgroup, while three further discrete subgroups of this turn out to also be relevant. So even in 2- d similarity

⁸E.g. differ homeomorphically at the topological manifold level, or a fortiori diffeomorphically at the differential manifold level, or furthermore isometrically at the level of Metric Geometry.

shape theory, strata make an appearance, provided that one considers one or both of mirror image identification or point-or-particle indistinguishability.

Remark 5 General bundles can be furthermore equipped as presheaves and then as sheaves, by which stronger gluing and localization methods become available. Note once again that the above three general bundles' base spaces are Hausdorff, second-countable and compact, so that whichever of the simpler and more worked out cases in [126]. (The attached entities are, moreover, also all Hausdorff, second countable and compact, with all bar one – $O(2)$ – additionally enjoying connectedness).

17.2 Picking representatives is choosing a section

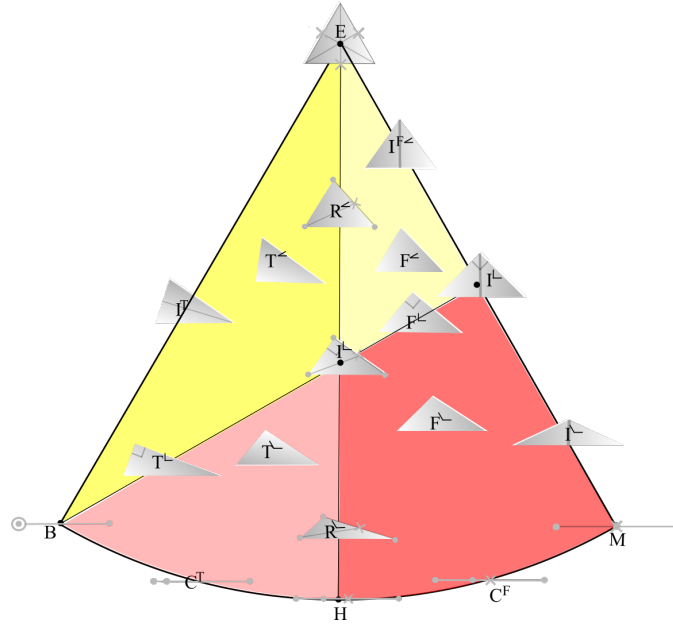


Figure 47: $\mathfrak{L}eib_{\mathfrak{S}}(3, 2)$ 'standing up' 'flat isosceles favouring' global section.

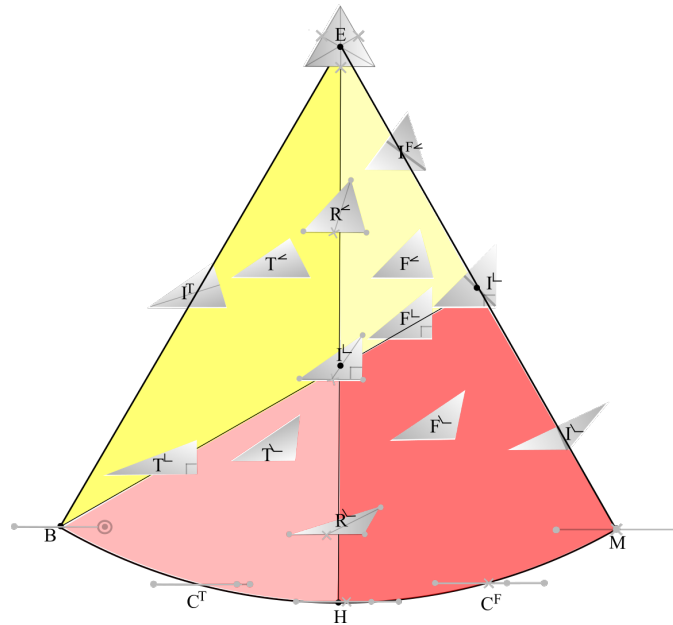


Figure 48: $\mathfrak{L}eib_{\mathfrak{S}}(3, 2)$ 'standing up' 'right-and-regular favouring' global section.

Remark 1 Let us now return to Kendall's labelling of points by triangles and identify it as a *choice of section*. In $\mathfrak{L}eib_{\mathfrak{S}}(4, 1)$ [and $\mathfrak{J}\mathfrak{S}(4, 1)$], while this is not a fibre bundle section, the notion of section straightforwardly extends to general bundles (and to sheaves). This case has the added advantage of supporting global sections. Figs (47) and

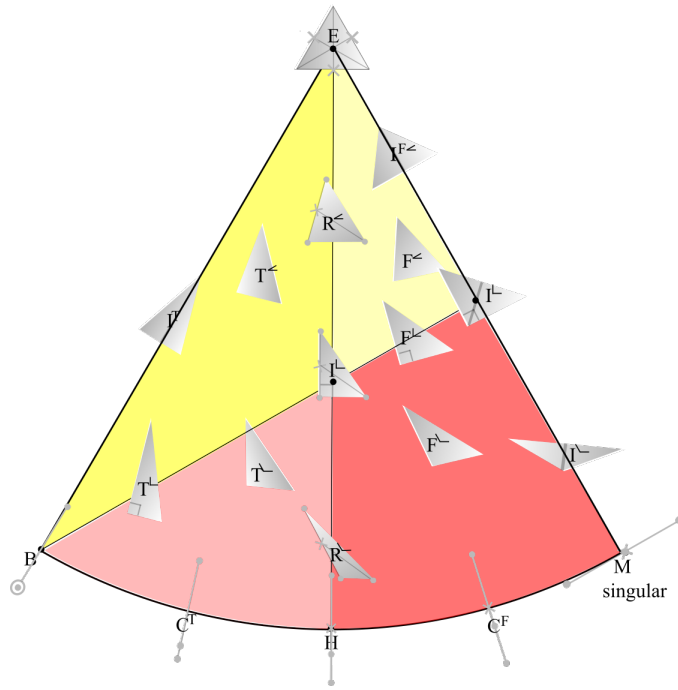


Figure 49: $\mathfrak{Leib}_5(3,2)$ non-global section which is not defined at the equilateral triangle and is discontinuous at M but is otherwise well-defined.

(48) are such, while (49) is an example which is not globally well-defined. $\mathfrak{Rep}\text{-}\mathfrak{Bun}(\mathfrak{S}(3,2))$ itself admits no global sections since it is the Hopf fibre bundle which is indeed a nontrivial fibre bundle.

Structure 1 All in all, the ‘shape-in-space to position-in-shape-space’ correspondence is to be built up into a bundle and sheaf construct in [126].

18 Triangleland's suite of monopoles

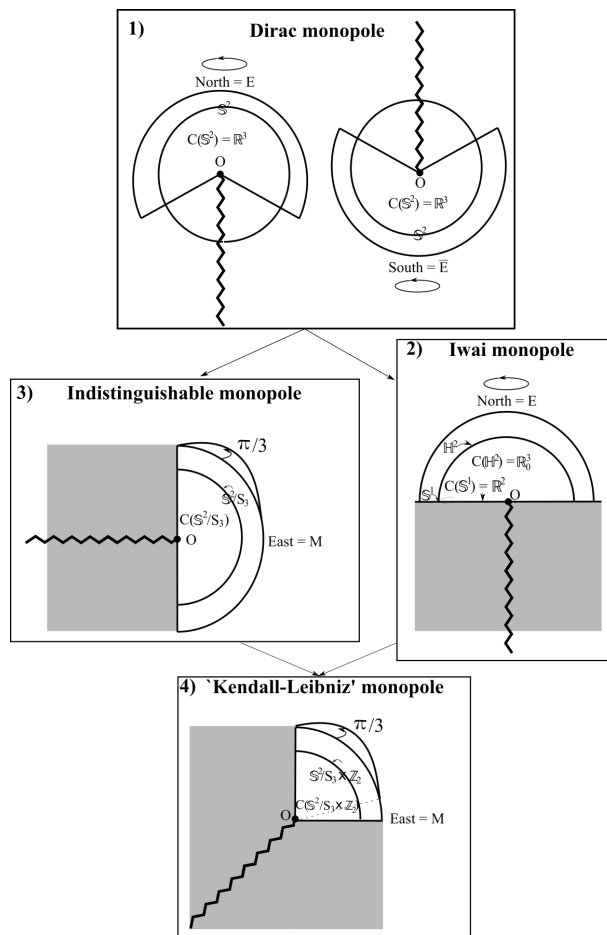


Figure 50: Relational triangleland suite of monopoles.

In 1), N and S are ‘North’ and ‘South’ stereographic coordinate chart patches which are large enough to overlap with each other. More shape-theoretic names for these use anticlockwise and clockwise equilateral triangle pole names E and \bar{E} rather than North and South.

In 2), N is now a hemisphere’s worth of ‘North’ (now orintetation-less equilateral triangle E) stereographic coordinate.

In 3), the chart is a third-hemisphere’s worth of ‘East’ (here the unlabelled M configuration) stereographic coordinate.

Finally, in 4) the chart is a sixth-hemisphere’s worth of ‘East’ (i.e. M) stereographic coordinate.

Iwai’s realization that the half-space from the 3-body problem carries a distinct monopole from Dirac’s whole-space version recurs for each of $\mathcal{IR}(3, 2)$ and $\mathcal{Leib}_{\mathcal{R}}(3, 2)$. Let us introduce the following terminology.

Definition 1 The $\tilde{\mathcal{R}}(3, 2)$ -monopole is a configuration space realization of the *Dirac monopole*, which is usually realized in space instead.

Definition 2 The $\mathcal{R}(3, 2)$ -monopole is the *Iwai half-space monopole*.

Definition 3 The $\mathcal{IR}(3, 2)$ -monopole is the *1/6th-segment monopole*.

Definition 4 The $\mathcal{Leib}_{\mathcal{R}}(3, 2)$ -monopole is the *half-of-a-1/6th-segment* alias *Leibniz–Kendall monopole*.

Remark 1 All four of these are depicted in Fig 50 and are further studied in [116]. As per Iwai’s monopole, the $\mathcal{IR}(3, 2)$ and Leibniz–Kendall monopoles’ Dirac string emanating from the maximal coincidence-or-collision O can be placed entirely in the corresponding non physically realized sector, by which a single chart or section description is afforded. On the other hand, for Dirac’s monopole, two charts or sections are required. The Iwai monopole is realized – in configuration space – in an important N -body problem setting: the mirror image identified 3-body

problem in $d \geq 2$, this identification being a fortiori non-optional in $d = 3$ (and higher; see Sec 12.4 as regards 2 versus $\geq 3-d$ distinction in structure). As far as the Author is aware, monopoles 3) and 4) are new.

Remark 2 Following on from the previous section, another reason to not conformally transforming to the flat metric on relational space is that this would dispense with the monopole structure emanating from O (but this is part of the physical properties of the system).

Remark 3 [116] studies 7 further cases of 2- d 3-body problems.

19 Conclusion

19.1 Results

The current Part III's triangle model's topological configurations reduce to partitions, a wider $d \geq 2$ feature in contrast with Part II's $d = 1$ feature. Part III's corresponding topological shape spaces are also considerably simpler than Part II's.

B) As special great circle arcs on triangleland shape space, we identified the equator of collinearity C and meridians of isoscelesness I. Collinearity splits clockwise and anticlockwise labelled triangles if regarded as distinct. Isoscelesness splits left-leaning and right-leaning triangles. As special points on triangleland shape space, we firstly identified E: equilateral triangle, B: binary coincidence-or-collision, and M = U(3, 1): the merger and most uniform collinear shape inherited from the (3, 1) model.

C) Bringing in the Jacobian notion of regularity R – equal base and median partial moments of inertia – which is also realized by meridians, we identify a final two types of significant point, H: the halfway shape also inherited from the (3, 1) model, and R[⊥]: the right-and-regular triangle.

D) The special B point maximizes clumpiness among the normalizable triangular shapes. On the other hand, uniformity, mass-weighted area per unit moment of inertia and perimeter per unit area are maximized by the special point E. Finally, M is the sole notion of merger in triangleland. All in all, more virtues are conferred on the equilateral triangle than are conferred on any one (4, 1) shape.

E) In Part III, we considered placing medians of triangles on the same footing as their sides due to Jacobi and Hopf motivation, both of these being structures entering the Shape Theory of the space of triangles. We first reformulated the medians–sides inter-relation as an involution \underline{J} . We observed that $\underline{J}(s)$ factor of $\frac{4}{3}$ has the same origin as the $\frac{4}{3}$ factor discrepancy between sides and medians in the standard Heron's formulae in space. Moreover, in both the involution \underline{J} and Heron's formula, this factor of $\frac{4}{3}$ is removed by the passage to the mass-weighted Jacobi coordinate version of the inter-relation and of the Heron's formulae. Thus the mass-weighted sides and mass-weighted medians versions of Heron's formula for the now also mass-weighted area are placed on an identical footing. We term these the *Heron–Jacobi formulae*. In the process, the original factor of $\frac{4}{3}$ is identified to be the ratio of the medians' Jacobi mass to the sides' Jacobi mass.

F) Triangleland is the smallest relational model with nontrivial relative angles. It realizes perpendicularity – in particular but not limited to rightness – and collinearity (but non-collinear parallelism is not possible for $N = 3$). It also realizes angle uniformity, of two angles in isosceles triangles, or all three in the equilateral triangle.

G) Considering right-angled triangles \perp as well, we additionally identified I[⊥] – the right isosceles triangle – as a special point, and also characterized regions of acuteness and obtuseness. Realizing \perp in shape space requires spherical cap – rather than great – circles. Via this, Shape Theory moreover provides an answer to Lewis Carroll's longstanding and conceptually interesting pillow problem pillow [5] of what is Prob(Obtuse) for a triangle, namely 3/4 [54, 100, 112]. We furthermore argued for this to be a prototype for mapping problems in flat space geometry⁹ to the corresponding shape spaces, where the problems take a prescribed differential-geometric form. Part III, we have indeed presented a substantial extension of this problem and its shape-theoretic solution.

One extension [112] is to finding the probability that an isosceles triangle is obtuse, as well as how obtuseness-or-acuteness condition with tallness-or-flatness and vice versa, with and without the extra assumption of isoscelesness.

⁹Or for constellations on other directly realized geometry, such as constellations on spheres [103] or tori [118] or real projective spaces [106, 107].

Another extension follows from viewing right-angled triangles as triangles whose maximal angle is right, and then passing to consider all the other possible values of maximal angle, $\alpha_{\max} = [\frac{\pi}{3}, \pi]$. This gives the *maximal angle flow* over Kendall’s shape sphere. We find that the three kissing cap-circles of rightness – that so readily provide the shape-theoretic resolution of Lewis Carroll’s original pillow problem – furthermore play the role of separatrix in the maximal angle flow; this flow is further discussed in [115]. We apply our new knowledge of the maximal angle flow over the shape sphere to find the probability that a triangle has nontrivially-located Fermat point. This corresponds to the critical angle $\alpha_{\max} = \frac{2\pi}{3}$. This is critical in the sense that if the angle is smaller than this (‘Fermat acute’), the Fermat point lies in the interior of the triangle, but if it is larger (‘Fermat obtuse’), the Fermat point just lies on the obtuse vertex.

H) E is moreover the centre of the $\mathfrak{S}(3, 2)$ hemisphere, whereas M is the $\mathfrak{IS}(3, 2)$ lune centre, whereas \perp^R provides a notion of $\mathfrak{Leib}_{\mathfrak{S}}(3, 2)$ centre. As in Parts I and II of this treatise, passing to Leibniz space involves paying the price of having a weaker notion of centre. Neither $\mathfrak{IS}(3, 1)$ nor $\mathfrak{Leib}_{\mathfrak{S}}(3, 1)$ admits a topologically characterized boundary – only the point B therein is. E, isosceles I, M and collinear C are all metric-level notions.

19.2 The Hopf map’s role in Shape Theory

I) The Hopf map is realized by the map from the preshape 3-sphere and the shape 2-sphere. In this realization, collinearity, isoscelesness and regularity occur as a package, firstly as mutually orthogonal Cartesian axes from the ambient \mathbb{R}^3 , which is also the triangle-land relationalspace. Thereby, Jacobi notions are to be considered alongside ‘geometrically more obvious’ Lagrangian notions. Secondly, the Hopf map is rooted in bundle mathematics, constituting a unified geometrical treatment of some traditionally geometric notions and other notions arising in the 3-body problem. We have also given parallels of the Hopf map for the mirror image identified half-sphere $\mathfrak{S}(3, 2)$ (due to Dragt [24]), $\mathfrak{IS}(3, 2)$, and $\mathfrak{Leib}_{\mathfrak{S}}(3, 2)$, and again for their (3, 3) counterparts (see Sec 12.4). This set of structures moreover transcends from fibre bundles to general bundles. Part IV extends this unified perspective to arbitrary N -a-gons. We moreover envisage this trend to grow with (c.f. Fig I.2) the affine quadrilateral, similarity tetrahedron, similarity pentagon, and subsequent increases in dimension d , point-or-particle number N , and redundant group \mathfrak{G} ’s number of generators. Application of the full extent of Hopf structure map has moreover only come to the attention of a subset of the literatures concerning or making use of shapes. By this, its prominent inclusion in the current Part is a useful complementation of some of the existing literatures.

J) We show that the elsewise well-known Hopf coordinates diagonalizing the Heron map \underline{H} , a fact that appears to have hitherto escaped attention. Indeed, in this manner, diagonalizing Heron’s map \underline{H} provides us with a new derivation both of the Hopf map, and of the shape space formed by the triangles being a sphere equipped with the standard round metric: Kendall’s Theorem. What occurs at the level of the Hopf formulation of the triangle is that Heron’s formula has become a ‘*Heron–Hopf*’ formula that is one and the same as the on-sphere condition determining that the shape space of triangles is a sphere. The factor of 4 in the Hopf quantity that, in its 3-body problem incarnation, is the ‘tetra-area’ is moreover accounted for in the current Part’s working as being none other than the prefactor of 1/4 in the expanded version of Heron’s formula.

K) The other two Hopf quantities are, in their 3-body problem incarnation, to be interpreted as ellipticity and anisoscelesness. In the current Part, these now receive the further enlightening interpretation of being Heron map \underline{H} eigenvectors, which are moreover also sides–medians involution \underline{J} eigenvectors by the commutation relation between \underline{H} and \underline{J} also established in this Part.

L) Our *Heron–Hopf formula* is obtained by diagonalizing the expanded Heron form, keeping mass-weighted area as the subject. This is moreover mathematically in the form of an on-sphere condition, which, if represented symmetrically, we term the *Heron–Hopf–Kendall formula* in honour of Kendall’s iconic shape sphere of triangles. We finally argued that one can (almost) just as well interpret ellipticity or anisoscelesness as the subject, giving two further concomitants of the Heron–Hopf formula.

M) We are now in possession of a considerable body of shape-theoretic results [62, 80, 106, 107, 89, 99, 102, 109, 110, 124, 122, 123]. Therein, topological and differential geometric methods open many doors as regards the study of figures in a wide range of geometries. The current treatise illustrates this for triangles in similarity geometry, whereas the last six references above entertain this for a wider range of problems in similarity and affine geometry.

N) The current treatise’s consideration of globally-valid Killing vectors over $\mathfrak{S}(3, 2)$, $\mathfrak{IS}(3, 2)$, $\mathfrak{Leib}_{\mathfrak{S}}(3, 2)$ and their (3, 3) counterparts is a crucial step for all of establishing Classical Dynamics conserved quantities on these. And also as regards finding and optimally formulating probability distribution functions over these, and quantizing over these [127, 129]. Knowledge of the Killing vectors feeds into conserved quantities, which play a bigger role for N -a-gons, and

then have the idea of not only Killing vector-respecting potentials but also of Killing vector-respecting formulating probability distribution functions. Detailed knowledge of the Killing vectors of each shape space are moreover crucial as regards giving a robust and topologically well-founded quantization of each of these very interesting models of triangular shapes. This refers both to getting the kinematical quantization right and to features of the dynamical quantization such as Killing vector respecting operator ordering, Killing vector invariant wavefunctions and Killing vector-invariant quantum operators.

O) We moreover reinterpret Kendall’s pictures of the shape sphere and spherical blackboard as sections of the Hopf fibre bundle and of a general bundle. We comment on which such pictures are global sections and which need to be covered by multiple local sections. We also discuss the spaces of all possible representatives at each point of shape space, i.e. the in-space interpretation of the fibres (or the general bundle’s inhomogeneous generalization thereof). This approach has considerable further applications for larger N , d and \mathfrak{g} .

P) The Hopf map moreover provides the fibre bundle theoretic description of the Dirac monopole [8, 11], which while usually realized in space, is realized *in relational space* by the mirror images distinct triangle-land. Iwai [41] moreover also pointed to the mirror images identified counterpart having a distinct monopole structure. The current Part completes this description by giving two novel monopole structures: the 1/6th-segment mirror-images-distinct indistinguishable-particle monopole and the ‘1/6th-hemisegment ‘Leibniz–Kendall’ monopole.

Q) Indistinguishable \mathfrak{S} and Leibniz $\mathfrak{L}eib_{\mathfrak{g}}$ shape spaces incur stratification and bundles even for $(3, 2)$. Understanding representatives as sections and the space of representatives as bundles or sheaves is an already classically useful observation, foundational for the 3-body problem, the geometry of triangles and Shape Statistics.

19.3 Comparison: $(3, 2)$ versus $(4, 1)$ models

See the summary Figure 51, including how each model extends the $(3, 1)$ model’s scope.

		(4, 1)	(3, 1)	(3, 2)	Comments
Topological level structure	Number of classes of topological shapes	more	less	less	Increasing N effect
	Number of representatives of each class of particle	more	less	less	complexity here is $1-d$ specific feature
	Topological level shape space structure	Cellular: faces, edges and vertices, giving a 24-face cubic-octahedron symmetry tessellation.	edges and vertices, giving a circle cut in six.	face and 3 vertices (no edges) giving the 'pair of pants'	$1-d$ to $>1-d$ distinction, and increasing N effect
	Topological level shape space graphs	more complex	less complex	less complex	
Metric level structure	shape information content	length ratio information only	length ratio information only	length ratio and relative angle information	$1-d$ versus $>1-d$
	Leibniz space metric structure	isosceles spherical triangle	arc	isosceles spherical triangle	
	most uniform state	$U(4, 1)$ is the centre of $\mathfrak{H}(4, 1)$ but only on the edge of $\mathfrak{Eib}_{\mathfrak{G}}(4, 1)$.	$M = U(3, 1)$ is the centre of $\mathfrak{H}(3, 1)$ but only an end point of $\mathfrak{Eib}_{\mathfrak{G}}(3, 1)$	$E = U(3, 2)$ has extra distinctions in space, pole position in $\mathfrak{H}(3, 2)$, centre of $\mathfrak{H}(3, 2)$, though it is just a vertex for $\mathfrak{H}(3, 2)$ and $\mathfrak{Eib}_{\mathfrak{G}}(3, 2)$	
merger	more types, some of which fold into catastrophes	has just 1 type, M	has just 1 type, M	Is $N=3$ versus $N=4$, independent of d	
Extrinsic and relational space structure	Cartesian axes	ρ_1, ρ_2, ρ_3 , are obvious Cartesian axes: a DDD system	ρ_1, ρ_2 are obvious Cartesian axes: a BM system	Cartesian axes are now less obviously realized via the Hopf map: $2\rho_1 \cdot \rho_2, 2\rho_1 \times \rho_3, \rho_3^2 - \rho_1^2$: an EBH system	this is $1-d$ versus $2-d$, in each case generalizing to all N
	relational space geometry	this \mathbb{R}^3 is flat	this \mathbb{R}^2 is flat	this \mathbb{R}^3 is not flat but is conformally flat	
Maximal collision		less distinguished or troublesome	less distinguished or troublesome	$SO(2)$ only acts as id on O , so it is a distinct gauge orbit stratum	this is $1-d$ versus $>1-d$
Killing vectors and isometry group	$Isom(\mathfrak{H})$ $Isom(\mathfrak{E})$ $Isom(\mathfrak{H})$ $Isom(\mathfrak{Eib}_{\mathfrak{G}})$	$SO(3)$ $U(1)$ id id	$SO(2)$ $SO(2)$ $SO(2)$ $SO(2)$	$SO(3)$ $SO(3)$ $U(1)$ $U(1)$	this is $1-d$ versus $>1-d$ Also stratum effects occur for $d > 2$, or even for $2-d$ in the affine case
Bundle structure		none	none	nontrivial shape representative spaces nontrivial sections of representative spaces some requiring more than just fibre bundles has relational space monopoles	} this is $1-d$ versus $>1-d$

Figure 51: (3, 2) and (4,1) compared, including as extensions of (3, 1).

19.4 Extensions of Part III's work

Let us end by pointing to various extensions of this work.

Extension 1) Our flow and area-ratio probability method can be applied to find further maximal critical angle dependent Flat Geometry triangles' properties' probabilities of occurring in the shape-theoretic sense of 'random triangles'.

Extension 2) Sec 13.10's maximal angle flow over the shape sphere's above-described features likely render the current treatise of interest as an example in Differential Geometry and Dynamical Systems.

Extension 3) A subsequent step is to plot and optimize the shape quantities $\mathcal{S}, \mathcal{M}, \mathcal{G}, \mathcal{H}, \Psi, \Lambda$ defined in Sec 11.6 and $\langle \widetilde{\text{linellip}} \rangle$ of Sec 15.14, over the shape sphere, much as Sec 13.1 did for mass-weighted area per unit moment of

inertia. This is considered in the subsequent paper [125], alongside plotting further geometrically significant functions for triangles over the shape sphere of triangles.

Extension 4) [100, 112, 115] and the current treatise's use of Shape Theory to answer questions about triangle inequalities and random triangles moreover extends to its use in answering questions about random quadrilaterals and polygons using the Differential Geometry of the N -a-gonland $\mathbb{C}\mathbb{P}^{N-2}$ [62, 90, 124, 130, 131]. This program uses Differential Geometry on Kendall's shape spaces to pose and/or solve probabilistic questions involving polygons by considering these to live on Kendall's natural shape space with uniform measure thereupon. Fermat's own problem has moreover a large number of generalizations as well – geometric means – which overlap well with the theory of polygons.

Extension 5) The current treatise's notion of similarity Shape Theory moreover itself extends to a wide variety of further notions of shape and shape space, such as affine, projective, conformal, Möbius... [80, 102, 108, 106, 107, 122, 123]. Many of Extension 4)'s considerations recur in this wider arena.

19.5 Comparison: (3, 2) versus (3, 3) models

Parallel 1 At the topological level, these have the same shapes and shape spaces.

Difference 1 At the metric level, however, only mirror image identified shapes are possible. So the number of configuration spaces is halved: only the right hand side of figures 3 and 7 survives.

Difference 2 Furthermore (3, 3)'s $SO(3)$ isometry group has a nontrivial subgroup, $SO(2)$, whereas (3, 2)'s isometry group is $SO(2)$.

This has the next four items as consequences.

Difference 3–Proposition 1 At the level of quotient configuration spaces,

$$\mathfrak{S}(3, 2) = \frac{\mathbb{R}^6}{Sim(2)} \quad (312)$$

is distinct from

$$\mathfrak{S}(3, 3) = \frac{\mathbb{R}^9}{Sim(3)} . \quad (313)$$

Also,

$$\mathcal{R}(3, 2) = \frac{\mathbb{R}^6}{Eucl(2)} \quad (314)$$

is distinct from

$$\mathcal{R}(3, 3) = \frac{\mathbb{R}^9}{Eucl(3)} . \quad (315)$$

A fortiori, $\mathfrak{S}(3, 3)$ and $\mathcal{R}(3, 3)$ are stratified, whereas $\mathfrak{S}(3, 2)$ and $\mathcal{R}(3, 2)$ are not.

Proof General G and collinear C configurations are on the same orbit in the first case, so $SO(2)$ acts fully on both. On the other hand, they are on distinct orbits in the second case, with $SO(3)$ acting fully on G but only an $SO(2)$ subgroup acting on C . \square

Difference 4–Proposition 2 The inertia tensor for 3 particles in 3- d is not invertible at C [63], whereas it is for 3 particles in 2- d [75].

Difference 5–Corollary 1 The dynamical problem can consequently be reduced for all configurations in the 2- d case, but only for general (non-collinear) configurations in the 3- d .

This is a global difference rooted on the difference in stratification structure, and can be further rephrased as follows.

Corollary 2 Wheeler's Thin Sandwich Problem's [19, 20] Best Matching Problem [37] generalization is globally solvable for 3 particles in 2- d but only locally solvable away from C for 3 particles in 3- d [108].

Remark 1) Proposition 1's stratification is moreover particularly benign in the following two ways.

Proposition 3 Eq (313) fits together particularly nicely, in the sense that it is not just a stratified manifold but a fortiori a manifold with boundary. More specifically, the two strata jointly constitute the *hemisphere with boundary*.

Proposition 4 The Ricci curvature scalar is regular at C [41].

Remark 2) This is moreover in contradistinction with $\tilde{\mathcal{R}}(N, 3)$ for $N \geq 4$, for which the Ricci curvature is singular at C.

Remark 3) Thus it is a stratum which is straightforward to attach. It is obvious where it fits (Proposition 3), which condition can be formulated entirely geometrically, and there is furthermore no curvature singularity obstruction to placing it there.

Parallel 2–Proposition 5 Both $\mathfrak{S}(3, 2)$ and $\mathfrak{S}(3, 3)$ have the same Killing vectors and thus isometry groups: $SO(2)$.

Proof These are just \mathcal{J} everywhere for the 2- d case. For the 3- d case, \mathcal{J} succeeds in being a Killing vector on both strata, by fitting both \mathbb{H}^2 and \mathbb{S}^1 's global specifications. The further Leibniz space boundary conditions are also met. \square

Remark 4 Propositions 3, 4 and 5 are key in kinematically quantizing 3 particles in 3- d [129].

Difference 6 The shape representative spaces, and bundles of representatives, are now as in Fig 52 rather than as in Fig 46.

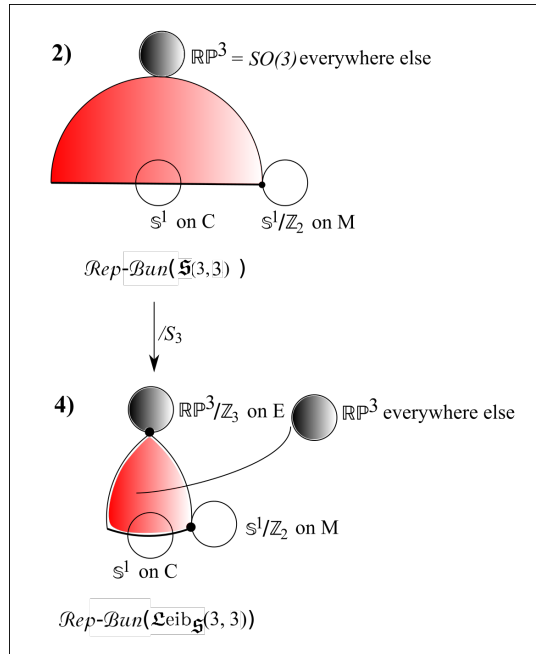


Figure 52: (3, 3) bundles of shape representatives.

Parallel 3 Sections of representatives, however, coincide for (3, 3) models and their two immediate (3, 2) counterparts.

Difference 7 Due to the above-mentioned stratification, (3, 3) has further need of general bundles than (3, 2) in the analysis of its spaces of shape representatives, and of shape representative sections over shape spaces. This is because the spaces of shape representatives of collinear configurations exceed those of generic shapes in dimension in the (3, 3) case.

Difference 8 For the (3, 3) model, variants of the Iwai and Kendall–Leibniz monopoles alone exist. These are not geometrically the same as in 2- d since now their collision plane and 1/6th-plane respectively, in each case excluding the origin, is now a separate stratum (Fig 53). So the current treatise points out that, at the level of stratified manifolds, there are in fact 2 distinct Iwai monopoles and 2 distinct Kendall–Leibniz monopoles. We note that *physical* investigation of topological defects in the presence of stratification remains in its infancy.

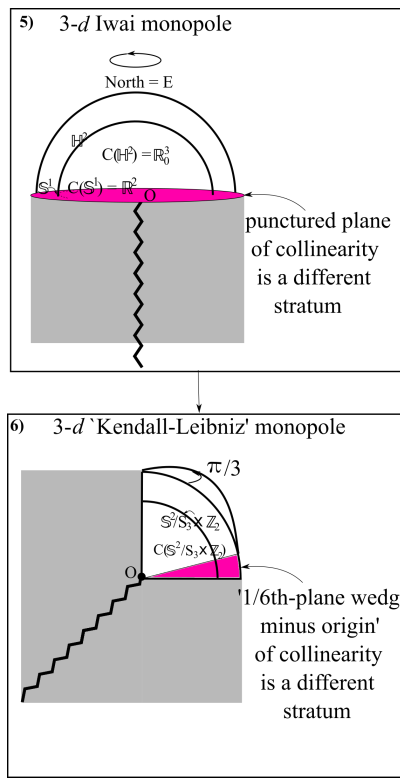


Figure 53: Relational triangleland monopoles in their most physically natural 3- d space setting.

5) 3- d Iwai monopole.

6) 3- d Leibniz–Kendall monopole.

[116] studies 2 further cases of 2- d 3-body problems.

Difference 8 Stratified manifolds can furthermore be usefully paired [66, 84, 108, 126] with sheaves [58, 42]. Better gluing and localization methods are then available to model the $(3, 3)$ case’s now inhomogeneous counterpart of shape representative space fibres. That $\mathfrak{S}(3, 3)$ and $\mathfrak{L}eib_{\mathfrak{S}}(3, 3)$ are Hausdorff, second-countable and compact, fortunately enables whichever of the simpler and more worked out cases outlined in [126] to apply. This includes via

$$(\text{Hausdorff and second countable}) \Rightarrow (\text{paracompact}) \quad (316)$$

and the very basic result that

$$(\text{compact}) \Rightarrow (\text{locally compact}) , \quad (317)$$

by the definition of this last concept [85, 64].

19.6 Advent of strata, general bundles and sheaves

These having been mentioned in the past four subsections, and also subsequently becoming the generic core of the subject of Shape Theory, let us end Part III with a more unified and referenced account of them.

Remark 1 As regards stratification, 1- d has no capacity for isotropy groups of different dimension. On the other hand, metric shape spaces for 2- d shapes avoid stratification issues. This is due to only involving $SO(2) = U(1)$, which acts in the same manner same on C and non- C configurations. However, in 3- d the C have only an $SO(2)$ subgroup of the $SO(3)$ acting upon them, so stratification ensues.

Remark 2 Plain N -stop metroland and N -a-gonland avoid stratification issues due to $SO(2) = U(1)$ ’s particular straightforwardness, whereas 3- d RPMs are not so fortunate.

See Appendices F, M and W of [108] for supporting outlines of fibre and general bundles, stratified manifolds, and sheaves respectively. The upcoming work [116, 126] provides further details.

Acknowledgments I thank Chris Isham for previous discussions, Jimmy York Jr for great motivation when I was young, and Don Page for discussions. Reza Tavakol, Malcolm MacCallum, Enrique Alvarez and Jeremy Butterfield for support with my career. I also thank Angela Lahee and the typesetting editors for my book manuscript this past summer for prompt and excellent work without which the current treatise could not have been completed by this date. I finally dedicate this paper to several friends who are going through considerably difficult times.

A Figure-webs of levels of structure for triangle-land

This Appendix is a useful end-summary in support of levels of structure discussed in Secs 4 to 8. It is presented all in one piece so as to exhibit the inter-relations between these structures, which are useful in building up these various structures and in understanding and remembering their content.

Structure 1 Figures 54, 55 and 56 exhibit 24 levels of structure for triangle-land, in which setting they are realized as 18 different structures. These figures are, respectively, for Leibniz space $\mathfrak{L}eib_{\mathfrak{G}}(3, 2)$, indistinguishable point-or-particle space $\mathfrak{I}\mathfrak{S}(3, 2)$, and a bird's eye view which coincides for plain and mirror-image-identified shape spaces $\mathfrak{S}(3, 2)$ and $\mathfrak{S}(3, 2)$.

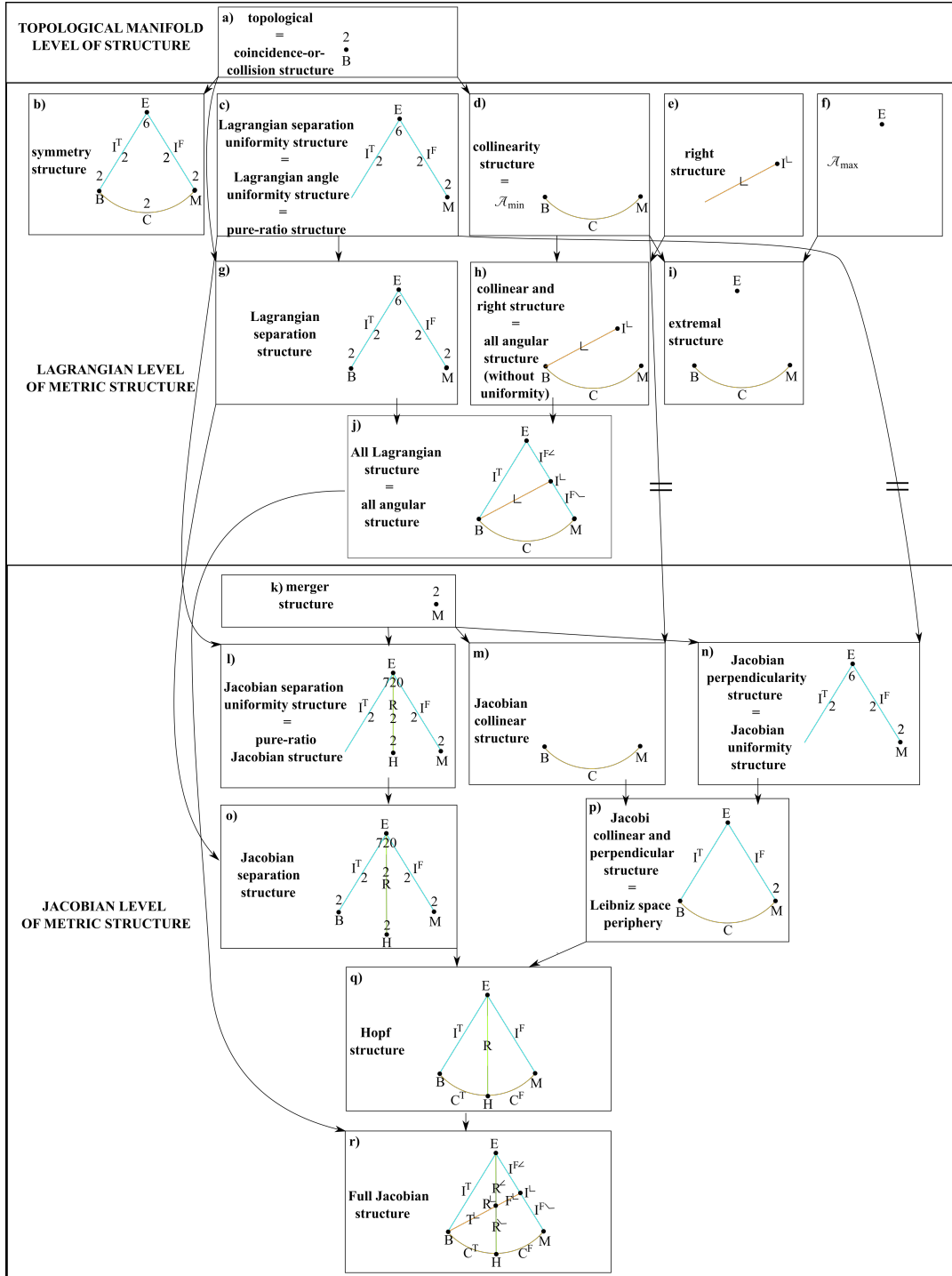


Figure 54: 24 levels of structure, which $\mathfrak{L}eib_{\mathfrak{G}}(3, 2)$ realizes as 18 distinct networks of points and arcs. These are viewed equatorially in the figure. The numbers indicated are, upon taking their logarithms, some of Part II's Appendices' quantifiers. This figure expands on eqs (I.255-256) for the (3, 1) model.

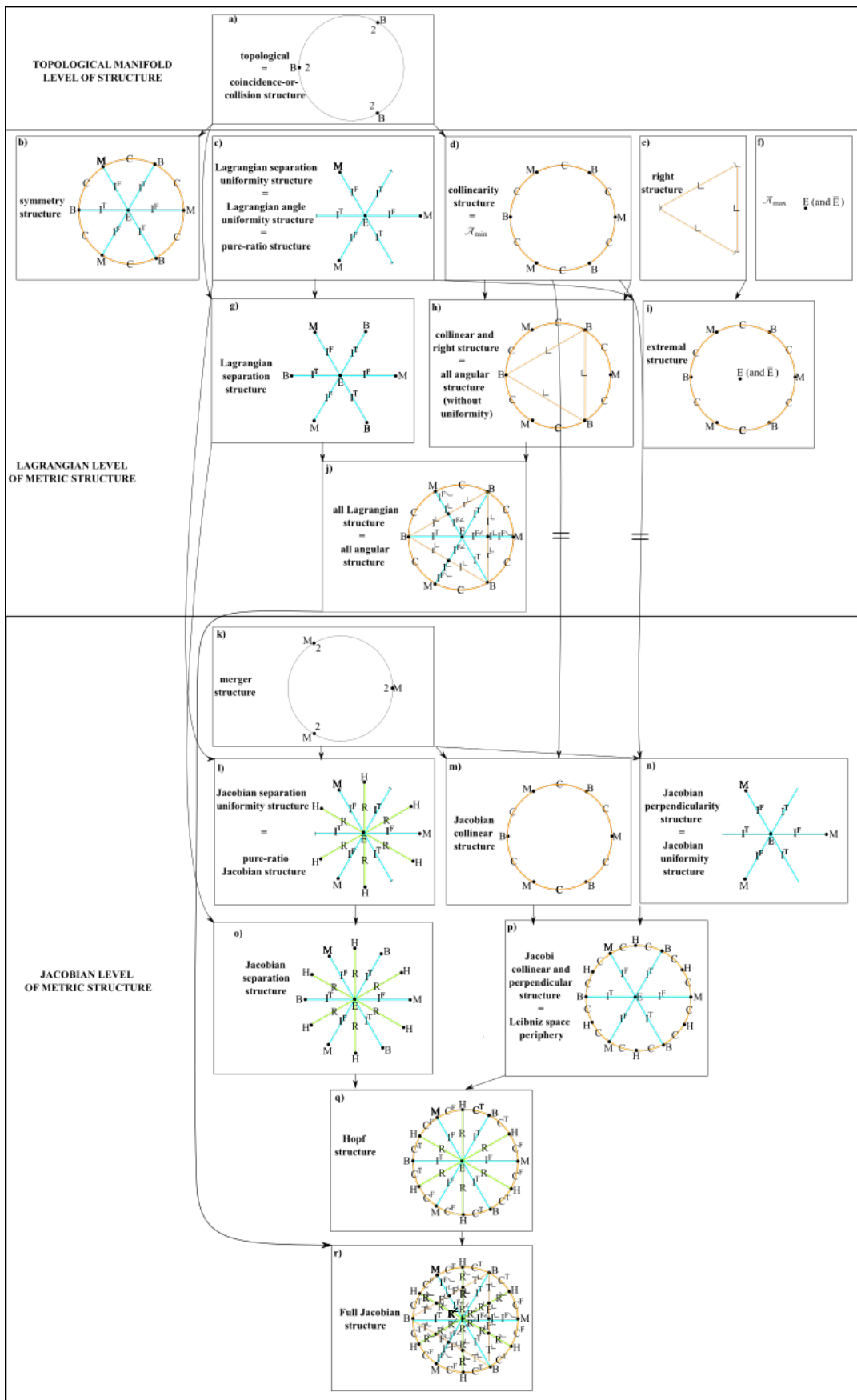


Figure 56: Bird's eye view 24 levels of structure, which are realized as 18 distinct networks of points and arcs in $\tilde{\mathfrak{S}}(3, 2)$ and 18 further such in $\mathfrak{S}(3, 2)$.

B Topological content of Part III's structures

Lemma 1 The sphere minus K points is topologically equivalent to the hemisphere minus $k = K - 1$ points, the disc minus k points and the k -bouquet. For K even ($= 2p$) these are topologically equivalent to the genus- p surface, i.e. the p -torus (where the 0-torus is the sphere), in each case with 1 point deleted. For K odd ($= 2p + 1$), these are topologically equivalent to the genus- p surface with a single puncture.

Proof See Fig 57. \square

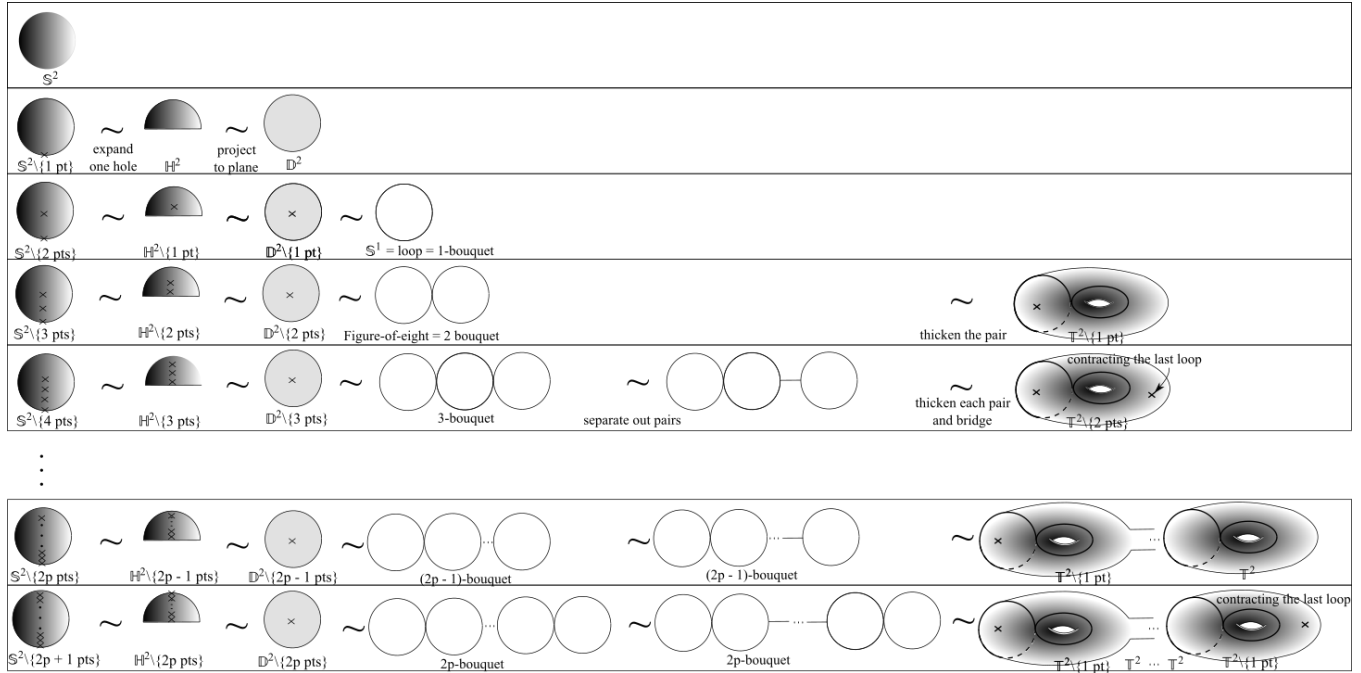


Figure 57: From circle to k -bouquet, with relation to punctured discs and (arbitrary hole number) tori. All of the previous section's structures are such objects or their disjoint union with further discs or points, as the next two figures tabulate.

Corollary 1 The topological content of the previous Appendix's structures is as tabulated in Fig 58 for the Lagrangian-level structures, and as in Fig 59 for the Jacobian-level structures.

shape space	coincidence-or-collision structure	symmetry structure	Lagrangian separation structure	collinearity structure	right	\mathcal{A}_{\max}	Lagrangian uniformity	collinear and right	extremal	all Lag
$\mathfrak{S}(3, 2)$	{1 pt}	\mathbb{S}^1	{1 pt}	{1 pt}	{1 pt}	{1 pt}	{1 pt}	{1 pt}	{1 pt}	$\mathbb{D}^2 \setminus \{2 \text{ pts}\}$
$\mathfrak{H}(3, 2)$	{1 pt}	$\mathbb{D}^2 \setminus \{2 \text{ pts}\}$	{1 pt}	{1 pt}	{1 pt}	{2 pts}	\mathbb{S}^1	{1 pt}	{1 pt}	$\mathbb{D}^2 \setminus \{4 \text{ pts}\}$
$\mathfrak{U}\mathfrak{S}(3, 2)$	{3 pts}	$\mathbb{D}^2 \setminus \{6 \text{ pts}\}$	{1 pt}	\mathbb{S}^1	{3 pt}	{1 pt}	{1 pt}	$\mathbb{D}^2 \setminus \{4 \text{ pts}\}$	$\mathbb{S}^1 \cup \{1 \text{ pt}\}$	$\mathbb{D}^2 \setminus \{12 \text{ pts}\}$
$\mathfrak{L}\text{eibg}(3, 2)$	{3 pts}	$\mathbb{D}^2 \setminus \{11 \text{ pts}\}$	$\mathbb{D}^2 \setminus \{2 \text{ pts}\}$	\mathbb{S}^1	{6 pt}	{2 pts}	$\mathbb{D}^2 \setminus \{5 \text{ pts}\}$	$\mathbb{D}^2 \setminus \{7 \text{ pts}\}$	$\mathbb{S}^1 \cup \{2 \text{ pt}\}$	$\mathbb{D}^2 \setminus \{23 \text{ pts}\}$

Figure 58: Table of topologies of various significant structures at the Lagrangian level

shape space	merger structure	Jacobian separation structure	Jacobian collision structure	Jacobian perpendicularity structure	Jacobian separation structure	Jacobian collision and perpendicularity structure	Hopf structure	full Jacobian structure
$\mathfrak{S}(3, 2)$	{1 pt}	{1 pt}	{1 pt}	{1 pt}	{1 pt}	\mathbb{S}^1	$\mathbb{D}^2 \setminus \{2 \text{ pts}\}$	$\mathbb{D}^2 \setminus \{4 \text{ pts}\}$
$\mathfrak{H}(3, 2)$	{1 pt}	\mathbb{S}^1	{1 pt}	{1 pt}	$\mathbb{D}^2 \setminus \{2 \text{ pts}\}$	$\mathbb{D}^2 \setminus \{2 \text{ pts}\}$	$\mathbb{D}^2 \setminus \{4 \text{ pts}\}$	$\mathbb{D}^2 \setminus \{8 \text{ pts}\}$
$\mathfrak{U}\mathfrak{S}(3, 2)$	{3 pts}	{1 pt}	\mathbb{S}^1	{1 pt}	{1 pt}	$\mathbb{D}^2 \setminus \{6 \text{ pts}\}$	$\mathbb{D}^2 \setminus \{12 \text{ pts}\}$	$\mathbb{D}^2 \setminus \{24 \text{ pts}\}$
$\mathfrak{L}\text{eibg}(3, 2)$	{3 pts}	$\mathbb{D}^2 \setminus \{8 \text{ pts}\}$	\mathbb{S}^1	$\mathbb{D}^2 \setminus \{2 \text{ pts}\}$	$\mathbb{D}^2 \setminus \{11 \text{ pts}\}$	$\mathbb{D}^2 \setminus \{11 \text{ pts}\}$	$\mathbb{D}^2 \setminus \{23 \text{ pts}\}$	$\mathbb{D}^2 \setminus \{47 \text{ pts}\}$

Figure 59: Table of topologies of various significant structures at the Jacobian level.

References

- [1] Euclid *Elements*, approximately 300 B.C; see e.g. *The Thirteen Books of Euclid's Elements* for an English translation and commentary by T.L. Heath (Dover, New York 1956).
- [2] Heron, alias Hero, of Alexandria, *Metrica* (60 A.D.).
- [3] G. Ceva, *De Lineis Rectis (On Straight Lines)* (1678).
- [4] M. Stewart, *Some General Theorems of Considerable Use in the Higher Parts of Mathematics* (Sands, Edinburgh 1746).
- [5] C.L. Dodgson (alias Lewis Carroll), *Curiosa Mathematica: Pillow-Problems, thought out during Sleepless Nights* (Macmillan, London 1893).
- [6] N.A. Court, *College Geometry* (Johnson, Richmond, Va. 1925), pp 60-61.
- [7] H. Hopf, "Über die Abbildungen der dreidimensionalen Sphäre auf die Kugelfläche", (Concerning the Images of S^3 on S^2), *Math. Ann.* (Berlin) Springer **104** 637 (1931).
- [8] P.A.M. Dirac, "Quantised Singularities in the Electromagnetic Field", *Proc. Roy. Soc.* **A133** 60 (1931).
- [9] T.H. Gronwall, "A Special Conformally Euclidean Space of Three Dimensions Occurring in Wave Mechanics", *Ann. Math.* **33** 279 (1932).
- [10] H. Whitney, "Complexes of Manifolds", *Proc. Nat. Acad. Sci. USA* **33** 10 (1946).
- [11] P.A.M. Dirac, The Theory of Magnetic Poles, *Phys. Rev.* **74** 817 (1948).
- [12] C. Lanczos, *The Variational Principles of Mechanics* (University of Toronto Press, Toronto 1949).
- [13] R. Courant and D. Hilbert, *Methods of Mathematical Physics* Vol. 1 (John Wiley and Sons, Chichester 1989, previously published in 1953).
- [14] P.M. Morse and H. Feshbach, *Methods of Theoretical Physics. Part I* (McGraw-Hill, New York 1953).
- [15] R. Thom, "Les Singularités des Applications Différentiables" (Singularities in Differentiable Maps), *Ann. Inst. Fourier* (Grenoble) **6** 43 (1955).
- [16] F.T. Smith, "Generalized Angular Momentum in Many-Body Collisions", *Phys. Rev.* **120** 1058 (1960).
- [17] N.D. Kazarinoff, *Geometric Inequalities* (Yale University, 1961).
- [18] F.T. Smith, "A Symmetric Representation for Three-Body Problems. I. Motion in a Plane", *J. Math. Phys.* **3** 735 (1962).
- [19] R.F. Baierlein, D.H. Sharp and J.A. Wheeler, "Three-Dimensional Geometry as Carrier of Information about Time", *Phys. Rev.* **126** 1864 (1962).
- [20] J.A. Wheeler, "Geometrodynamics and the Issue of the Final State", in *Groups, Relativity and Topology* ed. B.S. DeWitt and C.M. DeWitt (Gordon and Breach, N.Y. 1964).
- [21] J.L. Anderson, "Relativity Principles and the Role of Coordinates in Physics.", in *Gravitation and Relativity* ed. H-Y. Chiu and W.F. Hoffmann p. 175 (Benjamin, New York 1964).
- [22] H. Whitney, "Tangents to an Analytic Variety", *Ann. Math.* **81** 496 (1965).
- [23] J.L. Anderson, *Principles of Relativity Physics* (Academic Press, New York 1967).
- [24] A.J. Dragt, "Classification of Three-Particle States According to $SU(3)$ ", *J. Math. Phys.* **6** 533 (1965).
- [25] W. Zickendraht, "Configuration-Space Approach to Three-Particle Scattering", *Phys. Rev.* **159** 1448 (1967).
- [26] B.S. DeWitt, "Quantum Theory of Gravity. I. The Canonical Theory.", *Phys. Rev.* **160** 1113 (1967).
- [27] J.A. Wheeler, in *Battelle Rencontres: 1967 Lectures in Mathematics and Physics* ed. C. DeWitt and J.A. Wheeler (Benjamin, New York 1968).
- [28] B. Rich and C. Thomas, *Geometry* (McGraw-Hill, 1963).
- [29] W. Zickendraht, "Configuration-Space Approach to the Four-Particle Problem", *J. Math. Phys.* **10** 30 (1969).
- [30] R. Thom, "Ensembles et Morphismes Stratifiés" (Stratified Spaces and Morphisms), *Bull. Amer. Math. Soc. (N.S.)* **75** 240 (1969).
- [31] A.S. Posamentier and C.T. Salkind, *Challenging Problems in Geometry* (MacMillan, New York 1970, reissued by Dover, New York 1996).
- [32] W. Zickendraht, "Collective and Single-Particle Coordinates in Nuclear Physics", **12** 1663 (1970).
- [33] M. Abramowitz and I.A. Stegun, *Handbook of Mathematical Functions with Formulas, Graphs, and Mathematical Tables* (Dover, New York 1972).
- [34] W. Magnus *Noneuclidean Tessellations and their groups* (Academic Press, New York 1974).

- [35] T.T. Wu and C.N. Yang, "Dirac Monopole Without Strings: Monopole Harmonics", Nu. Phys. **B107** 365 (1976).
- [36] K.V. Kuchař, "Canonical Methods of Quantization", in *Quantum Gravity 2: a Second Oxford Symposium* ed. C.J. Isham, R. Penrose and D.W. Sciama (Clarendon, Oxford 1981).
- [37] J.B. Barbour and B. Bertotti, "Mach's Principle and the Structure of Dynamical Theories", Proc. Roy. Soc. Lond. **A382** 295 (1982).
- [38] D.G. Kendall, "Shape Manifolds, Procrustean Metrics and Complex Projective Spaces", Bull. Lond. Math. Soc. **16** 81 (1984).
- [39] V. Aquilanti, S. Cavalli and G. Grossi, "Hyperspherical coordinates for Molecular Dynamics by the Method of Trees and the Mapping of Potential Energy Surfaces for Triatomic Systems", J. Chem. Phys. **85** 1362 (1986).
- [40] R.T. Pack and G.A. Parker, "Quantum Reactive Scattering in Three Dimensions using Hyperspherical (APH) Coordinates. Theory", J. Chem. Phys. **87** 3888 (1987).
- [41] T. Iwai, "A Geometric Setting for Internal Motions of the Quantum Three-Body System", J. Math. Phys. **28** 1315 (1987).
- [42] J.L. Bell, *Toposes and Local Set Theories* (Clarendon, Oxford 1988 and Dover, New York 2008).
- [43] D.G. Kendall, "A Survey of the Statistical Theory of Shape", Statistical Science **4** 87 (1989).
- [44] H.S.M. Coxeter, *Introduction to Geometry* (Wiley, New York 1989).
- [45] C. Marchal, *Celestial Mechanics* (Elsevier, Tokyo 1990).
- [46] K.V. Kuchař, "The Problem of Time in Canonical Quantization", in *Conceptual Problems of Quantum Gravity* ed. A. Ashtekar and J. Stachel (Birkhäuser, Boston, 1991).
- [47] K.V. Kuchař, "Time and Interpretations of Quantum Gravity", in *Proceedings of the 4th Canadian Conference on General Relativity and Relativistic Astrophysics* ed. G. Kunstatter, D. Vincent and J. Williams (World Scientific, Singapore, 1992), reprinted as Int. J. Mod. Phys. Proc. Suppl. **D20** 3 (2011).
- [48] C.J. Isham, "Canonical Quantum Gravity and the Problem of Time", in *Integrable Systems, Quantum Groups and Quantum Field Theories* ed. L.A. Ibort and M.A. Rodríguez (Kluwer, Dordrecht 1993), gr-qc/9210011.
- [49] R. Guy, "There Are Three Times as Many Obtuse-Angled Triangles as There Are Acute-Angled Ones", Mathematics Magazine, **66** 175 (1993).
- [50] S. Portnoy, "A Lewis Carroll Pillow Problem: Probability of an Obtuse Triangle", Statist. Sci. **9** 279 (1994).
- [51] See e.g. D.C. Kay, *College Geometry: : A Discovery Approach* (Harper Collins, 1994).
- [52] D. Husemoller, *Fibre Bundles* (Springer, New York 1994).
- [53] R.G. Littlejohn and M. Reinsch, "Internal or Shape Coordinates in the N -body Problem", Phys. Rev. **A52** 2035 (1995).
- [54] C.G.S. Small, *The Statistical Theory of Shape* (Springer, New York, 1996).
- [55] R.G. Littlejohn and M. Reinsch, "Gauge Fields in the Separation of Rotations and Internal Motions in the N -Body Problem", Rev. Mod. Phys. **69** 213 (1997).
- [56] K.A. Mitchell and R.G. Littlejohn, "Derivation of Planar Three-Body Hyperspherical Harmonics from Monopole Harmonics", Phys. Rev. **A56** 83 (1997).
- [57] D. Giulini, "The Group of Large Diffeomorphisms in General Relativity", Banach Center Publ. **39** 303 (1997), arXiv:gr-qc/9510022.
- [58] G.E. Bredon, *Sheaf Theory* (McGraw-Hill, New York 1997).
- [59] J.B. Barbour, *The End of Time* (Oxford University Press, Oxford 1999).
- [60] K.A. Mitchell and R.G. Littlejohn, "Boundary Conditions on Internal Three-Body Wave Functions", physics/9908037.
- [61] K.V. Kuchař, "The Problem of Time in Quantum Geometroynamics", in *The Arguments of Time*, ed. J. Butterfield (Oxford University Press, Oxford 1999).
- [62] D.G. Kendall, D. Barden, T.K. Carne and H. Le, *Shape and Shape Theory* (Wiley, Chichester 1999).
- [63] L.Á Gergely, "The Geometry of the Barbour-Bertotti Theories I. The Reduction Process", Class. Quant. Grav. **17** 1949 (2000), gr-qc/0003064.
- [64] J.R. Munkres, *Topology* (Prentice-Hall, Upper Saddle River, New Jersey 2000).
- [65] J.R. Silvester, *Geometry Ancient and Modern* (Oxford University Press, New York 2001).
- [66] M.J. Pflaum, *Analytic and Geometric Study of Stratified Spaces*, Lecture Notes in Mathematics **1768** (Springer, Berlin 2001).
- [67] R. Montgomery, "Infinitely Many Syzygies", Arch. Rat. Mech. Anal. **164** 311 (2002).
- [68] See e.g. A. Benyi, "A Heron-type formula for the triangle", Mathematical Gazette **87** 324 (2003).
- [69] R. Montgomery, "Fitting Hyperbolic Pants to a 3-Body Problem", Ergod. Th. Dynam. Sys. **25** 921 (2005), math/0405014.

- [70] C. Rovelli, *Quantum Gravity* (Cambridge University Press, Cambridge 2004).
- [71] C. Kiefer, *Quantum Gravity* (Clarendon, Oxford 2004).
- [72] W.-Y. Hsiang and E. Straume, "Kinematic Geometry of Triangles and the Study of the Three-Body Problem ", math-ph/0608060; "Global Geometry of 3-Body Motions with Vanishing Angular Momentum. I", math-ph/0609076; "Global Geometry of Planary 3-Body Motions", math-ph/0609084.
- [73] D. Giulini, "Some Remarks on the Notions of General Covariance and Background Independence", in *An Assessment of Current Paradigms in the Physics of Fundamental Interactions* ed. I.O. Stamatescu, Lect. Notes Phys. **721** 105 (2007), arXiv:gr-qc/0603087.
- [74] E. Anderson, "Classical Dynamics on Triangleland", *Class. Quantum Grav.* **24** 5317 (2007), gr-qc/0702083.
- [75] E. Anderson, "Foundations of Relational Particle Dynamics", *Class. Quant. Grav.* **25** 025003 (2008), arXiv:0706.3934.
- [76] E. Anderson, Triangleland. I. Classical Dynamics with Exchange of Relative Angular Momentum", *Class. Quantum Grav.* **26** 135020 (2009), arXiv:0809.1168.
- [77] E. Anderson, Triangleland. II. Quantum Mechanics of Pure Shape", *Class. Quantum Grav.* **26** 135021 (2009) gr-qc/0809.3523.
- [78] E. Anderson and A. Franzen, "Quantum Cosmological Metroland Model", *Class. Quant. Grav.* **27** 045009 (2010), arXiv:0909.2436.
- [79] E. Anderson, "Shape Space Methods for Quantum Cosmological Triangleland", *Gen. Rel. Grav.* **43** 1529 (2011), arXiv:0909.2439.
- [80] D. Groisser, and H.D. Tagare, "On the Topology and Geometry of Spaces of Affine Shapes", *Journal of Mathematical Imaging and Vision* **34** 222 (2009).
- [81] E. Anderson, "Relational Mechanics of Shape and Scale", arXiv:1001.1112.
- [82] E. Anderson, "Quantum Cosmological Relational Model of Shape and Scale in 1- d ", *Class. Quantum Grav.* **28** 065011 (2011), arXiv:1003.4034.
- [83] E. Anderson, "The Problem of Time in Quantum Gravity", in *Classical and Quantum Gravity: Theory, Analysis and Applications* ed. V.R. Frignanni (Nova, New York 2012), arXiv:1009.2157.
- [84] M. Kreck, *Differential Algebraic Topology: From Stratifolds to Exotic Spheres* (American Mathematical Society, Providence 2010).
- [85] J.M. Lee, *Introduction to Topological Manifolds* (Springer, New York 2011).
- [86] I. Matić, Olympiad Training Materials, Geometric Inequalities, <http://www.imomath.com/index.php?options=601&lmm=0> (2011).
- [87] I. Matić, Olympiad Training Materials, Geometric Inequalities, <http://www.imomath.com/index.php?options=603&lmm=0> (2011).
- [88] I. Matić, Olympiad Training Materials, Geometric Inequalities, <http://www.imomath.com/index.php?options=604&lmm=0> (2011).
- [89] E. Anderson, "The Problem of Time and Quantum Cosmology in the Relational Particle Mechanics Arena", arXiv:1111.1472.
- [90] E. Anderson, "Relational Quadrilateralland. I. The Classical Theory", *Int. J. Mod. Phys. D***23** 1450014 (2014), arXiv:1202.4186.
- [91] E. Anderson, "Problem of Time in Quantum Gravity", *Annalen der Physik*, **524** 757 (2012), arXiv:1206.2403.
- [92] A. Bhattacharya and R. Bhattacharya, *Nonparametric Statistics on Manifolds with Applications to Shape Spaces* (Cambridge University Press, Cambridge 2012).
- [93] E. Anderson and S.A.R. Kneller, "Relational Quadrilateralland. II. The Quantum Theory", *Int. J. Mod. Phys. D***23** 1450052 (2014), arXiv:1303.5645.
- [94] E. Anderson, "Kendall's Shape Statistics as a Classical Realization of Barbour-type Timeless Records Theory approach to Quantum Gravity", *Stud. Hist. Phil. Mod. Phys.* **51** 1 (2015), arXiv:1307.1923.
- [95] E. Anderson, "Beables/Observables in Classical and Quantum Gravity", *SIGMA* **10** 092 (2014), arXiv:1312.6073.
- [96] J. Śniatycki, *Differential Geometry of Singular Spaces and Reduction of Symmetry* (Cambridge University Press, Cambridge 2013).
- [97] E. Anderson, "Background Independence", arXiv:1310.1524.
- [98] E. Anderson, "Problem of Time and Background Independence: the Individual Facets", arXiv:1409.4117.
- [99] E. Anderson, "Spaces of Spaces", arXiv:1412.0239.
- [100] A. Edelman and G. Strang, "Random Triangle Theory with Geometry and Applications", *Foundations of Computational Mathematics* (2015), arXiv:1501.03053.
- [101] E. Anderson, "Configuration Spaces in Fundamental Physics", arXiv:1503.01507.
- [102] E. Anderson, "Six New Mechanics corresponding to further Shape Theories", *Int. J. Mod. Phys. D* **25** 1650044 (2016), arXiv:1505.00488.
- [103] E. Anderson, "Spherical Relationalism", arXiv:1505.02448.
- [104] E. Anderson, "Explicit Partial and Functional Differential Equations for Beables or Observables" arXiv:1505.03551.

- [105] E. Anderson, "On Types of Observables in Constrained Theories", arXiv:1604.05415.
- [106] V. Patrangenaru and L. Ellingson "Nonparametric Statistics on Manifolds and their Applications to Object Data Analysis" (Taylor and Francis, Boca Raton, Florida 2016).
- [107] F. Kelma, J.T. Kent and T. Hotz, "On the Topology of Projective Shape Spaces", arXiv:1602.04330.
- [108] E. Anderson, *Problem of Time. Quantum Mechanics versus General Relativity*, (Springer International 2017), Found. Phys. **190**; free access to its extensive Appendices is at <https://link.springer.com/content/pdf/bbm%3A978-3-319-58848-3%2F1.pdf> .
- [109] E. Anderson, "The Smallest Shape Spaces. I. Shape Theory Posed, with Example of 3 Points on the Line", arXiv:1711.10054.
- [110] E. Anderson, "The Smallest Shape Spaces. II. 4 Points on a Line Suffices for a Complex Background-Independent Theory of Inhomogeneity", arXiv:1711.10073.
- [111] This was calculated using Maple 17.
- [112] E. Anderson, "Alice in Triangleland: Lewis Carroll's Pillow Problem and Variants Solved on Shape Space of Triangles", arXiv:1711.11492.
- [113] E. Anderson, "Two New Perspectives on Heron's Formula", arXiv:1712.01441.
- [114] E. Anderson, "Shape (In)dependent Inequalities for Triangleland's Jacobi and Democratic-Linear Ellipticity Quantities", arXiv:1712.04090.
- [115] E. Anderson, "Maximal Angle Flow on the Shape Sphere of Triangles", arXiv:1712.07966
- [116] E. Anderson, "Monopoles of Twelve Types in 3-Body Problems", arXiv:1802.03465.
- [117] E. Anderson, "Background Independence *Includes* Shape Theory", forthcoming 2018.
- [118] E. Anderson, "Background Independence and Shape Theory on the Torus, forthcoming 2018.
- [119] E. Anderson, "Shape Theory's Background-Independent Vertex-Primary Answer to Sylvester's Prob(Quadrilateral is Convex)", forthcoming 2018.
- [120] E. Anderson, "While Heron's Form is Shape-Theoretic, Coolidge's is not", forthcoming 2018.
- [121] E. Anderson, "Shape-Independent Inequalities for Quadrilaterals", forthcoming 2018.
- [122] E. Anderson, "Affine Shape Space. I. Topological Structure", forthcoming 2018.
- [123] E. Anderson, "Affine Shape Space. II. Riemannian Metric Structure", forthcoming 2018.
- [124] E. Anderson, "The Smallest Shape Spaces. IV. Quadrilaterals in the Plane", forthcoming 2018.
- [125] E. Anderson, "Geometrically Significant Functions for Triangles Plotted over the Shape Sphere of Triangles", forthcoming 2018.
- [126] E. Anderson, "Background Independence Leads to Study of Stratified Manifolds and Sheaves", forthcoming 2018.
- [127] E. Anderson, "Quantizing the Smallest Shape Spaces", forthcoming 2018.
- [128] E. Anderson, "Constraint Closure and the Problem of Observables: Outline of Sheaf-Theoretic Inputs", forthcoming 2018.
- [129] E. Anderson, "Quantum Triangles", forthcoming 2018.
- [130] E. Anderson, "Pentagonal Shapes and Shape Spaces", forthcoming.
- [131] E. Anderson, "Hexagonal Shapes and Shape Spaces", forthcoming.
- [132] E. Anderson, forthcoming.